2017

Ecological impacts of deforestation and forest degradation in the peat swamp forests of northwestern Borneo

BOSTON UNIVERSITY

GRADUATE SCHOOL OF ARTS AND SCIENCES

Dissertation

ECOLOGICAL IMPACTS OF DEFORESTATION AND FOREST DEGRADATION IN THE PEAT SWAMP FORESTS OF NORTHWESTERN BORNEO

By

HA THANH NGUYEN

B.Sc. Mount Alison University, 2009
M.A.Sc. Queen's University, 2011

Submitted in partial fulfillment of the
requirements for the degree of
Doctor of Philosophy
2017

Approved by

First Reader _____

Lucy R. Hutyra, PhD

Associate Professor of Earth and Environment

Second Reader _____

Mark Friedl, PhD

Professor of Earth and Environment

Third Reader _____

Curtis Woodcock, PhD

Professor of Earth and Environment

ACKNOWLEDGEMENTS

This dissertation would not have been made possible without the faith, generosity, support and patience that I have been fortunate to receive from many people. I owe my greatest gratitude to my parents and sister, who since I left home to study abroad 16 years ago have relentlessly stood by me and sacrificed tremendously to wait for this day. My father and mother have taught me to value scholarly pursuits, to follow my dreams with steadfast determination and integrity, and to honor my promise of making right their sacrifices. I would like to thank my supervisor Lucy Hutyra for her patience, guidance and dedication and for always upholding me for the highest quality of scholarly work. It has been an honor for me to have you fight for me and fight with me through the many challenges of this dissertation and to have been inspired by your knowledge and vision. I treasure every compliment you have given me and will always subject myself to the same scholarly standard you have 'raised' me in.

I would like to thank my committee members for their patience, attention and guidance over the years. I also have many colleagues of the Earth and Environment Department who have brainstormed with me, shared insight from other fields, and offered constructive critique for this work. Much of this dissertation will not be possible without the outstanding work of Dr. Zhe Zhu and Chris Holden, who have opened the path for many people including me to seamlessly explore and analyze the Landsat archives. I am indebted to Dr. Steve Raciti, Dr. Brady Getson-Hardiman, Dr. Dan Short Gianotti, Dr. Josh Gray and Dr. Andy Reinmann, for their in-depth knowledge and invaluable

assistance throughout this dissertation. I am grateful to the many members of the PhD community in the department, my co-inhabitants of CAS 338 and members of the Hutyra Lab who have shared with me all the ups and downs of the PhD process and made my time here a process of continuous stimulation, profound inspiration and maturation. A special shout-out to Dr. Zhan Li, Dr. Sohaila Bastami and (soon to be Dr.) Bin Li, who have grown with me and always been my loyal, true and honest audience. Opa and Oma, Mr and Mrs. Hulsman, thank you for giving the familial warm, and so much care and faith during my years studying abroad. I must also thank Mr. Pham Ngoc Tu, Mr. Pham Cuong and Mr. Nguyen Minh Duc, whose support and guidance have helped me keep my hopes alive and carry on through this journey.

Finally, I have to thank my partner Erwin Hilton who has always been by my side, offered confidence and advice and cheered me up as I strive towards the finish line. Behind a doctoral dissertation there is always a quiet co-writer and no one could have done a better job than you.

ECOLOGICAL IMPACTS OF DEFORESTATION AND FOREST DEGRADATION IN THE PEAT SWAMP FOREST OF NORTHWESTERN BORNEO

HA THANH NGUYEN

Boston University Graduate School of Arts and Sciences, 2017

Major Professor: Lucy R. Hutyra, Associate Professor of Earth and Environment

ABSTRACT

Tropical peatlands have some of the highest carbon densities of any ecosystem and are under enormous development pressure. This dissertation aimed to provide better estimates of the scales and trends of ecological impacts from tropical peatland deforestation and degradation across more than 7,000 hectares of both intact and disturbed peatlands in northwestern Borneo. We combined direct field sampling and airborne Light Detection And Ranging (LiDAR) data to empirically quantify forest structures and aboveground live biomass across a largely intact tropical peat dome. The observed biomass density of 217.7 ± 28.3 Mg C hectare^{-1} was very high, exceeding many other tropical rainforests. The canopy trees were ~65m in height, comprising 81% of the aboveground biomass. Stem density was observed to increase across the 4m elevational gradient from the dome margin to interior with decreasing stem height, crown area and crown roughness. We also developed and implemented a multi-temporal, Landsat

resolution change detection algorithm for identify disturbance events and assessing forest trends in aseasonal tropical peatlands. The final map product achieved more than 92% user's and producer's accuracy, revealing that after more than 25 years of management and disturbances, only 40% of the area was intact forest. Using a chronosequence approach, with a space for time substitution, we then examined the temporal dynamics of peatlands and their recovery from disturbance. We observed widespread arrested succession in previously logged peatlands consistent with hydrological limits on regeneration and degraded peat quality following canopy removal. We showed that clear-cutting, selective logging and drainage could lead to different modes of regeneration and found that statistics of the Enhanced Vegetation Index and LiDAR height metrics could serve as indicators of harvesting intensity, impacts, and regeneration stage. Long-term, continuous monitoring of the hydrology and ecology of peatland can provide key insights regarding best management practices, restoration, and conservation priorities for this unique and rapidly disappearing ecosystem.

TABLE OF CONTENTS

LIST OF TABLES

LIST OF FIGURES

LIST OF ABBREVIATIONS

LCLCC	Land Use Land Cover Change
LiDAR	Light Detection and Ranging
PSF	Peatswamp Forest

CHAPTER 1 - INTRODUCTION

Peatlands, ecosystems where soils are at least 30cm thick with more than 65% organic material (Rieley & Page 2005), play a very important role in the global carbon (C) cycle through both their vast carbon pools and their fluxes carbon dioxide (CO_2) and methane (CH_4) (Immirzi *et al.*, 1992; Strack, 2008). Formed in low relief, waterlogged, and high precipitation areas, which impede organic material decomposition, peatlands represent a very space efficient way to store carbon. Covering less than 3% of the Earth's land surface (Page *et al.*, 2011), peatlands store one third of global soil carbon (Parish *et al.*, 2008; Draper *et al.*, 2014). In the tropics, peat deposits co-exist with peat swamp forests (PSF) which have very high net primary productivity and provide the inputs to build the peat, providing crucial ecosystem services through sequestering carbon, regulating water budget and climate, and supporting biodiversity (Anderson, 1983; Page *et al*., 2011). Forested peatlands in insular Southeast Asia account for 56% the area of all PSFs worldwide and 70% the volume of global peat (Page *et al.*, 2011). In Northwestern Borneo, more than 12% of the coastal lowlands area is forested peatlands (Anderson and Muller 1975).

Peatlands have a convex form, raising above the surrounding landscape, with a vegetation cover that is well adapted to waterlogged, nutrient poor soils (Anderson 1983, Anderson and Muller 1975, Dommain *et al.* 2010). In Borneo, peat deposits are often found between river valleys adjacent to maritime fringes, in coastal plains and isolated basins. With a wet tropical climate, annual rainfall generally in excess of 2500 mm, they

mainly derived their nutrients from rain and are referred to as ombrogeneous ("rain-fed"). In Borneo, the rainfall is largely aseasonal, with either a long 'wet' season of 9–10 months alternating with a shorter 'dry' season of 2 or 3 months duration, or two 'monsoon' seasons (October to March and April to August) interspersed by two short 'dry' periods (Rieley and Page 2005). Periods are referred to as 'dry' if less than 100mm of rainfall is received.

Anderson and Muller (1975) and Anderson (1983) described the peatlands of northwestern Borneo, in terms of species composition and dominance, as a catenary sequence of forest types occurring from the periphery to the center of tropical peat swamps, with the timber valuable species *Shorea albida* predominant across most community types. This sequence is characterized by (i) an almost complete change in species composition from one forest type to the next; (ii) an increase in stem density and (iii) decreases in average size of a species in terms of height, girth and crown area. These transitions in forest composition and structure have been hypothesized to reflect changes in water and nutrient availability in the peat and ultimately the dome structure (Anderson 1983). Both the interdependence between belowground peat with aboveground vegetation (Page *et al.*, 1999) and the relation between peat carbon with the groundwater level can be strongly modified by land use activities (Hirano *et al.*, 2012; Carlson *et al.*, 2015). These render tropical peatlands in Southeast Asia extremely sensitive to disturbances and represent a crucial source of uncertainty in the global carbon cycle (Limpens *et al.*, 2008; Couwenberg *et al.*, 2010; Hooijer *et al.*, 2012).

The main carbon fluxes associated with peatland systems include photosynthesis by vegetation, peat accumulation, CO_2 release from peat decomposition, litter decay, carbon release by fires, and particulate organic carbon and dissolved organic carbon exported via waterways (Abrams *et al.*, 2016). There are CH_4 fluxes from both anaerobic peat and dissolved organic matter decay, the magnitude of which is less than 1% of the CO_2 emission from peat (Shimada *et al.*, 2016) and can be further reduced by drainage after logging (Jauhiainen *et al*., 2005, 2008; Melling *et al*., 2005, 2007; Couwenberg *et al*., 2010). According to recent radiocarbon dating study results, over the past 6,500 years, long term C sequestration in tropical peatlands in Borneo and Sumatra varies from 0.313 Mg C ha^{-1} $year^{-1}$ to 6.0 Mg C ha^{-1} $year^{-1}$ (Anderson 1964; Sieffermann *et al.*, 1988; Neuzil 1997; Page *et al.*, 2004; Dommain *et al.*, 2011). Mean annual net ecosystem CO_2 exchange (± a standard deviation) has been estimated as 1.74 ± 2.03 ha^{-1} $year^{-1}$ for an intact peat swamp forest in Indonesia (Hirano *et al.*, 2012). The carbon density in Indonesian peatlands have been estimated to be 2,772 Mg C ha^{-1} (based on a best estimate peat thickness of 5.5 m), which was much higher than typical values for aboveground peat swamp forest carbon density of 100-150 Mg C ha^{-1} (Page *et al.*, 2006).

Given their enormous carbon reservoirs, peatlands in SE Asia can become substantial sources of carbon when harvested and/or managed for agricultural development. Peatland destruction in Southeast Asia is a relative recent phenomenon (Dommain *et al.*, 2016). What started as cultivation schemes to boost national crop and rice production in undeveloped swamp areas in the 1970s, dramatically accelerated in the 1980s, and

continues to the present day due to growing global demand for timber, palm oil and pulp (Gaveau *et al.*, 2014, 2016; figure 1.1). These anthropogenic disturbances have led to substantial peat losses through enhanced oxidation and combustion (Page *et al.*, 2002; Hooijer *et al.*, 2006, 2010; Hirano *et al.*, 2012). During 2000-2010, PSF area in Borneo (comprising Brunei, Malaysia's Sarawak and Sabah, and Indonesia's Kalimantan) declined by as much as 2.2% yr^{-1} (Miettinen *et al.*, 2011). Drainage and burning released

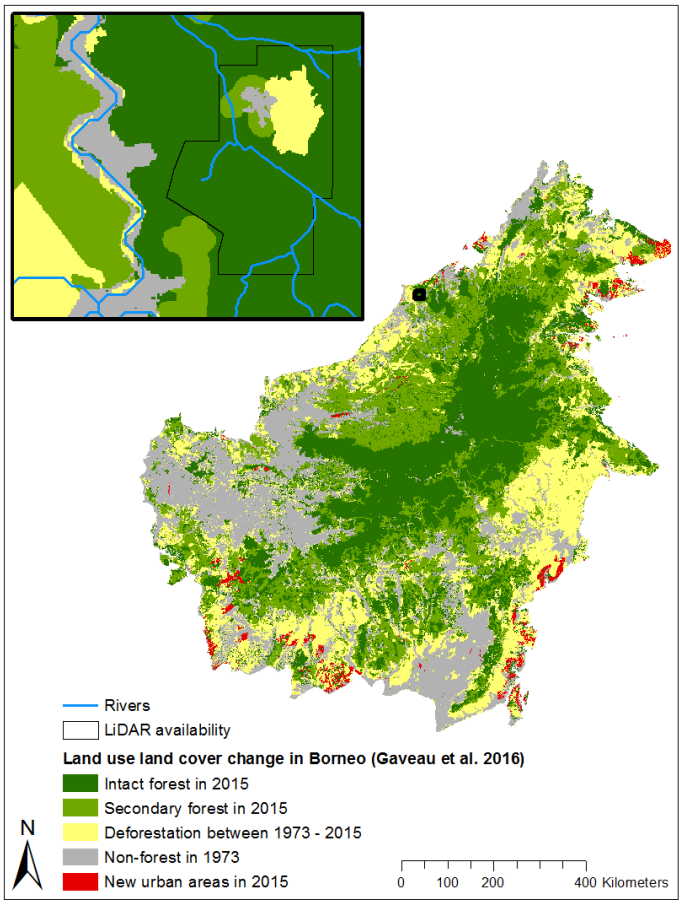

Figure 1.1: Land use land cover change on Borneo Island between 1973 and 2015. This figure was adapted from Gaveau *et al.* (2016). The study area of this dissertation was indicated in the black box.

an estimated 3.28 ± 2.04 and 4.99 ± 0.72 Mg C ha^{-1} $year^{-1}$, respectively (cf. Inubushi *et al.,* 2003; Melling *et al.,* 2005). Drainage results in a drying of the peat layer and oxygen availability within the peat, while logging increases the fuel load on the ground, both land use changes increase the susceptibility of PSF to fire. During the major 1997/98 and 2015/16 El Niño events, drought enhanced peat combustion contributed to the steepest rises in annual atmospheric CO_2 concentration since the beginning of the Mauna Loa record (Betts *et al.,* 2016; IPCC 2011; Page *et al.,* 2002) and contributed to approximately 20% of the annual global land use land cover change emissions (van der Werf *et al.* 2009). Moore *et al.* (2013) estimated that peatland disturbance since 1990 have resulted in an additional 22% C loss through fluvial organic carbon.

Compared to other major peatland areas in the world, peatland destruction in Southeast Asia is not only unprecedented in extent, speed and impact but also complex with various agents and drivers acting in the same area over time (Dommain *et al.,* 2016; Gaveau *et al.,* 2014, 2016; Bryan *et al.,* 2013; Miettinen *et al.,* 2011). Under a business as usual scenario of deforestation and forest degradation, SE Asian forested peatlands may vanish by 2030 (Hoojier *et al.,* 2010), releasing the rest of its 86.5 PgC, the equivalent of approximately 12% of the current amount of atmospheric CO_2 (Page *et al.,* 2011; La Quere *et al.,* 2015). In addition to emissions, land use land cover changes on PSF endanger the highly endemic flora and fauna (Posa *et al.,* 2011; Sodhi *et al.,* 2004), disrupt regional water regulation and global climate (Schrier-Uijl *et al.,* 2013), and harm both human health and regional economy (Dommain *et al.,* 2016; Koplitz *et al.,* 2016;

Varma 2003). As the regional population continue to grow, peatland conversion is unlikely to abate in the near future (Dommain *et al.*, 2016).

While tropical peatland degradation is commonly associated carbon emissions (Hooijer *et al.*, 2010; Miettinen & Liew, 2010), the ecological and other biogeochemical consequences of these disturbances are much less studied (Gandois *et al.*, 2013; Moore *et al.*, 2013). Southeast Asian countries are starting to recognize the need to reduce such emissions, developing restrictions on peatland conversions and restoration/conservation plans. For example, Indonesia enacted a Logging Moratorium from 2011-2015 and has established a Peat Restoration Agency in 2016. This dissertation explores the spatial and temporal patterns of peatland ecology with respect to harvesting and management practices through a combination of ground measurements, optical and microwave remote sensing imagery. Chapters 2, 3, and 4 are presented as self-contained scientific papers. The study sites for the dissertation are a pair of peat domes which are part of the Baram-Belait peat complex in northwestern Borneo.

The Baram-Belait complex is one of the most widely documented peat complexes in northwestern Borneo (Sarawak, Malaysia and Belait, Brunei), it is approximate 4,500 km^2 in size and 4,500 years in age and among the few peat domes that exhibited a full catena of vegetation (Wetlands International 2010, Staub and Esterle 1994, Anderson 1983, 1964, 1961). This complex was formed approximately around 2,200 years before present on mangrove clay in the lower catchment of Sungai Belait. Present day tidal flooding can still reach north of the Damit dome (Caline and Huong 1992). The Baram-

Belait peatland complex, has experience variable management and disturbance regimes and includes intact forests, logged only areas, and logged and drained regions.

In chapter two of this dissertation, I combined direct field sampling and airborne Light Detection And Ranging (LiDAR) data to empirically quantify forest structure and aboveground live biomass (AGB) across the largely intact tropical peat dome at Ulu Mendaram. I quantified how forest structure parameters, including biomass, stem density, stem height, crown area, crown roughness, gap size, and frequency vary on a landscape scale across ~1,662 ha of PSF and 4m of elevational gradient. In chapter three, I developed and implemented a multi-temporal change detection algorithm to detect forest disturbance trends and events in an aseasonal tropical peatlands, and analyzed a time series of 208 Landsat images between 1991 and 2014 for Mendaram and Damit domes. The algorithm explicitly tracked changes in vegetation moisture over time assuming that (i) land cover disturbances were rare phenomena for a relatively large area within a short time period; and (ii) a change must warrant a substantial and detectable drop in vegetation moisture. Quantitative metrics, such as the magnitude, rate and time of forest cover change in each pixel, were derived from the resultant logistic equations. However, if such a trend fitting procedure could not work due to data scarcity, we then assessed whether a pixel was perceived as change from the statistical distribution of its neighbors. Finally, in chapter four, I examined the regrowth dynamics of PSF in terms of ecology and hydrology as a function of harvesting and management practices, output of chapter three, in both the short- and long-term. Specifically, I examined (i) regrowth dynamics

with respect to time since last disturbance (logging and pathogen); (ii) the mesoscale patterns of hydrology with respect to disturbance dynamics and (iii) how the co-dependence between hydrology and forest structure determines the contrasts in structure and environmental conditions between intact and logged forests.

Finally, in chapter five I summarize the main findings of this dissertation in the context of tropical peatlands in a time of global environmental changes and discuss future research direction. This research was supported by collaborative grant NSF 454111, the Evelyn Pruitt Dissertation Fellowship and the Arnold Arboretum Research Fellowship on Tropical Biology.

CHAPTER 2 - CHARACTERIZING FOREST STRUCTURE VARIATIONS ACROSS AN INTACT TROPICAL PEAT DOME USING FIELD SAMPLINGS AND AIRBORNE LIDAR

2.1 Introduction

2.1.1 Tropical forests and global environmental changes

High net primary productivity (NPP) and large carbon pools make tropical ecosystems particularly important within the global carbon cycle (Dixon 1994, Lewis *et al.,* 2009; Malhi *et al.,* 2014). Tropical peat swamp forests (PSFs) are among the most carbon dense ecosystems on the globe. Page *et al.,* (2006) estimated typical aboveground biomass in PSFs to be 100 -150 Mg C ha^{-1}, whereas belowground carbon storage as peat is ~2,772 Mg C ha^{-1} based on estimated peat thickness of 5.5m in Indonesia. Forested peatlands in insular Southeast Asia account for 56% of all PSFs worldwide (Page *et al.,* 2011), but comprise only 5% of the total regional forest cover (Miettinen *et al.,* 2011).

PSFs are undergoing extensive loss due to deforestation and conversion to oil palm plantations (Page *et al.,* 2002, 2011). During 2000-2010, PSF area in Borneo (comprising Brunei, Malaysia's Sarawak and Sabah, and Indonesia's Kalimantan) declined by as much as 2.2% yr^{-1} (Miettinen *et al.,* 2011). Both natural and anthropogenic disturbances within these tropical PSF can result in exceptionally large carbon losses to the atmosphere (Langner *et al.,* 2007; Hirano *et al.,* 2014). In the major 1997-1998 El Niño

event, estimated emissions from fires and logging in Southeast Asian peatlands were equivalent to 13-40% of mean annual global greenhouse emissions from fossil fuel combustion (Page *et al.*, 2002). Recent studies have raised concerns over the long-term, large-scale changes of tropical ecosystems caused by ongoing global environmental changes and the implications of such ecological changes (Lewis *et al.*, 2009; Malhi *et al.*, 2014). The exceptionally high carbon density of PSFs' and their sensitivity to land use land cover changes makes understanding the structure and function of these ecosystems particularly important in the context of global environmental changes.

Despite demographic observations on the dominant species within Borneo's PSFs since the 1960s (Anderson 1961, 1964), relatively little is known about the structure, spatial distribution of biomass, and interdependence between vegetation and peat depth within these forests (Page *et al.*, 1999; Mirmanto 2010). Moreover, previous observations were based on relatively small field plots. Forest structure is directly tied to various types of disturbances, which function on different spatial and temporal scales (Palace *et al.*, 2008) and which drive the biomass turnover rate (Lewis *et al.*, 2013). Forest structure is also closely related to light capture, which drives carbon gain (NPP), and the rate at which trees recruit into the upper canopy layers (Iida *et al.*, 2011). Through its influences on carbon gain and loss (susceptibility to disturbances), forest structure determines aboveground biomass (AGB). PSFs also exhibit interdependence between aboveground vegetation structure and belowground peat (Page *et al.*, 1999). An improved understanding of factors causing within-landscape variation in forest structure can

improve estimates of PSF carbon density and its spatial distribution across the landscape (Clark & Clark 2000*)*.

Large-scale natural disturbance events are thought to provide sufficient light to drive secondary succession and hence influence forest community composition and carbon storage rates (Hubbell *et al.*, 1999; Chambers *et al.*, 2013). Chambers *et al.*, (2013) found that inclusion and adequate sampling of disturbance events of intermediate and large scales is particularly important for assessing the broad-scale tropical forest carbon balance. In contrast, Esparto-Santo *et al.*, (2014) found that frequent, small-scale events account for the majority of AGB losses, however, large/infrequent disturbance events are poorly captured by small, long term monitoring plots (Clark 2004). Differences in gap derivation method (field based or remotely sensed), gap height, and study scale (plot scale or landscape scale) might explain the different gap size distributions and different conclusions for aboveground biomass patterns and forest dynamics (Lobo and Dolling 2014). Further, existing gap definitions from the Neotropics might not apply for Borneo's PSFs, which experience a unique cyclone and wind regime and have different soil structure (Whigham *et al.*, 1999) which may affect rates of gap formation. To date, gap studies in Borneo's PSF were carried out via stereoscope over aerial photos (Bruenig 1968, 1973, 1989) and hence were limited in scope and in their linkages to other spatial characteristics. Light Detection and Ranging (LiDAR) is a powerful tool for studying gap dynamics (Lobo & Dalling 2014) and forest structure at the landscape scale (Clark & Clark 2000) and for scaling ecological results beyond the field plot scale (e.g. Kronseder

et al., 2012). Characterization of vegetation structure, biomass and its spatial distribution for a vast, intact tropical peat dome can help generalize our understanding of PSF's ecology throughout northwestern Borneo. Improved ecological understanding also will inform the conservation priorities for the remaining intact peat swamp forest as well as the ecological consequences of previously disturbed PSF areas.

2.1.2 Development and structure of tropical peat swamp forests

Forested peatlands comprised 12.5% of the coastal lowlands in Northwestern Borneo (Sarawak and Brunei) (Anderson and Muller 1975). Tropical peat domes are characterized by convex topography due to massive peat accumulations that increase from the rivers towards the center of a dome. Profile studies suggested a steep elevational gain in the periphery of the swamp, which levels off to a rise towards the center of less than 1m km^{-1} (Anderson 1983; Page *et al.,* 1999). The water table is typically close to the peat surface due to obstructed soil drainage arising from compacted, undecomposed or semi-decomposed woody material buried within the peat. Water table depth is more variable near the center of the dome (Ashton & Hall 1992).

Anderson and Muller (1975) and Anderson (1983) described, in terms of species composition and dominance, a catenary sequence of forest types occurring from the periphery to the center of tropical peat swamps, with *Shorea albida* predominant across most community types. This sequence is characterized by (i) an almost complete change in species composition from one forest type to the next; (ii) an increase in stem density

and (iii) decreases in average size of a species in terms of height, girth and crown area. These transitions in forest composition and structure have been hypothesized to reflect changes in nutrient availability in the peat and ultimately the dome structure (Anderson 1983). Previous studies have shown that compared to surface peat in the periphery of the swamps, surface peat in the center of the swamps had lower bulk density, lower mineral content and higher C/N ratio (Anderson 1983; Page *et al.,* 1999; Gandois *et al.,* 2013). As long as tree roots can reach the mineral soils underlying the peat and nutrients circulate between living plants and the peat, high biomass *S. albida* dominated forests has been found to grow. As the peat layer thickens and peat surface flattens, restricted drainage reduces root access to mineral soil and makes the soil more anaerobic and infertile (Momose & Shimamura 1992).

2.1.3 Objectives & Hypotheses

In this study, we combined direct field sampling and LiDAR measurements to characterize the structure of an intact tropical peat forest in Sungai Mendaram, Brunei, which is representative of the lowland peatlands in Northwestern Borneo (Anderson 1983). We hypothesized that

(i) From the dome margin to the center, stem height follows a concave pattern with the most stunted forests found on the top of the peat dome. Stem density increases while crown area and crown roughness decrease along successive vegetation communities.

These patterns in forest structure are expected due to decreased nutrient availability and increased water level fluctuations towards the dome center.

(ii) The gap size distribution will follow a power law relationship on a landscape level, with more variation in gap size (very small gaps and very large gaps) in the forest occupying the dome interior.

(iii) Aboveground biomass will decrease towards the dome interior as a function of decreasing tree height and diameter.

To test these hypotheses we examined how forest structure parameters, including biomass, stem density, stem height, crown area, crown roughness, gap size and frequency vary on a landscape scale across ~1,662 hectares of forest within an intact peat dome. Using both field and remotely sensing observations we empirically quantified forest characteristics, estimated aboveground biomass, the spatial variations in each. We interpret the observed patterns and test the PSF-specific hypotheses put forth by Anderson (1961, 1964, 1983) and Ashton and Hall (1992) within a global context of tropical forests and their response to a changing environment.

2.2 Materials and Methods

Ecological study of the Belait peat swamp, located on the Mendaram peat dome in northwestern Borneo, began over 50 years ago (Anderson 1961, 1964, 1983; Bruenig 1964, 1973; Whitmore 1984; Ashton and Hall 1992; Page *et al.*, 1999). In this study, we combined field sampling with spatial analysis of LiDAR data to characterize vegetation

structure across the extent of the peat dome. Field observations of canopy structure and tree biomass were used to calibrate LiDAR observations and to scale from plot to landscape estimates of forest structure and biomass.

2.2.1 Site description

The Mendaram peat dome is located between the Baram River in Malaysia and the

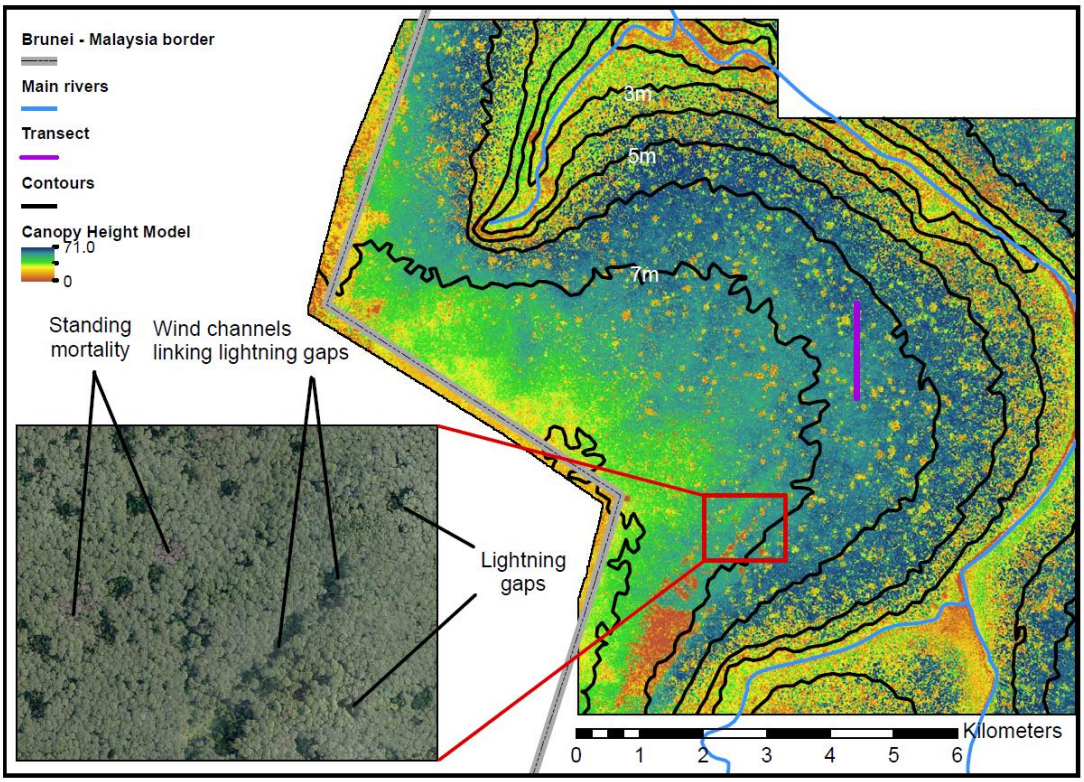

Figure 2.1: The canopy height model in 0.5m resolution for the Mendaram peat dome. The elevational gradient is steep near the river but levels off within 2km inland. Inset figure shows different types of disturbance.

Belait River in Brunei (114.35 E, 4.36 N; Fig.2.1). The full areal extent of the dome is difficult to determine due to deforestation on the Malaysian side, but the intact dome area in Brunei is approximately 4,000 hectares. Aside from deforestation across the border on the Malaysian side of the dome, there is no record of contemporary anthropogenic disturbances in Mendaram. Mean monthly temperature is 27^{o}C (Kumagai *et al.*, 2004), with minimal seasonal variation in precipitation and temperature (Whitmore 1984). Although annual precipitation exceeds 3000mm, with mean monthly precipitation between 100 and 400mm, the forest does occasionally experience dry spells (Bruenig 1969; Kumagai *et al.*, 2004) where total monthly precipitation can drop to 60-100mm (Whitmore 1984). Overall the climate regime is classified as Koppen's type A (perhumid, aseasonal) (Bruenig 1969, Whitmore 1984).

Whitmore (1984) characterized forests in this area as having a 3-tiered stratification: (1) the canopy layer contains the largest trees which commonly emerge as isolated or grouped above a continuous layer; (2) the subcanopy contains trees in the building phase, some of which might mature to be the canopy trees; and (3) the understory contains young, short stature individuals. This structural layering not only reflects stratification by height, but also grouping of species and age classes (Whitmore 1984). For northwestern Borneo, the topmost layer is composed mostly of the Dipterocarpaceae and Leguminosae and can attain heights between 45 and 60m. Burseraceae and Sapotaceae are abundant in the subcanopy layer while the understory contains Euphorbiceae, Rubicaceae and many Annocaceae, Lauraceae and Myristicaceae species.

This forest experienced widespread fungal infection and moth defoliation in the 1950s (Anderson 1961), but no evidence of this infestation could be identified in the 2010 aerial photos. Lightning and wind throw are common causes for crown damage in the taller, uneven canopies of *S. albida* co-dominated marginal forests, while severe wind damage is prevalent where the canopy dominated species (including *S. albida*) turned pole-like towards the dome interior (Bruenig 1964, 1973; Anderson 1964). Lightning damage is also present in the pole-like forest but to a lesser extent due to the smaller and more even crowns. Gaps formed by wind throws can be identified from aerial photos, whereas the standing mortality associated with pathogens appears as leafless, moribund branches. Lightning gaps appear circular and wind throw gaps align themselves along the dominant wind direction (Fig.1 inset).

2.2.2 Field measurements and biomass estimation

A belt transect with an area of 20 m x 1000 m (2 ha) for biometric survey was established in a north-south orientation (Fig.2.1). The central point of this plot was located at 518804.87m latitude and 482619.88m longitude (UTM zone 49N). A 10m grid marked with PVC poles was laid out across the full transect. We surveyed all live and standing dead trees across the transect between April and October 2014. All live stems with a minimum diameter at breast height (DBH, measured at a height of 1.37m, or above the buttress) ≥ 5cm were tagged, measured, mapped (with ~1m), and identified to species. All trees were visually assigned a canopy status based on their canopy position using Whitmore 1984's 3-tiered forest stratification (emergent/canopy; subcanopy; understory)

and any deformation in morphology was noted (Osunkoya *et al.,* 2007). The tall and dense canopy made it difficult to obtain clear measurements of canopy height, so we established a subplot in a forest gap identified from the 2010 aerial photos and still easily locatable during the 2014 field survey. The stem frequency counts, stem location relative to the grid, DBH and height of canopy dominant trees bordering the gap were measured for use as validation data for automated extraction of stem density, tree height calibration, and biomass estimation from LiDAR.

All standing dead trees (snags) greater than 5 cm in diameter and taller than 1m (height) were tagged, measured, and mapped (with ~1m). The base (above the base swell, ~10cm) and DBH were measured (as above) and top diameter was measured or visually estimated if measurement was not possible. The height of the snags was measured using a hypsometer.

The Chave *et al.,* (2005) allometric relationship for moist tropical forests was applied to estimate AGB from the field biometric survey. Other allometries could have been used, but the Chave *et al.,* (2005) equation was developed from an extensive database containing several sites in Southeast Asian Dipterocarp forests and has been widely applied in pan-tropical studies, including several that we compared with. AGB (kg) was estimated using DBH (cm) and wood density (ρ; in g cm^{-3}) such that

$$\mathrm{AGB} = \mathrm{S} * \mathrm{e}^{-1.499+2.148*\ln(\mathrm{DBH})+0.207*(\ln(\mathrm{DBH}))^2-0.0281*(\ln(\mathrm{DBH}))^3} \qquad (2)$$

Wood density of 0.619 g cm^{-3} was used for *S. albida* (Monda *et al.*, 2015) and 0.6 g cm^{-3} was applied for all other species (Osunkoya *et al.*, 2007). To account for the very strong tendency of large *S. albida* individuals to be hollow, we multiplied their estimated dry mass from (2) by 0.577, using the average fraction of dense wood volume for *S. albida* in Sarawak, Malaysia observed in Monda *et al.*, (2015).

The volume of standing dead biomass was estimated as a frustum of a cone (Harmon and Sexton 1996) using a radius R measured at breast height and another, smaller radius r measured at the snag's top height. When this smaller radius was not available, we approximated r as a function of R (Chambers *et al.*, 2000), we then multiplied volume by an average wood density of the current snag's decay class (Rice *et al.*, 2004; Keller *et al.*, 2004) to estimate biomass. When both top radius and snag height were not available, we calculated the wood volume based on Chave *et al.*, (2005), but replaced live wood density based on snag's decay class. Wood density for decay class 2 (Rice *et al.*, 2004) was higher than for live *S. albida* so we adjusted the decay wood density by a factor of 0.6 to account for branch loss.

2.2.3 LiDAR data pre-processing

LiDAR observations covering approximately 4,000 hectares of Sungai Mendaram were acquired in 2010 with an airborne multi-pulse scanning laser altimeter (Optech ALTM Gemini, Optech, Inc., Ontario, Canada). The scan angle was 12^{o} from zenith, giving a total field of view of 24^{o}. The average point spacing is 0.584m, with vertical and

horizontal accuracy of 0.15m and 0.20m, respectively. Returns were classified by the accompanying TerraScan software, with class 2 representing ground returns and classes 1, 3, 4, and 5 corresponding to canopy returns. Class 5 (tall vegetation) accounted for more than 80% of total returns. The accompanying photo imagery was not ortho-rectified and was therefore only used for illustrative purposes.

Ground and vegetation LiDAR returns were separated and interpolated to create a Digital Elevation Model (DEM) and a Digital Terrain Model (DTM), both at 0.5m resolution (Popescu and Wynne 2004, Vaukhonen *et al.,* 2011) – both DEM and DTM were created in ArcMap (version 10.1). The DEM was subtracted from the DTM to produce a Canopy Height Model (CHM). The CHM was subsequently filled for voids and iteratively Gaussian smoothed to reduce anomalies and data drop-offs (negative height or height value more than 2 standard deviations from the median height of neighboring pixels within a 3x3 window) (Popescu *et al.,* 2002, Popescu and Wynne 2004, Vaukhonen *et al.,* 2011). The resulting CHM was a map of LiDAR top-of-canopy height (hereafter referred to as LiDAR height) at 0.5m resolution (Fig.2.1).

We limited our analysis to exclude areas within 750m from the river since the riverine forest is more of an open mixed swamp forest (Bruenig and Huang 1989) and buffered 500m from the Malaysian border to exclude the edge effect from deforestation (Gaveau *et al.,* 2014). Filtering reduced the area of analysis from 3,800 to 1,662 hectares. Many existing theories about PSF structure and community dynamics are based on radial location within the dome. In the absence of peat depth measurements and a precise

location of the dome center, we used dome elevation as proxy for distance from the dome center and for peat depth (with higher elevations being closer to the dome center).

2.2.4 Stem identification

We utilized a local maxima filtering (LMF) with varying window sizes on the canopy height model for stem identification (Popescu *et al.*, 2002; Popescu and Wynne 2004). We assumed that crown width varies as a function of tree height, so as the code 'swept' through the CHM, diameter of the search window varied as a function of the height of the central pixel and was equal to predicted crown diameter. The relationship between canopy height (H) and crown width (W_2) for the Dipterocarp family calculated according to

$$W_2 = 0.42 * H^{0.79} \quad (4)$$

with allometric scaling parameters for species at our site provided by Iida *et al.*, (2011). If the value of the current pixel was not the maximum of all the pixels falling into the search window, no treetop was returned and the code moved on to the next pixel until all pixels were processed. Gaussian smoothing resulted in multiple pixels being flagged as tree top for every tree (Popescu and Wynne 2004). Hence, we used a simple hierarchical clustering procedure to group them into the same tree they correspond to. We compared the use of both square and circular search windows and found that, as expected, circular windows performed better due to their conforming to the shape of a crown in a continuous canopy.

2.2.5 Crown segmentation

We used LMF-identified stem positions as priors for the crown segmentation procedure. In the absence of a standard crown segmentation methodology for closed canopy forests (Feret & Asner 2012), we tested several widely used approaches with the same set of centroids found through LMF process including k-means clustering on 3D cloud points, k-means clustering on CHM, and k-means clustering vs. Gaussian mixture. We then developed an algorithm for a seeded growing region, the results of which compared best to existing aerial photography of the transect. Following Solberg *et al.* (2006) and Vega *et al.* (2014), the final algorithm used the LMF identified tree positions as 'seeds' and ran sequentially from the tallest treetop to the shortest treetop. For each treetop, we first 'grew' the crown to an area predicted from the allometric relationships presented in Iida *et al.*, (2011). We then compared each edge pixel's value with its neighbors in a circular neighborhood to determine whether the crown should be expanded. If the height of an edge pixel was lower than at least half of its neighbors, the crown expansion stopped. We examined the histogram of height for all stems in our transect and found that pixels with height differences >10m from the tree top were either anomalies (e.g. when the LiDAR pulses reaches a branch below the canopy) or did not belong to that crown at all. Hence, if a given pixel was more than 10m lower than a local maximum, the pixel was not included in the segmented crown volume. Additionally, if a pixel was taller than at least half of its neighbors by at least 10m, the segmentation would not continue from that pixel. Finally, all adjacent crowns that either overlapped by at least

25% or that were located within a crown radius from each other in planar distance and within 2m difference in vertical height were merged. Crown shapes from the crown segmentation were compared with aerial photos to provide a qualitative validation while the number of crowns was compared with the number of canopy stems from the field survey.

2.2.6 Crown roughness, crown area, and canopy gaps

A number of crown structural characteristics were calculated from the CHM and segmentation procedures to test hypotheses for how vegetation structure varies across the peat dome. Crown area was calculated from each segmented tree crown as the projected crown area based on the number of 0.5m by 0.5m pixels representing each crown. Canopy roughness for each detected crown was calculated as the standard deviation of heights of all pixels representing that crown following Parker *et al.*, (1995) and Falkowski *et al.*, (2008). The segmentation process described above prescribed that no pixels within one crown could be more than 10m apart vertically from the height of that crown. Thus, crown roughness cannot exceed 10m.

Many different operational definitions for tropical forests gaps exist in the literature. We defined a gap as a vertical hole in the canopy that extends downward from the foliage at the gap edge to a height of 30m or less (or ~ ½ of the height of the emergent trees – Bruenig 1964), with minimum area of 40 m^2, which is similar to gap size threshold in a PSF in Indonesia (Shimamura & Momose 2005). This minimum size threshold roughly

corresponded to mean crown area and is large enough to eliminate instances of partial crown (branch) mortality. The vertical threshold was included to guarantee inclusion of old gaps where trees have grown tall in the middle of the gaps. Partial gaps at the boundary of the LiDAR coverage were excluded from analysis. Using maximum likelihood estimation we fitted a discrete Pareto distribution to the gap counts where gap sizes were binned every $50m^2$ and used bootstrapping to estimate the shape factor (λ) within 95% confidence interval (Lobo and Dalling 2014). Gap coverage across the dome was calculated as the percentage of area per 1 ha that is within a gap and then inferred the distribution of gap coverage using kernel density estimation. This method does not assume any underlying distribution of gaps. As gap count per area and mean gap size changed with respect to size of the survey area unit and where the survey plot was spatially placed, the use of percentage gap coverage instead of gap counts and mean gap size enabled analysis of gap statistics over a large area from remote sensing in the absence of extensive gap survey from ground and in lieu of interpretation under stereoscope and hand digitization (Bruenig 1964, 1973). Further, this method allowed for assessment of the spatial distribution of forest gaps. The probability for a given percentage of gap coverage was the infinitesimal area under the density curve.

2.2.7 Upscaling from the transect to the dome

We used gaps which were present in the field sample transect and present in aerial photos four years prior to the survey as landmarks to aid in spatially registering live tree survey results with spatial data, especially with stem recognition results from LMF. Gap-

edge trees identified in both field survey and LMF were used to position the survey grid with respect to a 10m by 10m grid that covers our DEM and CHM such that (i) the GPS measured central transect point lies on the central line and (ii) the transect completely lies over 200 pixels of this grid.

We compared stem density of canopy trees identified in the field survey with that of canopy trees identified by local maxima filtering by dividing the transect into 20m x 60m subplots and summing the number of canopy trees found by field survey ($S_{tall,\ field}$) and LMF (S_{lmf}) within each subplot. The size of the subplot was chosen to allow for error in estimating stem position in the field and for the cases where the apex of the canopy is not the same with the position of the trunk. We developed a regression between $S_{tall,field}$ and S_{lmf} and apply it on the number of LMF found canopy trees within each 1 ha to estimate the number of canopy trees. In the absence of additional ground survey data across different forest types, we assumed that ratio between density per hectare of the canopy trees (namely *S. albida*) and that of total live trees (including understory trees that the LiDAR could not detect) is the same across the dome as in the *S. albida* consociation (where the transect was located). We multiplied the estimated number of canopy trees in the field with this ratio to give the total number of live stems per hectare across the entire dome.

To upscale field-measured biomass to the entire dome, we sought a relationship between mean LiDAR height (from the CHM) and field-measured biomass. We anticipated a power-law functional relationship between mean LiDAR height and AGB

(Mascaro *et al.*, 2011; Kronseder *et al.*, 2012; Jubanski *et al.*, 2013, Englhart *et al.*, 2013). Using the Levernberg-Marquadt method we fitted such a relationship between mean LiDAR heights at a 20m resolution and the field-measured biomass.

2.2.8 Statistical Analysis

Statistical analysis was conducted using R Statistical Software 3.1.3. Unless specifically noted otherwise, all reported errors in the text and figures reflect 95% confidence intervals. Biomass sampling uncertainties and confidence intervals were calculated by bootstrap analyses (Efron and Tibshirani 1994) due to heteroscedasticity within the data distributions. Bootstrap samples were drawn 1000 times with replacement to estimate 95% confidence intervals around mean. Error estimates do not include allometric or spatial scaling errors. An alpha-value of 0.05 was used to denote significance. For the non-linear fits, a pseudo R^2 was calculated as 1 – residual sum of squares/ sum of squared variances while the root mean squared error (RMSE) was calculated as the squared root of the residual sum of squares divided by the number of samples subtracted by the number of equation parameters.

2.3 Results

2.3.1 Field biometric survey

We surveyed 2064 trees across 2 ha, with 145 snags and 1919 live trees. The understory held 67.8% of total live trees surveyed, with 1282 stems in the smallest DBH classes (5-20cm; Fig.2.2). Understory and sub-canopy trees (5-40cm DBH) comprised

19.0% of the total AGB. Canopy trees (40-130cm DBH) made up only 7.8% of total number of live trees surveyed, but accounted for 81.0% of the total AGB. All of the canopy trees were identified as *S. albida*. We observed *S. albida* density to be 100 stems ha^{-1}, suggesting the transect was located within the *S. albida* consociation (Anderson 1975, 1983).

LiDAR data indicated that the transect passed through several forest gaps and we found stem density within the closed canopy portions and within the gap portions of the forest followed a similar exponential decay with DBH (Fig.2.2A). The smallest size class (5-10cm) accounted for 60% and 40% of the total number of live trees in the forested and gap portions of the transect, respectively. However, gaps had a higher relative fraction of stems within the medium size bins (10-40cm), despite having similar stem density. The ratio between the forested (1.76 ha) and gap areas (0.24 ha) was 7.3, while the ratio between total number of live trees within the forested area (1107 stems) and that within the gap area (812 stems) was only 1.3. Therefore, while the stem density did not differ within DBH classes less than 50cm (stem density and DBH slope of -0.13 ± 0.007 and -0.10 ± 0.012 or the forested and closed canopy portions, respectively), the overall stem density and biomass did differ due to the absence of larger diameter trees (Fig.2.2). There were no trees with DBH larger than 90cm within the gap areas.

Sub-dividing the transect into 0.01 ha subplots, we found that biomass density in both the forested and gap subplots did not follow a normal distribution (Fig.2.2B), with a particularly long tailed distribution within the closed canopy forest. Mean observed field

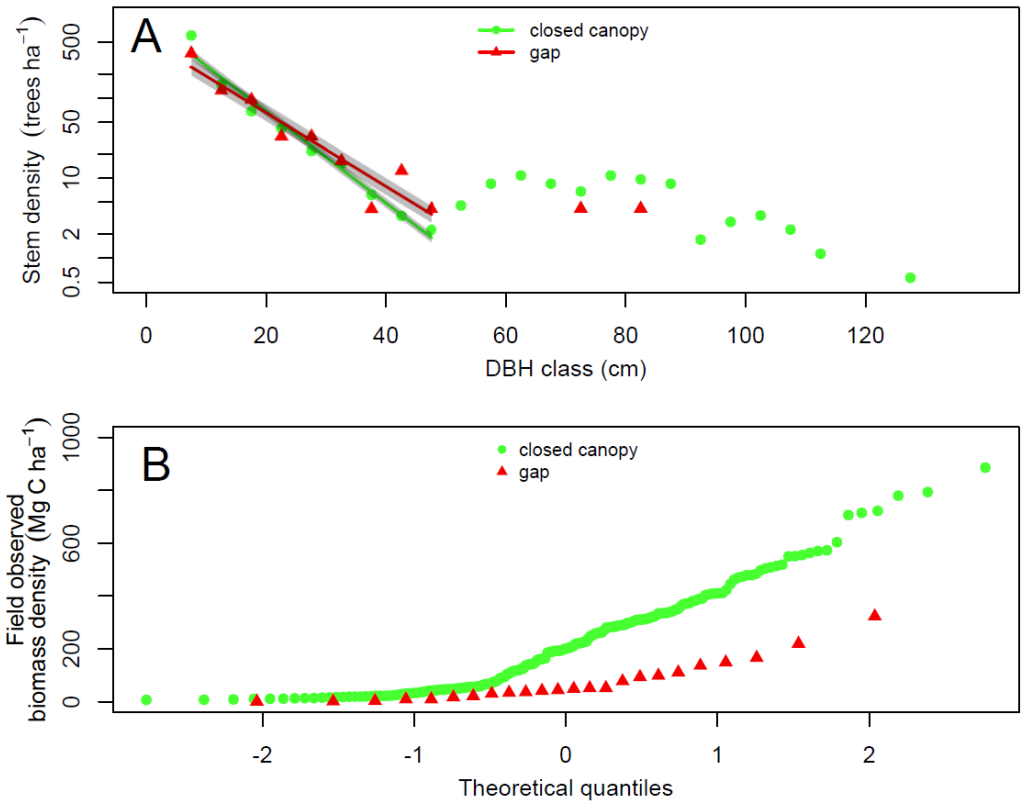

Figure 2.2: Forest structure within the forested and gap portion of the 2 ha field survey transect. A: Total live trees stem density as a log scale function of DBH size class. Shading represents the confidence intervals. B: A comparison between theoretical quantiles, assumed that subplots biomass density follow a normal distribution, and actual distribution of biomass density across 200 10m x 10m subplots.

live biomass density was 217.7 ± 28.3 Mg C ha^{-1} and with an additional 29.8 ± 13.6 Mg C ha^{-1} in standing dead biomass. For the gap portion, live and standing dead biomass was 70.4 ± 27.3 Mg C ha^{-1} and 63.9 ± 49.7 Mg C ha^{-1}, respectively.

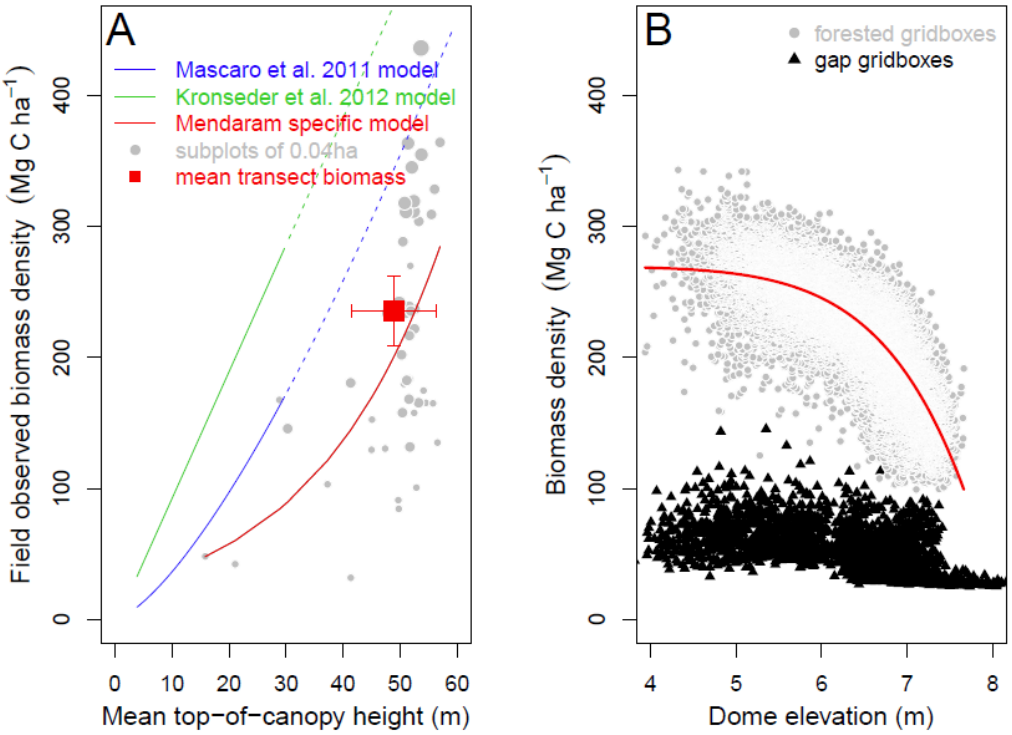

Figure 2.3: A: The relationship between mean LiDAR top-of-canopy height (m) and live biomass density over a 20m x 20m grid. Dashed lines indicate allometric curves that have been extrapolated outside their parameterized range (for illustration purposes only). Grey points with varying sizes indicate the number of *S. albida* trees present in field subplots (ranging between 1 and 7 trees per subplot). B: Live biomass density estimates across the dome as estimated by the locally derived height relationship in (A).

Aggregated to 0.04 ha subplots, a comparison of biomass and height diverged from previous height-biomass relationships reported for SE Asia (Fig.2.3A). The outliers at 40m and 50m heights with very low biomass density were likely the result of new gaps since the 2010 LiDAR observations. However, the variability in canopy height was ~3x less than biomass (stem diameter); the coefficient of variation for mean LiDAR height

and DBH are 0.08 and 0.23, respectively, which is consistent with the low model R^2 of 0.28 and large overall RMSE was 80 Mg C ha^{-1}. This model (Fig.2.3A), when applied across the peat dome, showed a strong decrease in biomass density as a function of dome elevation and tree height (Fig.2.3B). Within closed canopy forest areas, the biomass density followed a parabolic function and decreases towards the center of the dome (Fig.3B). Using the DBH-based allometry from Chave *et al.,* (2005) with adjustment for *S. albida* hollow trees, biomass density estimate for the transect was 239.9 ± 26.3 Mg C ha^{-1}. Using our own Mendaram model mean biomass density for the entire forested (not gap) portion of the dome was 222.4 ± 40.4 Mg C ha^{-1} (Fig.2.3B). The gap areas of the dome had mean biomass density of 52.9 ± 18.4 Mg C ha^{-1}. These differences highlighted both the high biomass density in a PSF and the spatial variation of biomass within this ecosystem.

2.3.2 LiDAR derived stem density and crown characteristics

A direct comparison of the stem counts produced from our local maxima filtering and the field survey found 155 and 150 canopy trees within the transect area, respectively. The LiDAR data was acquired in 2010 and field surveys were conducted in 2014. Tree heights (h_{2014}) were measured from the ground for 12 trees in a 2014 gap. LiDAR height (h_{2010}) was extracted from the same trees based on the local maxima filtering and the CHM. Despite inherent hypsometer error, presence of stems broken by lightning, treetops missed by the LiDAR footprint, and the difficulty of measuring true tree height in

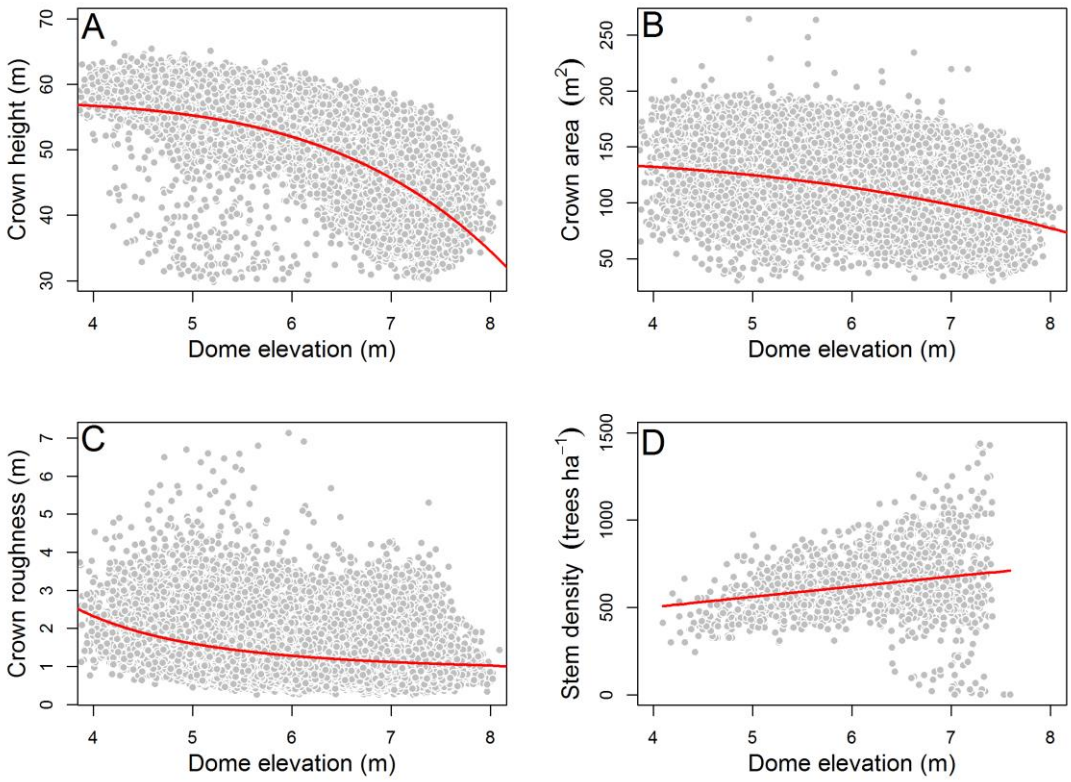

Figure 2.4: (from top down, left to right): A: crown height as function of dome elevation; B: crown area as a function of dome elevation; C: crown roughness as a function of dome elevation; and D: stem density as a function of dome elevation. Each point in panels A-C represents a canopy individual while each point in panel D represents 1 ha.

lowland Dipterocarp forests (Englhart *et al.*, 2013), mean h_{2010} and mean h_{2014} were nearly identical (53.2 ± 3m and 53.1 ± 2.5m, respectively).

Tree height estimated with the CHM ranged from 32m in the dome interior to 60m near the river (Fig.2.4A). Tree heights decreased parabolically over the 4m dome elevation range. The mean crown size was found to vary from 150 to 80m^2, decreasing

linearly with dome elevation (Fig.2.4B). Crown roughness decreased as a parabolic function with dome elevation, indicating that tree crowns become more even in the more interior communities (Fig.2.4C). Finally, we found that stem density increased linearly with dome elevation, with stem density in the dome interior being 3-fold higher than that near the dome margin (Fig.2.4D). There were a few anomalies in stem density that corresponded to very large gaps (e.g. Fig.2.1 inset).

2.3.3 Dome gap and biomass distribution

Gaps covered 7.7% of the peat dome (128 ha out of 1,662 ha). The number of gaps as a function of gap size followed a power law distribution, which has been reported for other tropical forests (Kellner & Asner 2009; Lobo & Dalling 2014). The shape factor λ for our area was 1.76 ± 0.06. The power law relationship persisted with shape factor λ decreasing from 1.76 ± 0.06 to 1.89 ± 0.08 and 2.27 ± 0.08 as the gap height threshold was kept constant at 30m but the gap map resolution increased from 0.5m to 1m and 5m, respectively. Moving from the dome margin towards the interior, the kernel densities of gap coverage (the percentage of a 1 ha area that falls into a gap) persistently followed a Gamma distribution form with decreasing mode (Fig.2.5). Multi-modality appeared where we observed very large gaps (>1ha in area) near the dome interior where dome elevation was at least 6m (Fig.2.5 inset). The biggest gaps had very low biomass density (Fig.2.1 and Fig 2.3B), which contributed to the wide scattering around the mean in the distribution of live biomass density for gaps (Fig.2.3B).

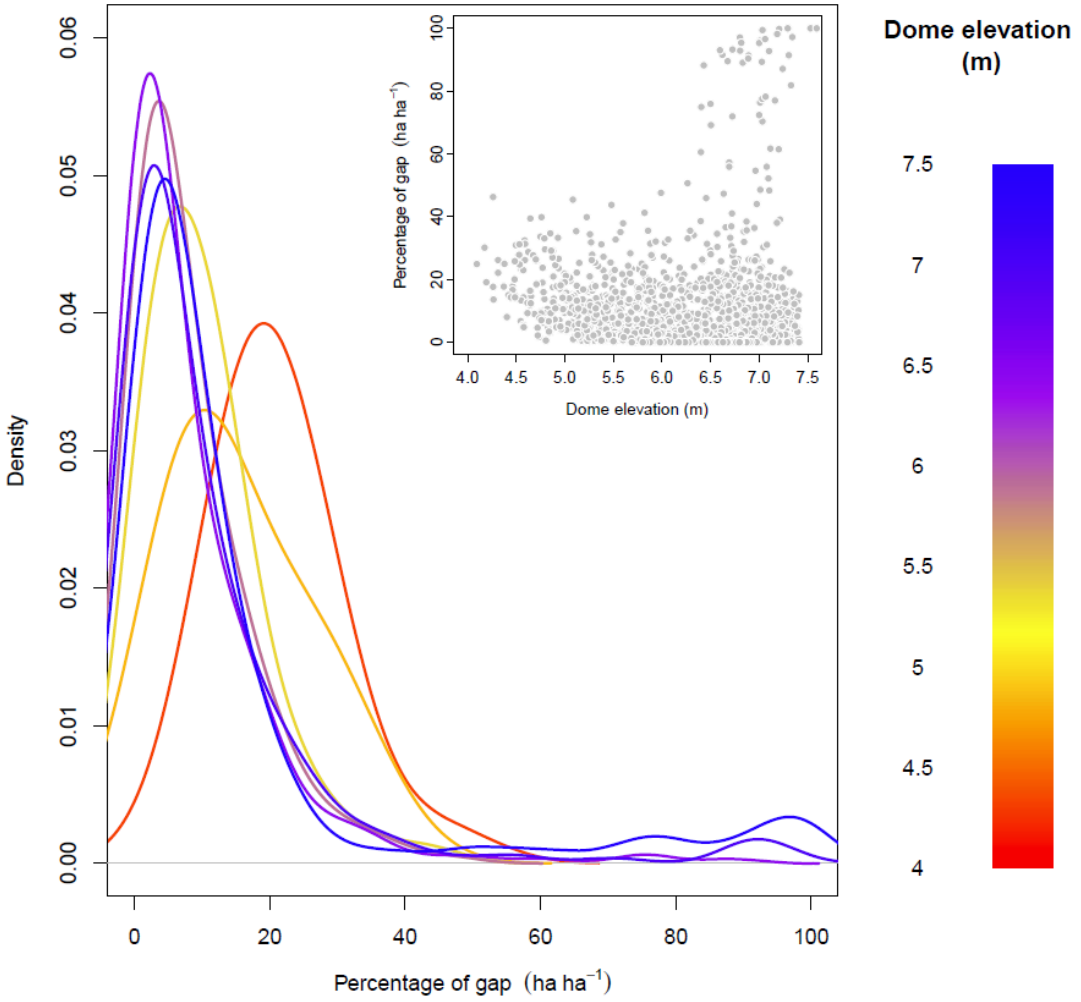

Figure 2.5: Kernel densities for percentage of gap shows the variance in percentage of gap coverage increases towards the dome interior. Density is proportional to the probability of encountering a corresponding percentage of gap coverage. The inset shows the data that were used to generate the distribution curves.

2.4 Discussions

2.4.1 Spatial patterns in forest structure

We observed dramatic differences in canopy height, stem density, and crown roughness across a 1,662 ha tropical peat dome with a gain of 4m in elevation (Fig.2.1). Consistent with the catena characterization by Anderson (1975, 1983) and Whitmore (1984), the forest showed, from the dome margin to the dome interior, an increase in canopy stem density and in density of total live trees but decreases in average size of the canopy individuals in terms of height, crown area and crown roughness. These sequential characteristics have been qualitatively reported from field plots in PSFs elsewhere in Borneo (Page *et al.,* 1999; Mirmanto 2010) and reinforce the hypothesized co-limiting factors of drainage condition and peat fertility on forest structure and productivity (Anderson 1983; Ashton and Hall 1992; Page *et al.*1999, Mirmanto 2010). Less soil aeration and lower nutrient and water availability combine to give rise to shorter interior stands and in particular, shorter stature for the canopy individuals (Anderson 1983). However, on the dome margin where nutrient supply is enhanced by water availability, trees were much taller with larger crown areas (Fig.2.4A, 2.4C). The fact that their density in the peripheral stands was lower than in the interior stands (Fig.2.4D) has been explained by individual mortality resulting from occasional droughts (Ashton & Hall 1992). While these relationships have long been hypothesized, this LiDAR-based study allowed for robust quantification on a landscape level and direct correlation between forest structure and dome elevation as a proxy for drainage condition and peat fertility.

We found that 7.7% of the forested peatland area was in gaps, consistent with the typical gap area fraction for tropical forests (Whitmore 1984). However, mean gap size in

the study area was 0.04 ha, whereas in nearby Sarawak mean gap size was 0.09 ha (Bruenig 1973). The overall gap frequency followed an expected power law distribution. Our shape factor λ ranged between 1.76 and 2.27 across increasing gap map resolutions (0.5m, 1m and 5m), which overlapped with the range of 1.70 – 2.45 found in Panama (Lobo & Dalling 2014) despite a gap height threshold three times higher (30m vs. 10m).

Gap dynamics in PSFs are driven by spatial patterns in gap formation through lightning and wind throw, operating in opposing directions across the dome. Near the margin of a peat dome in Sarawak, where the forest was taller and co-dominated by *S. albida*, lightning that strikes several trees at once (group lightning) prevailed, with mean lightning gap size ranging from 0.19 and 0.33 hectare (Bruenig 1964). Percentage of lightning gap coverage was observed to decrease from between 0.5 and 2.6% in the periphery to as low as 0.1% in the dome interior (Bruenig 1964). At the same time, the gaps created by wind throw tended to be diffuse and quickly filled by expansion of *S. albida* crowns and regeneration under very high sunlight (Anderson 1964; Bruenig 1964). Hence, wind damage was more commonly observed within the less structurally stable interior forest and can be particularly severe (Anderson 1964). Percentage gap coverage in Mendaram's marginal forest had a single mode between 15 and 19.1% (Fig.2.5), enough to cover a group of standing dead *S. albida* crowns (Fig.2.3C). The modal percentage gap coverage then decreased by a factor of 4 between the margin and the interior (Fig.2.5), which was a similar magnitude of difference reported by Bruenig (1973) and Bruenig and Huang (1989). If the several particularly large gaps in the dome

interior (more than 10 hectares) are excluded from the analysis, the distribution of percentage of gap coverage diminished towards the dome interior, with lightning damage dominating the marginal stands and wind damage dominating the interior stands (Bruenig 1973; Bruenig & Huang 1989). On the other hand, the inclusion of these few large gaps doubled the mean gap coverage near the dome periphery from 27.5% to 50% (Fig.2.5) and lowered the biomass density of gap areas (Fig.2.3B). Hence, we find that the very large and less frequent gaps have a disproportionately large effect on forest structure and carbon dynamics.

2.4.2 Comparison with other Neotropical and Paleotropical forests

The observed transect carbon density at 217.7 ± 28.3 Mg C ha^{-1} reflected the current AGB for *S. albida* dominated peat swamp forest. This AGB was higher than van der Meer *et al.*'s (2011) estimation at 198 ± 5.71 Mg C ha^{-1} for the same forest type from Anderson's field samplings in Sarawak, Malaysia and higher than the remote sensing based predicted biomass density for this area (175 Mg C ha^{-1} according to Saatchi *et al.*, 2011 and 155 Mg C ha^{-1} according to Baccini *et al.*, 2012). Given that neither of these remote sensing studies contained direct field observation from northwestern Bornean PSF and were at medium resolutions, our transect based and dome wide estimations of AGB met the IPCC Tier 3 standards in terms of spatial variation for reporting carbon stock values (IPCC 2006) and should help improve future efforts in pan-tropical biomass mapping (Langner *et al.*, 2014).

A compilation of published field biomass observations from Dipterocarp forests in lowland northwestern Borneo, the flora of which distinguished it from the rest of Borneo (Ashton and Hall 1992; Potts *et al.,* 2002; Slik *et al.,* 2003), yielded an area weighted mean carbon density of 269.7 Mg C ha^{-1} (Table 2.1). There are several points to consider when comparing regional ecological and biometric studies. Firstly, although hollow and brittle trunks are common in tropical trees, sampling for such stem characteristics is rare and difficult (Anderson 1983, Monda *et al.,* 2015). Our study accounted for hollow trunks and heart rot, both of which can significantly reduce wood density and hence AGB estimations compared to previous PSF studies. Allometric equations used in AGB estimation vary widely between studies (Table 2.1). The Chave *et al.,* (2005) equation was updated in 2014 (Chave *et al.,* 2014), wherein the DBH-only allometry had an environmental variable (E) added to account for temperature seasonality, climatic water deficit and precipitation seasonality. This revised Chave *et al.,* (2014) allometry yielded a 33% increase in biomass for this site, relative to Chave *et al.,* (2005) equation. Given the aseasonal climate in northwestern Borneo and in order to be conservative, consistent, and comparable with previous works on tropical forests, this paper relied on the Chave *et al.,* (2005) allometry. Secondly, the large values of the Ashton's 1967 plots might be due to the fact that these plots are located on elevations higher than that for PSF. Finally, the high biodiversity in this region is such that the collective term 'mixed Dipterocarp lowland forest' is not always appropriate for ecological interpretations of forest types at local scales (Small *et al.,* 2004). Peat swamp forests are an extremely variable forest type

where within the same co-dominant species *Shorea albida*, tree physiology and wood density varied across different phasic communities (Monda *et al.*, 2015 and personal communication with P.S.Ashton). Our remote sensing-based results highlight the dramatic changes in the physiognomy of canopy individuals in an intact peat swamp forest whereas our transect study exemplifies structure and biomass density from the most carbon dense vegetation community within this PSF. More extensive sampling across forest types, elevational range, and allometric patterns are necessary to provide a more complete picture of stand structure and function in this ecosystem.

Despite a large hollow stem volume (43.2% on average according to Monda *et al.*, 2015) compared to the Neotropics (1.7% hollow according to Clark & Clark 2000), our observed AGB estimates were still higher than the mean AGB across field plots in Amazonia, which ranged between 150 and 163.5 Mg C ha^{-1} (Malhi *et al.*, 2006). The higher AGB on Borneo can be linked to the differences in abundance of large trees (Appendix 3 from Paoli *et al.*, 2008) and the height characteristics between two regions (Paoli *et al.*, 2008; Banin *et al.*, 2014). Northwestern Borneo (Sarawak, Sabah and Brunei) had comparable total stem density with the rest of Borneo, but much higher stem density for larger DBH size classes (> 50cm). The higher densities of large trees on Borneo could reflect a higher productivity due to the warm, aseasonal insular climate (Banin *et al.*, 2014). Alternately, differences in stature could be linked to historical biogeographical factors that favored the predominance of ectomycorrhizal Dipterocarpaceae on Borneo, but led to the family's rarity in the Neotropics (Ashton

1982; Hart *et al.,* 1989; Curran 1994). A third possibility was that a milder disturbance regime on Borneo has enabled biomass accumulation over longer periods, leading to a higher equilibrium biomass. Banin *et al.,* (2014) suggested that the exceptional productivity of Bornean forests may be driven by floristic elements. The current paucity of data prevented further evaluation as to which of these factors (or combination thereof) explained higher aboveground biomass on Borneo (Paoli *et al.*, 2008).

The dominance of the Dipterocarpacae family in Southeast Asia, and of *S. albida* for the PSFs in northwestern Borneo, was clearly an important driver of aboveground live biomass and its spatial variation. In our study, canopy trees held more than 80% the aboveground live biomass, in contrast to ~33% in Panama (Chave *et al.,* 2003) and 60% in West Kalimantan (Paoli *et al.,* 2008). Taken as a whole, this suggested that the same disturbances (deforestation, drainage and burning) in PSFs are likely to produce higher biomass losses with more severe ecological consequences (Bruenig 1977; Paoli *et al.,* 2008) than elsewhere. Investigations into the implications of land use changes in this area should pay particular attention to the impact of these disturbances on the ecology of *S. albida*. Types of disturbance should be evaluated in terms of their ability to alter the forest floor, which in turn will alter the nutrient and water availability to *S. albida* and the subsequent changes in aboveground biomass (Cole *et al.,* 2014).

2.4.3 LiDAR models in tropical forests

The methods and algorithms developed in this study focused on airborne small footprint discrete returns LiDAR in a broadleaf, closed canopy forests, in absence of other supporting remote sensing ancillary data (e.g. high resolution, orthorectified aerial photos and other high resolution satellite data). This data limited scenario is common in remote, wet tropical locations where clear sky satellite data acquisitions are rare. We carried out stem identification and crown segmentation sequentially by identifying tree apices through the detection of local maxima on a CHM interpolated from raw LiDAR returns. The information loss associated with the reduction of the initial 3D point cloud to a single-layer CHM in this forest type was ameliorated by the dominance of the canopy layer, representing 81% of biomass and 80% of the LiDAR returns. We chose a very fine grid size (0.5m by 0.5m) for the CHM to optimize the quality of the CHM, significantly aiding in the identification of the crown apices and hence accurate crown segmentation. The difference between field surveyed canopy stems (150 trees) than those found through LMF (155 trees) might be due to a combination of the following: (i) LiDAR missing the top of the canopy and/or there may be more than one apex per tree; (ii) the LiDAR acquisition and survey were approximately 4 years apart; and (iii) LMF might be over sensitive to the inherent structural complexity of a closed canopy, broadleaved tropical forest (Vaukhonen *et al.*, 2011, Vega *et al.*, 2014). We found a strong correlation between field surveyed stem density and LMF-found tree density with an R^2 of 0.7, comparable to the spatial regression between field-surveyed stems and aerial photo derived crown map on Barro Colorado Island (Garzon-Lopez *et al.*, 2014).

With only canopy tree heights (from LMF), which comprise less than 10% of the total live tree stems but account for more than 80% AGB, we applied a moving region-of-interest approach and developed a model to upscale mean LiDAR height to biomass over the entire peat dome. While the noisy fit between subplot biomass and mean LiDAR height (Fig.2.3A) is a long-standing problem when point-based estimates of biomass are correlated with moving region-of-interest based height statistics, this problem is particularly challenging for peat swamp forests where the R^2 for previous regressions between mean LiDAR top-of-canopy height metrics and field estimated AGB ranged between 0.40 and 0.66 (Kronseder *et al.*, 2012, Englhart *et al.*, 2013). Several factors likely account for the different biomass density values. First, the range of mean LiDAR top-of-canopy height for Mendaram's PSF was between 15 and 60m, twice the range observed in Panama (Mascaro et al., 2011) and Central Kalimantan (Kronseder *et al.*, 2012; Englhart *et al.*, 2013) where the maximum canopy height was only 30m. Mascaro *et al.,* (2011) also observed large scattering in biomass at the high end of the canopy height range. Secondly, although the SE Asia specific equation developed by Saatchi *et al.*, (2011) had an R^2 of 0.73, the height metric was weighted by basal area with the majority of the values concentrated in the range of 20-30m. Saatchi *et al.*'s sample plots did not include any from northwestern Borneo, which was known to be floristically rich and distinct from the rest of the island (Slik *et al.*, 2003). Finally, we scaled the field estimated AGB to account for hollowness, which was rarely accounted for in previous

ecological studies in PSF (Monda *et al.*, 2015). These differences highlight the challenges of applying universal height-AGB models in upscaling AGB for carbon dense PSF.

2.5 Conclusions

Forested peatlands comprised 12.5% of the coastal lowlands in Northwestern Borneo (Anderson and Muller 1975) and account for 5% forest cover in insular Southeast Asia (Miettinen *et al.*, 2011), but contain some of the highest forest carbon densities on the planet. In this study we combined direct field sampling and LiDAR to empirically quantify forest structure and aboveground live biomass across ~1,662 hectares of a large tropical peat dome. Across 4m gain in dome elevation, we observed an increase in stem density but decreases in height, crown area and crown roughness in the canopy. In peat swamp forests, nutrient and hydrological dynamics influenced the forest structure and stature of the dominant species, leading to reduced productivity towards the dome interior. In turn, forest structure and productivity influenced the extent of gaps and selects for the dominant gap formation factor. Rare but extreme disturbance events appeared to have a disproportionately large effect on gap dynamics and the spatial variation of biomass. Lower productivity combined with higher rates of gap-forming disturbances that are also more variable in size give rise to lower AGB towards the dome interior. It is currently unknown how anthropogenic disturbance events will interact with the local environments and the underlying gap dynamics. In this study we demonstrated the utility of LiDAR data in characterizing forest structure and exploring gap dynamics across a large tropical peat dome. LiDAR data, when acquired at high temporal resolution and

over long periods of times, can aid the detection of rare, but spatially extensive events as well as those with high turnover rates.

Ground-based (2 ha sample) and dome-wide estimates of ABG were 217.7 ± 28.4 Mg C ha^{-1} and 222.4 ± 24.4 Mg C ha^{-1}, respectively. The dome-wide estimated AGB was derived from mean top-of-canopy height. AGB and its spatial variability were dominated by the canopy individuals, suggesting that the ongoing disturbances (deforestation, drainage and burning) to a peat swamp forest, which target these canopy individuals, are likely to produce higher biomass losses with more severe ecological consequences than in other tropical regions.

Acknowledgements

We thank the Brunei Forestry Department who were critical in making this project possible through access to data and field sites, as well as assistance in the field. We are grateful for Charley Harvey, Alex Cobb, Kang Min Ngo, Haji Bohari and the field crew in Brunei for their invaluable assistance in data collection. We would like to also thank Conor Gately, Andy Reimann, Jackie Getson-Hardiman, Andrew Trlica, Brittain Briber and Victoria Dearborn for very helpful comments which improved this manuscript. The study is supported by NSF grant number EAR-1114155, Singapore – MIT Alliance for Research and Technology (SMART) and the Evelyn L. Pruitt Dissertation Fellowship from the Society of Women Geographers.

Table 2.1: Carbon density across biometric plots in northwestern Bornean mixed Dipterocarp lowland forests. Results unpublished by Dr. P.S. Ashton and by Poulsen *et al.* (1996) were provided by Slik *et al.* (2010).

Source	Location	Survey year	Plot (ha)	Carbon density Mg C ha^{-1}	Allometry Applied
Ashton unpublished	Brunei	1964	20.0	218.7	DBH-only Chave *et al.*, 2005
Poulsen *et al.*, 1996	Brunei	1992	1	271.9	DBH-only Chave *et al.*, 2005
This study	Brunei	2014	2.0	337.5	DBH-only Chave *et al.*, 2005
This study	Brunei	2014	2.0	217.7	DBH-only Chave *et al.*, 2005 + hollow adjustment after Monda *et al.*, 2015
Lee et al., 2015	Brunei	2014	3.16	316.8	Basuki *et al.*, 2009
Ashton unpublished	Sarawak	1967	2.4	176.2	DBH-only Chave *et al.*, 2005
Ashton unpublished	Sarawak	1967	6.0	309.2	DBH-only Chave *et al.*, 2005
Ashton unpublished	Sarawak	1967	9.0	277.1	DBH-only Chave *et al.*, 2005
Ashton unpublished	Sarawak	1967	9.0	292.4	DBH-only Chave *et al.*, 2005
Ashton unpublished	Sarawak	1967	18.0	270.6	DBH-only Chave *et al.*, 2005
Ashton unpublished	Sarawak	1967	6.0	365.5	DBH-only Chave *et al.*, 2005

Ashton unpublished	Sarawak	1967	3.0	389.3	DBH-only Chave *et al.*, 2005
Ashton unpublished	Sarawak	1967	3.0	278.4	DBH-only Chave *et al.*, 2005
Ashton unpublished	Sarawak	1967	3.0	292	DBH-only Chave *et al.*, 2005
Ashton unpublished	Sarawak	1967	1.2	225.2	DBH-only Chave *et al.*, 2005
Ashton unpublished	Sarawak	1967	0.6	302.2	DBH-only Chave *et al.*, 2005
Ashton unpublished	Sarawak	1967	0.6	292.7	DBH-only Chave *et al.*, 2005
Proctor *et al.*, 1983	Sarawak	1983	0.95	325.0	Dawkins' regression
Kho *et al.*, 2013	Sarawak	1992	1	234.8	DBH and height Chave *et al.*, 2005
Kho *et al.*, 2013	Sarawak	1992	1	259.2	DBH and height Chave *et al.*, 2005
Kho *et al.*, 2013	Sarawak	1997	1	207.2	DBH and height Chave *et al.*, 2005
Kho *et al.*, 2013	Sarawak	1997	1	270.2	DBH and height Chave *et al.*, 2005
Kho *et al.*, 2013	Sarawak	2003	1	216.0	DBH and height Chave *et al.*, 2005
Kho et al., 2013	Sarawak	2003	1	250.2	DBH and height Chave *et al.*, 2005
Kho et al., 2013	Sarawak	2008	1	227.4	DBH and height Chave *et al.*, 2005
Kho *et al.*, 2013	Sarawak	2008	1	263.4	DBH and height Chave *et al.*, 2005
Field survey area weighted mean				269.7	

CHAPTER 3 – LAND USE DYNAMICS IN NORTHWEATERN BORNEO PEATLANDS DURING 1991-2015.

3.1 Introduction

CO_2 emissions from land use land cover change (LULCC) accounted for 12.5% of the total annual anthropogenic emissions during 2000 – 2009 (Houghton *et al.*, 2012) and as much as 25% of 2015 total annual anthropogenic emissions (Le Quere *et al.*, 2015). LULCC fluxes are dominated by tropical deforestation with many uncertainties concerning (i) the true extent and rate of deforestation; (ii) biomass and soil carbon content of different forest types; (iii) the spatial distribution of these forest types (Achard *et al.* 2008) and; (iv) the inclusion of different feedbacks and management types (Houghton *et al.* 2012). Uncertainties in LULCC CO_2 emissions are up to 50% of the actual estimates (Houghton *et al.* 2012). An improved understanding of the temporal and spatial patterns of tropical deforestation and forest degradation will help reduce LULCC uncertainties in estimates of emissions and better constrain the terrestrial C budget.

Borneo, a key global biodiversity hot spot, has experienced substantial forest loss driven largely by shifting agriculture and demand for timbers (Bryan *et al.*, 2013; Gaveau *et al.*, 2014). During the 2000s, lowland mixed Dipterocarp forests in Southeast (SE) Asia, especially peat swamp forests (PSF), disappeared at twice the annual rate of other regional lowland evergreen forests (Miettinen *et al.*, 2011a). PSF is a forest type that

develops on water logged, nutrient poor peat soil but supports a high degree of endemism in flora and fauna, and stores large amounts of carbon both above and belowground (Page *et al.* 2011, Nguyen *et al.* 2016). Accounting for less than 6% of global peatland area, but about 14% of global peat carbon, these PSF ecosystems become a large C source when disturbed. The major El Nino events of 1997/1998 and 2015/2016 see fire emissions from peatlands accounted for between 13% and 40% annual anthropogenic CO_2 emissions (Page *et al.,* 2002, van der Werf 2015). Under a business as usual scenario, these forests may vanish by 2030 with profound consequences to the emissions budget, ecosystem services, biodiversity and the global climate *(Hoojier et al., 2010, Miettinen et al., 2011a).*

The environmental and societal impacts of peatland conversion underlie the importance of having continuous and accurate updates on the precise rate of conversion and the trends it shows. Previous efforts to map forest cover and forest activities have revealed the complex history of forestry practice in Borneo (Bryan *et al.,* 2013; Gaveau *et al.,* 2014) and highlighted it as a global deforestation hotspot (Miettinen *et al.,* 2011b; Hansen *et al.,* 2013). Most of the historical deforestation took place as early as the 1970s in the coastal lowlands (< 500m above sea level), where peat swamp forests grow extensively. An initial period of booming exploitation occurred between the 1970s and the 1990s, followed by a slower expansion into the remaining, more marginal forests in the 2000s and recently a steady move inland and upland (Bryan *et al.* 2013; Gaveau *et al.* 2014). As a result, between 1972 and 2010, the forested area in Borneo dropped by 30%,

with the largest losses in Malaysian Sabah and Indonesian Kalimantan. By 2010, only 22% of land surface in Sarawak and Sabah remained as intact forests, compared to 54% in Brunei.

Approaches to map land use land cover change can be methodologically categorical or continuous (Bontemps *et al*., 2012). The categorical approaches include post-classification comparison techniques and algorithms based on mathematical combinations of snap shots in time (e.g. 1990, 2000, and 2010) such as image differencing, image regression, change vector analysis, principal component analysis, and spectral mixture analysis. Classification-based techniques typically compare single-date classifications ('wall to wall') to identify diverging areas, and thus their efficiency depends on prior classification accuracy (Cardille and Foley 2003). An alternative approach to using categories considers change as a continuous variable, whereby change was detected through measurement of the degree or probability of change in the concentration, percentage, etc. of a variable (e.g. the forest cover) through time (Rogan and Chen 2004).

For the Borneo region, several recent attempts have been carried out to map and assess rates of land cover change. Bryan *et al.* (2013) used the Carnegie Landsat Analysis System (CLASlite) and assumed a 350m distance from roads as proxy for degradation level to develop a map of Borneo Land Use Land Cover Change for '2009' based on a mosaic of images from 2007-2009. A particular pixel was deemed to be forest or non-forest based on whether its end members exceeded prescribed thresholds. Gaveau *et al.* (2014) used ALOS PALSAR, Landsat, a 700m maximum buffer from main logging

roads and a MODIS based tree cover map in a supervised classification scheme to map deforestation on the island between 1973 and 2010. Both Miettinen *et al.* (2011b) and Langner *et al.* (2007) ran unsupervised classification of individual MODIS scenes and compared pairs of images across the period of analysis to map changes. Post classification comparison subjects the change maps to accuracy of single date LULCC maps. On a global level, errors in mapping where forests were and where deforestation took place can often be bigger than the expected land change rates (Bontemps *et al.*, 2012).

The major constraint of the wall-to-wall, continuous approach to land cover change detection has been data availability, especially in tropical areas where cloud-free periods can be rare. The challenges of cloud cover necessitate the practices of mosaicking and compositing, thereby preventing a precise date to be determined (Langner *et al.,* 2007). A sampling based approach (e.g. Stibig *et al.,* 2014) could circumvent data scarcity but did not ensure the inclusion of all the deforestation hot spots in the sampling, which could result in the omission of significant changes (Bontemps *et al.,* 2012). Another way to ensure spatial coverage and maximize the number of cloud free observations uses medium spatial resolution (250–1000 m) time series from the satellite Pour l'Observation de la Terre (SPOT; e.g. Bontemps *et al.,* 2012) and the Moderate Resolution Imaging Spectroradiometer (MODIS; e.g. Langner *et al.,* 2007, Miettinen *et al.,* 2011b) with daily coverage. However, the gain in temporal coverage is balanced, by the restricted range of spatial details that can be detected.

Using a continuous approach, Hansen *et al.* (2013) mapped global gross forest loss from all Landsat imagery between 2000 and 2012 using decision trees. The decision trees classified Landsat pixels by first defining classes based on relations between Landsat metrics and training data (e.g. Quick bird tree crowns, MODIS tree cover and previous Landsat based forest cover maps) and then predicting the class membership of the remaining pixels. Class membership of observations can be assessed by comparing the observed statistical distribution with the expected statistical distribution using such metric distance as the Mahalanobis distance. Bontemps *et al.* (2012) segmented SPOT images of Borneo into units ('objects') of homogeneous spectral reflectances across space and time and then computed Mahalanobis distance to assess the departure from the unchanged reference of each object. By setting a threshold on this distance metric, a set of 'changed object' can be identified.

Previous studies using discrete and continuous approaches have been informative for estimating total area of forest (or deforestation) within a certain epoch or regions, but for areas with very high cloud cover and extensive ongoing deforestation, additional detail is critically needed. In Borneo, we still do not know exactly where intact, logged and degraded forests were on the ground for any given year, especially in the early 1990s, an epoch that has been largely neglected by remote sensing studies with particularly high uncertainties in regional LULCC (Kim *et al.,* 2015). The condition of the post logging (non)forests or the drivers behind the disturbance-regrowth dynamics are also regionally uncertain (Bryan *et al.,* 2013; deVries *et al.,* 2015). Such knowledge on forest health,

degradation levels and regrowth dynamics is essential for the conservation of an ecosystem undergoing massive and rapid changes such as peat swamp forests.

Recent efforts in LULCC mapping have shifted away from the conventional wall-to-wall approaches and towards exploring the temporal evolution of land use/ cover as a continuous variable (DeVries *et al.,* 2015; Dutriex *et al.,* 2015; Zhu and Woodcock 2014; Kennedy *et al.,* 2010). Through the opening of the Landsat archive, it is now possible to detect even subtle land cover changes, such as forest degradation, if they have a distinct temporal spectral signature that can be reliably identified (DeVries *et al.,* 2015; Ahmed *et al.,* 2014; Song *et al.,* 2014; Zhu and Woodcock 2014; Broich *et al.,* 2011; Kennedy *et al.,* 2007, 2010). A focus on the temporal structure of the data is advantageous for monitoring near real time disturbance and post disturbance regrowth dynamics (Kennedy *et al.,* 2010, DeVries *et al.,* 2015). Kennedy *et al.* (2010) grouped these multi-temporal change detection algorithms by whether they seek trends or seek deviations. Deviation seeking algorithms capture persistent land cover changes that move the spectral signal away from a presumed stable condition, whereas trend seeking algorithms rely on time series fitting techniques to separate long lasting changes from year-to-year noise. Since human and natural disturbance and successional changes can be either abrupt or gradual, it is important that algorithms be flexible enough to capture both types of changes.

In this chapter, we described a proof-of-concept needed for how a multi-temporal change detection algorithm can be applied to detect forest disturbance trends and events in a tropical peat dome, including strategies to address the challenges of cloud cover and

data gaps. The methods were built from the Continuous change detection and classification (CCDC) algorithm (Zhu and Woodcock 2014) and the Landsat-based detection of Trends in Disturbance and Recovery (LandTrendr) algorithm (Kennedy *et al.,* 2007, 2010; Ahmed *et al.,* 2014). Our method detected *both* durable changes, which required the temporal smoothing of spectral noise in long-duration signals in trend seeking approaches, *and* abrupt events, which called for the unsmoothed capture of spectral change in deviation seeking strategies. The detection scheme directly worked on the entire time series, without calibration with external higher resolution data (e.g. Hansen *et al.,* 2013), in order to produce precise timing of disturbances and extract other information on the post disturbance recovery dynamics (Dutrieux *et al.,* 2015). The strategy described here can be readily integrated into existing forest monitoring systems and extended to apply to more seasonal types of tropical forests, as well as other types of land use activities (e.g. agricultural expansion and fire).

3.2 Methods

3.2.1 Study area

Forested peatlands comprised 12.5% of the coastal lowlands in Northwestern Borneo (Sarawak and Brunei) (Anderson and Muller 1975). Tropical peat domes were characterized by convex topography with peat thickness of at least 3m above sea level near the rivers and increasing towards the center of a dome. The water table was typically

close to the peat surface due to obstructed soil drainage arising from compacted,

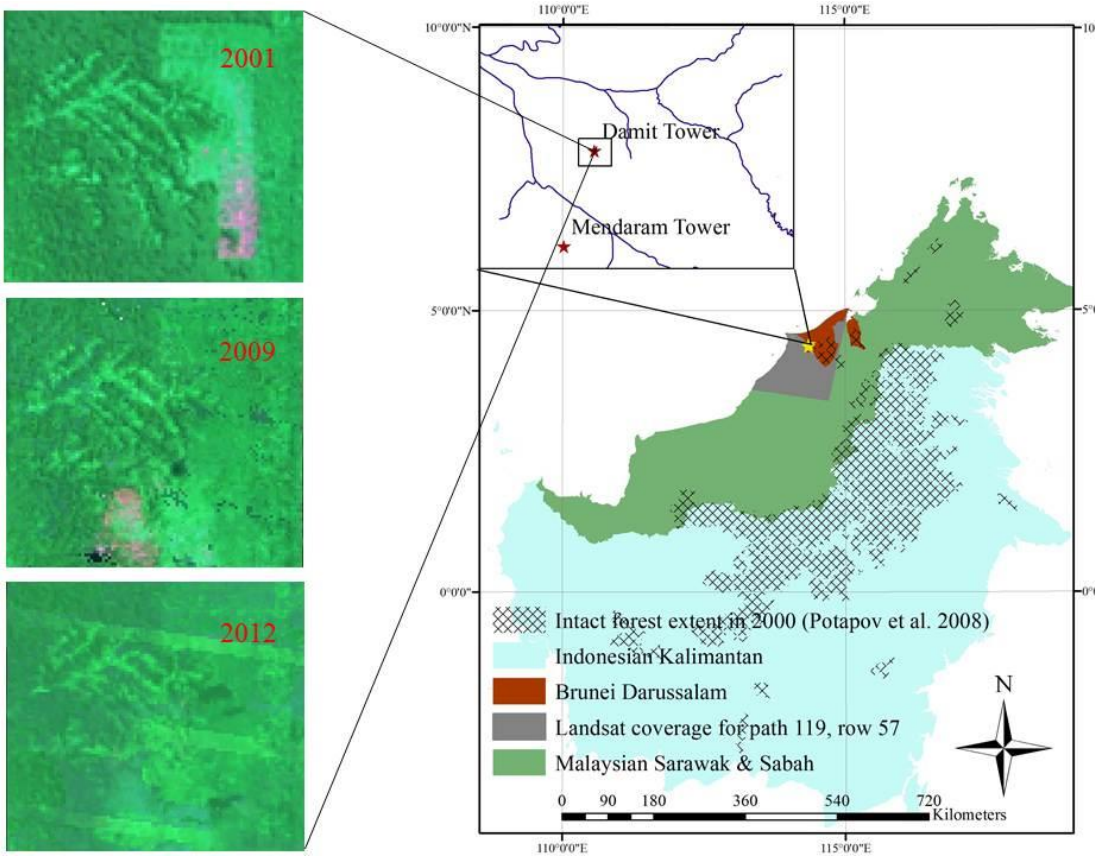

Figure 3.1: Geographical information about the Damit dome. Three Landsat snapshots (2001, 2009 and 2012) illustrated the spatial extent of logging and the quick recovery of the forest.

undecomposed or semi-decomposed woody material buried within the peat. The system is ombrotrophic with most nutrients coming from precipitation. The aboveground live biomass typically exceeds 200 Mg C hectare^{-1} with approximately 10 times additional biomass stored belowground (Nguyen *et al.*, 2016; Page *et al.*, 2011).

By 2010, Brunei has maintained more than 80% of its forest cover (Bryan *et al.*, 2013), with the Belait peat swamp being the largest contiguous peat swamp complex in

the whole of Borneo (Government of Brunei Darussalam 2009). The high forest cover is due to the country's concentration on the petroleum and shale gas extraction and the 1990s policy to reduce the national production of timber by half to 100,000 m^3 $year^{-1}$ since 1990 (Siddique 1992). Our study region is a peat dome at (Sungei) Damit (4° 27'N, 114° 21'E) (Figure 3.1). At 4,400 hectares, Damit accounts for 5% the area of the Belait peat swamp and was systematically logged between 1972 and 2010 (Government of Brunei Darussalam 2009). In contrast, the nearby Ulu Mendaram peat dome has remained intact until today (Nguyen *et al.*, 2016).

3.2.2. Overall processing flow

This LULCCC analysis approach used individual pixel-level reflectances and vegetation indices for change detection. For each pixel, a time series of vegetation index values was built, screened for clouds and noise and assessed to determine whether there was a shift in its temporal trend or a change in the pixel's value with respect to the scene-wide statistical distribution during the analysis period (1991 – 2015; Fig.3.2). Our algorithm explicitly tracked changes in vegetation moisture over time assuming that (i) land cover disturbances were rare phenomena for a relatively large area within a short time period; and (ii) a change must warrant a substantial and detectable drop in vegetation moisture (Song et al., 2014). Outliers due to clouds and haze and candidates for changes were identified from the majority of unchanged pixels in two separate steps: first the cloud, cloud shadow and haze (section 3.2.3.3), and second, the true changes (section 3.2.4.4). Then for each pixel, the algorithm tracked continuous changes in

vegetation moisture over time by fitting one or more nonlinear curves to the cloud free time series of proxy values for vegetation moisture. Our goal was to capture the sigmoid or "S" shape of forest cover change using logistic functions which best described the actual physical process of land cover change on the ground (Viedema *et al.*, 1997,

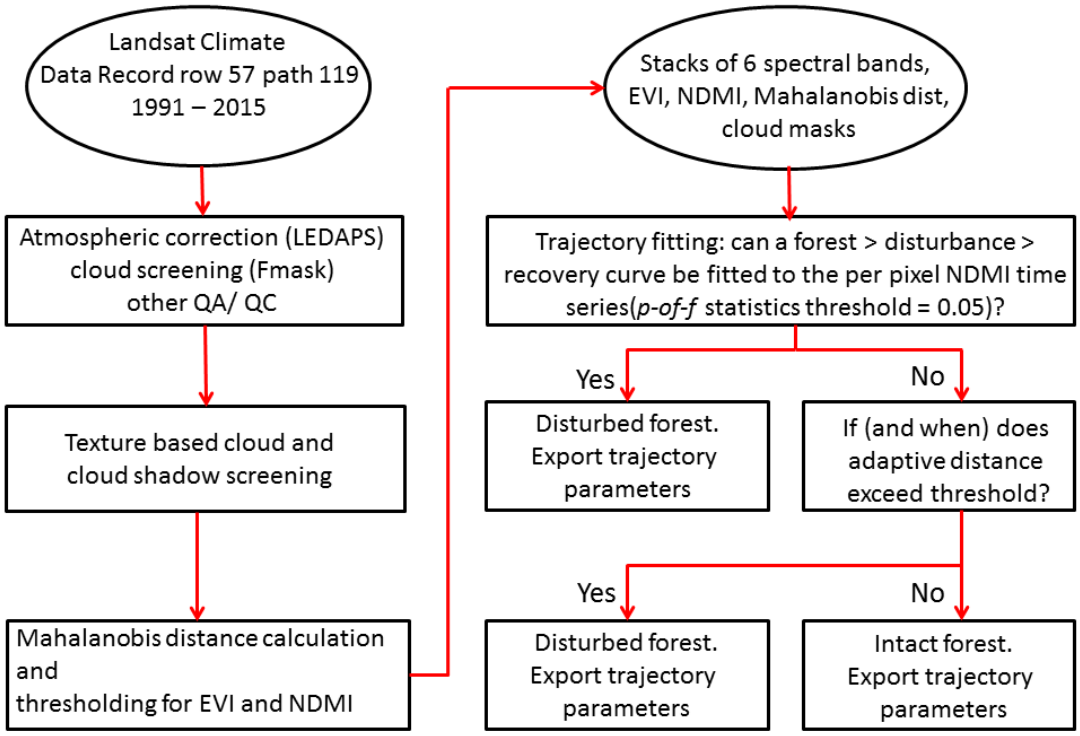

Figure 3.2: Processing steps

Kennedy *et al.*, 2010, Ahmed *et al.*, 2014). Quantitative metrics, such as the magnitude, rate and time of forest cover change in each pixel, were then derived from the parameters of the resultant logistic equations. However, if such a trend fitting procedure could not work due to data scarcity, we then assessed whether a pixel was perceived as change

from the statistical distribution of its neighbors, informed earlier in the process (section 3.2.4.4). If and when that occurred, a disturbance event was again recognized, but this time without other disturbance metrics. Disturbance events picked up by the adaptive outlier detection were tested against LiDAR derived canopy heights. The final map was validated with IKONOS high resolution imagery.

3.2.3 Preprocessing

From the Landsat Surface Reflectance Climate Record Data (CDR) we obtained 208 Landsat Thematic Mapper (TM) 5 and Enhanced Thematic Mapper (ETM) 7 for row 119 and path 57 that covered Damit and were acquired between 1991 and 2014. The imagery was atmospherically corrected and cloud screened using the standard Landsat Ecosystem Disturbance Adaptive Processing System (LEDAPS**,** NASA CDR Product Guide) and Fmask (Zhu and Woodcock 2012) algorithms, respectively. We also downloaded several vegetation indices including the Enhanced Vegetation Index (EVI), Normalized Burnt Index (NBR), and Normalized Difference Moisture Index (NDMI).

3.2.3.1 Vegetation indices

The choice of spectral band or index used in the disturbance-regrowth analysis was an important determinant of the method's sensitivity to forest change dynamics. We excluded the Normalized Difference Vegetation Index (NDVI) from our consideration since it was shown to perform poorly as a measure of forest cover and structure (Freitas, Mello, & Cruz, 2005), and tended to saturate over dense forest (Gamon *et al.*, 1995;

Huete *et al.*, 2002). EVI was known to be more sensitive to succession, phenology, photosynthetic activity and productivity (Glenn *et al.*, 2008), while NDMI was associated with canopy water content (Jin and Sader 2005) and hence was referred in the rest of the chapter as vegetation moisture. The sensitivities of EVI and NDMI to fluctuations in greenness and moisture, respectively, caused by logging made them suitable candidates for trend seeking algorithms to monitor forest changes (Kennedy *et al.*, 2010, Ahmed *et al.*, 2014). In addition, works by Dr. Sulla-Menashe (personal communications) showed that there was no bias in NDMI between Landsat 5 and 7, thereby eliminating the need for spectral normalization prior to the trend and deviation seeking steps.

3.2.3.2 Adaptive outlier detection

An adaptive outlier detection approach was applied for both cloud screening and land cover change identification. This method originated with the recognition that to detect outliers in a multivariate case, both the distance of an observation to the centroid of the data and the shape of the data should be considered. The shape and size of multivariate data can be quantified by the covariance matrix and a distance metric known as the Mahalanobis distance, which represents the distance from a data point to a statistical distribution and hence indicates class membership of that data point. Assuming that errors in repeated measurements of a variable of land use/ cover were independent and identically followed a normal distribution, then measurements of stable locations over time also followed a normal distribution while those of disturbed locations were outliers of that distribution. Therefore, the squared Mahalanobis distances of the pixels can be

expected to approximate a chi square distribution (Filzmoser *et al.*, 2005). Compared to a standard chi square distribution, the observed data, including outliers, had a fatter tail and was skewed to the right. For outlier detection we implemented a deviation seeking procedure that adapts to sample size (Filzmoser *et al.* 2005). For every cloud free scene within the 208 images, we computed the theoretical chi square distribution of the Mahalanobis distances of all pixels given a covariance matrix of values of a chosen variable (e.g. spectral value or index) taking into account the size of the population. Next, we simulated the empirical distribution of the data by selecting half the population, computing the sample covariance matrix and the new Mahalanobis distance with respect to the sample covariance matrix, repeating for 1000 times. A critical value was computed as a function of the size and dimension of the data, which set the upper limit to the difference between the empirical distribution and the theoretical distribution for data of the same dimension and numbers of variables. Using the theoretical distribution and the critical value, we then back calculated the threshold on Mahalanobis distance, beyond which we compared the tails of two distributions. Any pixel whose Mahalanobis distance exceeded the scene-wide theoretical chi-square distribution by more than the critical value was marked as 'changed'.

3.2.3.3 Cloud, cloud shadow and haze screening

Landsat imagery available upon request from the United States Geological Survey included the standard Fmask for initial land/water segmentation and cloud screening. Additional cloud screening was carried out to remove missed clouds, cloud shadows and

haze in the images that Fmask did not pick up and to avoid false positives in the final change detection. Given the extensive regional cloud cover, we developed a single scene texture based cloud screening procedure using the grey scale co-occurrence matrix (GLCM) textures. On every scene within the 208 images, variance of variance for band 2, 4 and 5, ratio between band 1 and band 7 (Goodwin *et al.* 2013) and the Tasseled Cap Haze index (Richter 1995) were calculated on a window of 3 by 3 pixels and in 4 directions to identify cloud, cloud shadows (Ouma and Tateishi 2006) via the adaptive oulier detection described in section 3.2.3.2.

3.2.3.4 LiDAR processing

Light Detection and Ranging (LiDAR) observations covering approximately 3,600 hectares of Sungai Damit were acquired in 2010 with an airborne multi-pulse scanning laser altimeter (Optech ALTM Gemini, Optech, Inc., Ontario, Canada). The scan angle was 12^{o} from zenith, giving a total field of view of 24^{o}. The average point spacing was 0.584m, with vertical and horizontal accuracy of 0.15m and 0.20m, respectively. Returns were classified by the accompanying TerraScan software, with class 2 representing ground returns and classes 1, 3, 4, and 5 corresponding to canopy returns. Class 5 (tall vegetation) accounted for more than 80% of total returns. The accompanying photo imagery was not ortho-rectified and was therefore only used for illustrative purposes. From the raw point clouds, Canopy Height Model (CHM) for Damit at 0.5m resolution was produced following the procedure described in Nguyen *et al.* (2016).

Due to challenges associated with the signal of vegetation moisture from open mixed swamp forests, we limited our analysis to forests dominated by *Shorea albida*, which were most affected by human activities. As there was no clear boundary to mark the transition from riverine, open mixed swamp forest to other phasic forest communities (Anderson 1983, Bruenig and Huang 1989), we limited the analysis area using information of peat depth and drainage. Therefore the analysis area was produced in ArcGIS using a minimum elevation of 3m and a maximum slope of 0.10 as proxy for poor drainage. Since three meters was the reported peat depth that was beyond tidal influence and that was most like subjected to human disturbances (Esterle and Ferm 1994; Hoojer 2004; Wosten *et al.*, 2008), we assumed that a minimum elevation of 3m could help delineate the area of at least 3m peat depth. The final analysis area was 1,980 hectares. Subsequent extraction of forest structures (gap fraction, canopy stem density, canopy stem position and height) followed the methodology set out in Nguyen *et al.* (2016). We derived a fractional canopy cover map using our CHM and a forest definition from Food and Agricultural Organization (FAO 2012).

3.2.4. Trajectory formulation and selection

3.2.4.1 Parameterizing trajectories

Within a QGIS framework implemented by C. Holden, we inspected the landscape and derived three land use land cover trajectories as priors for the subsequent temporal fitting algorithm: intact forest, clear cut with regrowth prior to the start of the time series

(1991), and logging after 1991 followed by regrowth. After identifying three candidate trajectories, we developed appropriate analytical functions to describe them. The functional forms of these trajectories were adapted from Viedma *et al.* (1997), Kennedy *et al.* (2010) and Ahmed *et al.* (2014). Intact forest and forest disturbed prior to 1999 shared the same single, flat line functional form due to cloud and large gap in data acquisition for the tropics during the 1990s. We relied on the predictive power of the adaptive outlier detection (section 3.2.3.2) for classification of intact vs pre-1999 disturbances. For forest disturbed after 1999 with revegetation, the NDMI shows a pre-disturbance, linear state similar to intact forest, a sharp dip representing the disturbance event followed by a logistic growth for recovery. The functional form for this disturbance type had three shape parameters to represent (i) NDMI value immediately after disturbance; (ii) the stabilizing NDMI that revegetation reached and (iii) the rate at which NDMI changed from immediately post disturbance to stability.

3.2.4.2 Identifying breakpoints

The problem of detecting forest changes in our case was a problem of segmenting a time series of vegetation characteristics. The goal was to partition the input time series into segments that represent homogenous vegetation condition e.g. intact, logging and post-logging. By this definition, each segment represented a state of vegetation condition and the time points between one segment to the next a state change of vegetation conditions. In other words, segmentation of time series involved identifying the time points at which the statistical behavior of a pixel changed in a time series. As such, it was

essential that segmentation takes place after removal of noise from cloud, cloud shadow and haze and additional smoothing.

Our segmentation strategy was a top down technique that considered every possible partition and split the time series at the best locations. We started by identifying the observation with the largest drop in the NDMI time series. Observations between this point and the end of the time series constituted a post disturbance state, while those between it and the beginning of the time series represented the pre-disturbance state and/or a during-disturbance state. If a break point existed, two linear segments were fit for the pre-disturbance and during-disturbance phases, respectively. Otherwise, only one linear segment would be fit. In order to decide on such a break point, we followed the Kendall-Theil Robust Line method, otherwise known as the Theil-Sen line (Fernendes & Leblanc 2005), and assessed the pair-wise slopes of each segment between the minimum NDMI and each of its preceding observation. The maximum of these slopes would belong to the segment formed between the minimum NDMI value and the break point that separated the pre-disturbance phase from the disturbance event and post disturbance phase. To identify the break point, we incorporated an existing script that implemented the Kendall-Theil Robust Line method written by Daniel Rothenberg (https://code.google.com/p/ccfhomogenization/source/browse/code/mw2009/chgptmodels.py)

3.2.4.3 Fitting trajectories (or trend seeking)

For each per pixel time series we created initial estimates of shape parameters for the three forest change models (intact, clear cut and regrowth before 2001, logging after 2001 and regrowth). We fit the pre-disturbance and post-disturbance portions of the trajectory using a linear model and a nonlinear model, respectively. The linear model indicating pre-disturbance state was fit between the minimum NDMI, at which disturbance occurred and the break point (section 3.2.4.2). The non-linear model was a logistical growth curved with three shape parameters initialized by (i) the minimum NDMI value; (ii) the mean NDMI of the last 10 observations of the time series and (iii) the difference between the log value of the immediately post disturbance NDMI and that of the at-stability NDMI. Non-linear curve fitting employed the Levesque-Marquadt nonlinear least square regression and optimization to adjust these initial parameters to find the best fit of the potential trajectory to the observed trajectory (Kennedy *et al.*, 2010, Ahmed *et al.*, 2014). By assuming that disturbance warrants a substantial and detectable drop in vegetation moisture and by comparing curves fit to a time series with and without cloud screening, we set a threshold so that a drop in NDMI had to be at least 0.11 for the algorithm to accept it as a disturbance event. If NDMI values were negative, which indicated exposed soil, we set the value to 0, to facilitate convergence of shape parameters. No logistic growth curve would be fit if the single disturbance event of the time series happened after 2011, when records confirmed the end of logging operation, or happened within the last 5 observations of the time series.

Assessment of goodness of fit was summarized in terms of a standard *f*-statistic, and the probability of that *f*-statistic (*p-of-f*) was calculated (Kennedy *et al.,* 2007). The *f* statistics is a function of the sum of squared model (SSM), the sum of squared errors (SSE), the number of cloud free observations minus the number of model parameters minus 1 and the number of model parameters. In turn, SSE was calculated as deviations of predicted from actual empirical values of data and SSM as deviations of predicted values from mean value of data. We built a cumulative distribution for the *f* statistics and back calculated the *p-of-f* statistics for a null hypothesis (no trend, single linear line) and for the fit trajectory. High *f*-values indicated that the fit trajectory described the observations well. The model with the lower p value was the one with higher probability of observing *f* statistics more extreme than the null hypothesis, and hence showing better agreement between the fit trajectory and the observations. We only considered a hypothesized trajectory if its *p-of-f* value did not exceed 0.05 (Kennedy *et al.*, 2007, 2010).

The model with the lowest p-value was selected. The trajectory type and all the parameters describing that model were saved as separate layers of the output image and the fitting statistics (*f*-statistic and *p-of-f*) were output as a text file. The model parameters written to the output images described key aspects of the disturbance regime, including year of disturbance, change in NDMI at disturbance (a proxy for intensity of disturbance), and rate of recovery of NDMI (a proxy for regrowth). This process was repeated for all 20,006 pixels in the study region.

3.2.4.4 Deviation seeking

We ran the adaptive outlier detection procedure on the cloud free EVI and NDMI for each scene separately. Candidate change pixels were those that, across their respective time series, exceeded the threshold calculated for the scene-wide chi-square distribution of Mahalanobis distances with respect to the scene-wide mean and covariance of the vegetation index of interest, namely EVI or NDMI. If outliers were flagged in the EVI or NDMI layers, the pixel was classified as changed. The trend seeking approach only worked if there was sufficient data for a fitting to be completed. However, large data gaps due to sporadic acquisition in the 1990s, scan line corrector failure since 2003, and clouds led to large data gaps corresponding to loss of data for historical disturbance and recovery. When *p-of-f* statistics returned a straight line (i.e. no trend; section 3.2.4.3), we turned to deviation seeking, whereby if and when the vegetation index of a pixel exceeded the adapted threshold defined for that scene, that observation was flagged as change for the pixel's time series.

3.2.5. Processing, assembly and validation of final results.

Texture based cloud screening and adaptive outlier detection were carried out the statistical software R. Using a processing framework implemented by C. Holden (2015) in Python and QGIS, we assembled a stack of 12 images for each observation date and processed and output forest disturbance trajectory parameters and statistics for each pixel. A separate script read in results by parameter type (e.g. time, and intensity of disturbance,

recovery rate) and output one raster for each parameter. Any pixel that had no trajectory output due to its having less than a desired number of observation (e.g., less than 15 over 25 years) were assigned a trajectory and disturbance status from the dominant disturbance status of its 8 neighbors. Any pixel who disturbance status was significantly different from those of its 8 neighbors (e.g., an 8 years different in time of last disturbance events) was reassessed based the disturbance status and parameters of its 8 neighbors.

We designed a pixel-based stratified random validation scheme to compensate for the lack of high resolution aerial imagery of the area and to conform as much as possible to recommended good practices in estimating accuracy and area and quantifying uncertainty in land use land cover change detection (Olofsson *et al.,* 2013, 2014). We visually assessed pixel-level LULC labels and distinguished between natural and anthropogenic disturbances against the two IKONOS aerial images at 1m resolution for 2001 and 2013 available from Google Earth. Each pixel was assessed by its status as well as the statuses of its 8 neighbors. To account for misalignment and differing viewing angles at different acquisition date, we relied on tree fall gaps, forest edge and crown shape to make sure we were looking at the same area on the 2001 and 2013 IKONOS images. In addition, we compared top-of-canopy heights of forest and deforested Landsat pixels for scenes from the early 1990s as an independent check on the accuracy of our outlier detection (Fig.3.5, section 3.2.3.3).

3.3. Results and Discussions

3.3.1 Forest disturbance trajectories and rates

The Damit study area was dominated by forests that were disturbed before 2001 (53.8% of the total area), intact forests (31.2%) and forests disturbed after 2001 (15.0%) (Fig.3.3). The majority of deforestation happened in the 1980s spreading north to south and from east to west through access along the tributaries of the Belait river. Annual rate of deforestation dropped by almost an order of magnitude: from ~ 300 ha year^{-1} during the early 1990s to ~40-50 ha year^{-1} during the 2000s, which reflected the government's policy to limit timber production (Siddique 1992). The spatial pattern and areal rates of logging showed an initial period of booming exploitation that lasted until the early 1990s, followed by a slower expansion into the remaining, more marginal forests in the 2000s. Similar patterns have been previously been observed in Sarawak (Malaysian Borneo) (Ichikawa 2007, Kaur 1998). The dominance of disturbance contrasted our study area with other forest change mapping studies, where change was assumed to be rare events and hence only constituted no more than 10% of the landscape (Olofsson *et al.*, 2014; Song *et al.,* 2014, DeVries *et al.,* 2015). The landscape dominance of deforestation has increasingly become the norm for Borneo's peat swamp forests, which further highlighted the need to examine their post-disturbance conditions (Bryan *et al.* 2013).

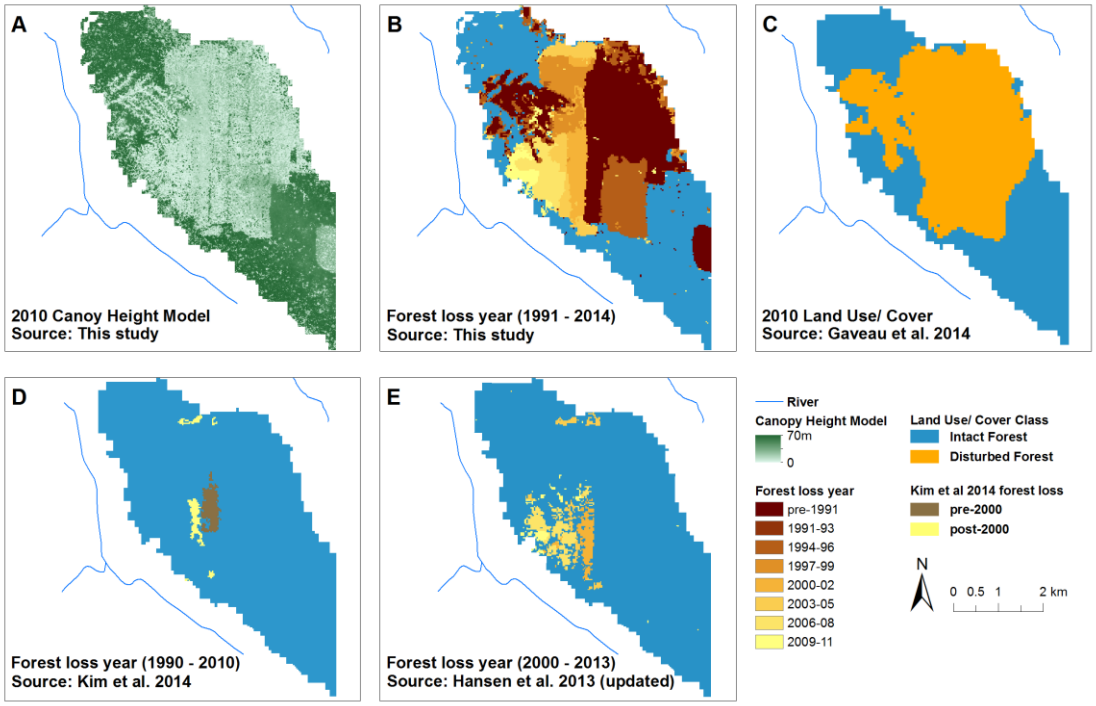

Figure 3.3: Change detection results for Damit and comparison with other global and regional LULCC products: From clockwise, the 2010 LiDAR based Canopy Height Model (panel A), this study's LULCC maps by class and by year of disturbance (panel B), an LULCC map for Borneo in 2010 by Gaveau et al. (2014) (panel C), a global LULCC map zoomed in for Borneo by Kim et al. (2015) (panel D) and Hansen et al. (2013) (panel E). The area of analysis was designated to correspond to peat depth of at least 3m and slope of at most 0.10 (Section 3.2.3.5).

Our algorithm identified the shape, the duration and rate of disturbance events, as well as disturbance type and timing of last disturbance event across a peat dome that was logged for almost 40 years (circa 1972 – 2010). Figure 3.4 illustrated each example of curve fitting output for the multiple forest disturbance trajectories (intact, logging before 1991, logging in 1999 followed by regrowth and logging in 2009 followed by regrowth)

with collocated observations in 2010 aerial imagery and the LiDAR canopy height.

Although the final NDMI values for each example across three disturbance trajectories

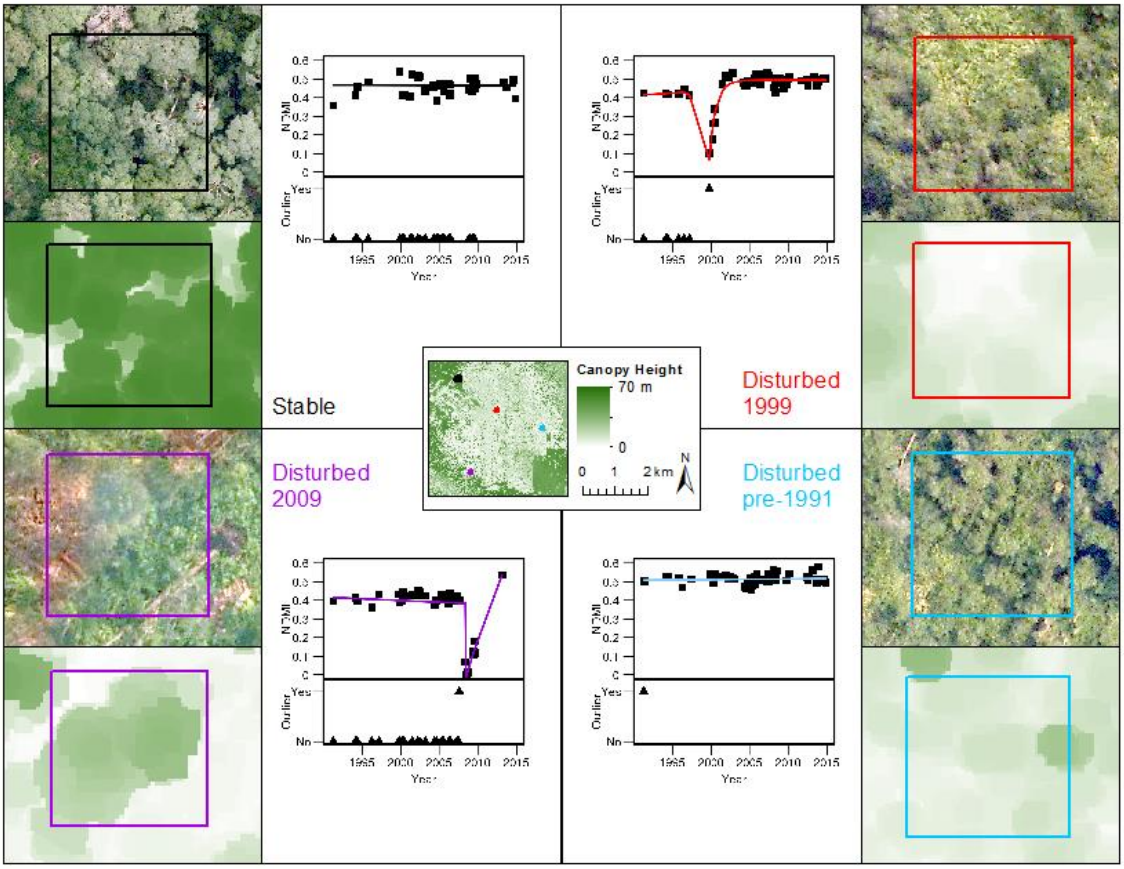

Figure 3.4: Examples of the disturbance trajectories. The center image shows the LiDAR based canopy height model and color coded sample trajectory pixels. Clockwise from the top left are examples of a stable forest pixel (black), a forest pixel disturbed before 2001 (red), a forest pixel disturbed after 2001 (purple) and a forest pixel disturbed before 1991 (blue). For each example a 2010 unorthorectified aerial photo zoomed in for the canopy height adjacent to the NDMI time series observations and disturbance models are included. The square within each image is the 30m x 30m Landsat pixel area color coded for the disturbance type.

were similar (~ 0.5), a pixel that was clear-cut in 1999 was shown to be structurally different from another pixel selectively logged in 2009 in terms of regrowth rate and tree height. The former had uniformly short vegetation stature, most of which was dominated by *Pandanus andersonii* and *Nephrolepsis biserrata* (Kobayashi 2000), whereas the latter had a few tall, poor quality trees left behind by the loggers. Post logging, vegetation moisture increased, which should be taken as caution due to NDMI's susceptibility to contamination to shadow from within pixel tall canopy, moisture in the regenerated ferns and the water saturated condition in the soil (Jin and Sader 2005). Tree cover as seen from the CHM did not distinguish old deforestation patches from newly logged ones. Whereas the traditional, wall-to-wall mapping approach often assumed that reduction in forest cover meant deforestation and hence resulted in a one time, binary assessment of forest condition i.e. logged or intact, the use of time series can provide extra information such as the mode of deforestation (clear cut vs. selective logging) and the subsequent rate of recovery.

3.3.2 Comparisons with other products

The extent of pre-1991 deforestation closely followed that from the field observations report by Kobayashi (1999). By 2010, deforestation was shown to have expanded and matched the pattern in the map produced by Gaveau *et al.* (2013) (Fig.3.3 C) using selected Landsat imagery and Phased Array L-band Synthetic Aperture Radar data on board the Advanced Land Observing Satellite (ALOS PALSAR). Our results agreed better with Gaveau *et al.* (2013)'s map than with the global products by Kim *et al.* (2015)

(Figure 3.3D) and Hansen *et al.* (2013) (Fig.3.3E). Note that all four products were at the 30m Landsat resolution. Both Hansen *et al.* (2013) and Kim *et al.* (2015) used decision trees to predict class membership of Landsat pixels using relationships between Landsat spectral reflectance metrics and data on tree crown and tree cover. Since Hansen *et al* (2013)'s analysis period was restricted to be post-2000, their product broadly agreed with our map in terms of extent and year of tree cover loss for the same period. Also using decision trees, Kim *et al.* (2015) extended the analysis period to the 1990s. Based on a sample of pixels whose vegetation cover stayed 'forest' or non-forest' between two given dates, they calculated the possibility of being 'forest' or 'non-forest' as a function of surface reflectance and temperature. A categorical map of forest change was then produced by assigning each pixel to the category with highest probability. It was possible that cloud cover excluded many pixels from the training data for Kim *et al.* (2015), resulting in these deforested pixels not chosen for training the trees and hence their product seemed to miss a lot of deforestation in the Damit study area. In addition, both Hansen *et al.* (2013) and Kim *et al.* (2015) relied on global tree cover to inform forest change. The extraordinary height and vigorous regrowth of tropical peat forest (Kobayashi 2000) meant that even post-logged forests were rendered intact forests under FAO's definition. The practice of detecting forest change by epoch, despite being necessitated by the paucity of data in tropical region, resulted in both studies missing deforestation that occurred before the studied period. This comparison made clear how land use land cover change products can differ just by the choice of a cloud mask or the

change detection technique and called for a more uniform framework for continuous monitoring of forest disturbance and regrowth especially in the tropics.

3.3.3 Accuracy assessments

We tested whether our algorithm captured the extent of logged forest by calculating fractional forest cover from LiDAR within the disturbed Landsat pixels. Fractional canopy cover was computed as the ratio between the number of LiDAR pixels with minimum elevation of 30m (Figure 2.5) and total number of LiDAR pixels in each Landsat pixel and the ratio had to be 10% minimum (FRA 2015). The mean fractional forest cover for the disturbed forest was 0.2, which showed that our algorithm was sensitive to both clear cut and partial logging at Landsat resolution.

Our algorithm achieved clear separation between disturbed and intact forests in terms of NDMI and mean top-of-canopy height. Figure 3.5 showed how all pixels in a cloud free NDMI scene were grouped into intact (blue) and disturbed (orange) pixels as a result of the adaptive outlier detection procedure and the corresponding NDMI and top-of-canopy height distributions for each group. The distributions of NDMI values showed similar shapes but a shift in centroid and great overlapping between the intact and the disturbed forest pixels, which would be very challenging to resolve without the adaptive outlier detection. Similarly with the independent measure of canopy height, we observed that intact forests were taller than disturbed forests, as expected. The overlap in height between intact and disturbed forests was due to (i) poor quality canopy trees left behind

by loggers, which increased the mean height of the collocated Landsat pixel and (ii) sub pixel canopy gaps, which reduced the mean height of the collocated Landsat pixel.

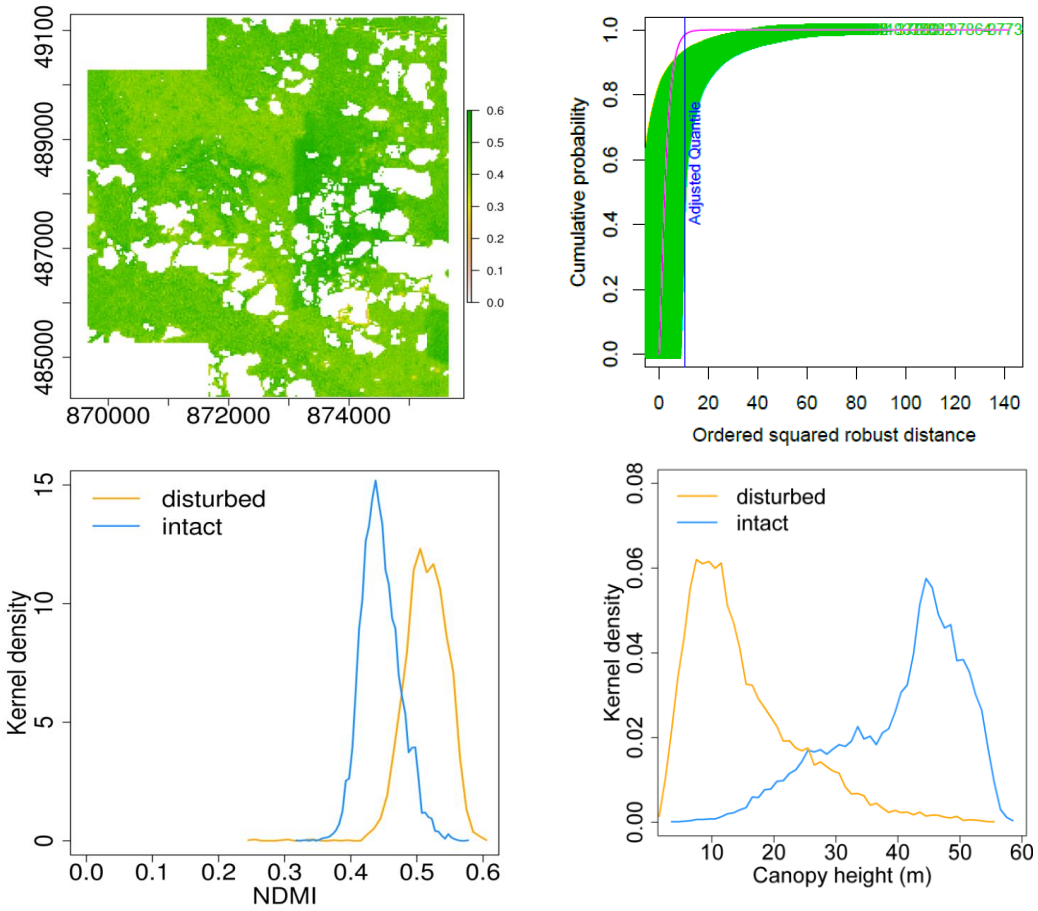

Figure 3.5: Detecting changed pixels: we started with a cloud free scene (NDMI was shown as example) and plotted its theoretical (purple) and simulated (green) chi square distributions. The resultant intact (blue) and disturbed (orange) pixels were plotted by NDMI and mean top-of-canopy height values.

Our pixel-based stratified sampling validation scheme for disturbance type and timing of last disturbance event closely followed Olofsson *et al.* (2013, 2014)'s guidelines. We calculated a total sampling size of 650 pixels assuming that all classes achieved user's accuracy of 85% and standard error of 0.014. From this, we assigned stratified sampling

sizes of 225, 312 and 113 pixels to intact forest, disturbed forest before 2001 and disturbed forest after 2001 respectively. The sample size of 113 was to ensure that every year after 2001 would show up in the selected samples. The sample count statistics were summarized in Table 3.1:

Table 3.1: Error matrix of sample counts for the three land use land cover classes. Map categories are the rows while the reference categories are the columns.

Observation / Algorithm	Intact forest	Disturbed prior to 2001	Disturbed during 2000s	Map area (hectares)	Fraction of total landscape
Intact forest	211	10	4	793.5	0.40
Disturbed prior to 2001	6	284	22	891.3	0.45
Disturbed after 2001	5	5	103	297.1	0.15

Table 3.2 summarized user's and producer's accuracies and areal estimates with 95% confidence level. Our LULCC areal estimates in table 3.1 were within 95% confidence intervals for the true areas (Table 3.2). Our user's and producer's accuracies were in the upper range among the most popular tropical deforestation studies (DeVries *et al.* 2015).

Table 3.2: Estimated error matrix with accuracy measures ± a 95% confidence interval.

Class	User's accuracy (percentage)	Producer's accuracy (percentage)	Areal estimates (hectares)
Intact forest	0.94 ± 0.032	0.95 ± 0.051	772.7 ± 30.5
Disturbed prior to 2001	0.91 ± 0.032	0.95 ± 0.027	878.7 ± 37.5
Disturbed after 2001	0.91 ± 0.053	0.80 ± 0.052	329.4 ± 32.7

We further analyzed forest structure associated with the validation pixels. Many pixels located at the edge of logging swatch in one year only became detected in later years by the algorithm when at least an additional 50% of the pixel's canopy cover was removed or when the cloud cover for that area was low enough for successful detection, which was encountered elsewhere in the temperate forest (Ahmed *et al.,* 2014). The algorithm detected all natural gaps bigger than 20 hectares, which occurred in 4 separate locations due to pest pathogen in the late 1940s (Anderson 1961). For natural gaps that were one Landsat pixel or smaller, the canopy cover had to reduce by 50% of the pixel area or 50% of the original canopy height in order to be detected. As such, only a few pixels with pixel to sub-pixel natural gaps were detected. Gap opening was not the main objective of the development of our method and will be treated separately in another section.

3.3.4 Change Detection Methodological tradeoffs

Differences of data sources, acquisition streams, analysis strategy, spatial extent and resolutions prevent simple standardization of continuously updated land use/ cover change product that was highly versatile for different research purposes (carbon accounting, climate change projections and biogeochemical modeling). The algorithm introduced in this paper is a major step towards a framework for continuous monitoring of forest disturbance and regrowth by contributing a means to map forest disturbance in an aseasonal tropical forest at annual resolution using time series analysis. Here, NDMI as proxy for vegetation moisture is used as an illustration of the algorithm. Like other time series change detection methods (e.g., VCT (Huang *et al.* 2010), BFAST (Breaks for Additive Season and Trend) Verbesselt *et al.* 2010, LandTrendr Kennedy *et al.* 2010), our method has the statistical advantage of increased degrees of freedom over the wall-to-wall change detection methods. A candidate change event is confirmed by a time series (instead of a pair) of observations before, during and after the change in order to be detected and identified. In addition to our primary design for change detection algorithm, we provide a texture based cloud mask to better screen cloud, cloud shadow and haze, which is important and useful for other tropical areas with similar cloud cover challenges. Our algorithm accounts for *both* continuous changes and abrupt changes (or events in sparse data density), assuming that NDMI values for disturbed pixels either change gradually (e.g., resulting from natural growth) over time or differ substantially from the statistical distribution of their neighbors from observation date to observation date.

The methodological foundation is based on well-characterized, parametric statistical models and offers computational simplicity. Large-area land cover mapping or change detection often requires intensive human involvement or automation, which entails sophisticated algorithm parameterization, substantial computing facilities or both. Our method follows established statistical theory with little parameter fine-tuning. It includes (i) careful screening of cloud, cloud shadow and haze to prevent false positive and (ii) adaptive detection of candidate change pixels to provide the algorithm the initial values. Further, this method captures continuous natural and anthropogenic changes in land cover at fine spatial resolution and has the potential to capture subtle and long-term changes, such as forest degradation in the absence of a universal, definite method designed for forest degradation and in light of the rapid but uncharacterized forest degradation in Southeast Asia (Miettinen *et al.*, 2014). This application to a dense, cloudy tropical peat swamp forest provides the exact location, the timing and the mode of disturbance for an area understudied in current global environmental change research, under-reported in national forest inventory but that has been undergoing fast and substantial disturbances. This method can contribute to current efforts in monitoring for both Deforestation and Degradation in the context of REDD+.

This approach does not need to be limited to tree cover or imagery resolution and frequency. Although our proof of concept of the algorithm uses NDMI, the general method has no specific requirement on the thematic type or spatial or temporal resolution. Therefore, it may be applicable to continuous fields of other land cover types generated

using satellite data from different sensors at the sampling frequency, resolution and spectral indices that optimize the research purpose(s). However, there are several limitations of the current algorithm that require additional refinement. First, the algorithm currently operates on time series of single pixels without any consideration for its neighbors and spatial correlation is only considered in the post processing of the results. We may expect spatial correlation between different pixels and serial correlation between observations of a given pixel taken over time. The effect of spatiotemporal correlation on change detection needs to be investigated in the future. Moreover, the current algorithm is optimized for detecting single and dominant forest disturbances (e.g., clear cutting) whereas changes can be multiple (logging and burning) or repeated, such as fires and crop rotations. Another big assumption is that any change has to result in a prominent, detectable drop in vegetation greenness or moisture while events such as crop intensification might only shift the mode of the vegetation time series. Secondly, although both natural and anthropogenic disturbances are captured, the distinction between the natural and anthropogenic cause is only by visual inspection, instead of registering each cause with a distinctive temporal signature. To this end, more indices should be investigated to best suit a variety of disturbances e.g. wind, pathogen, fire etc. Finally, our current algorithm evaluation is only demonstrated in the tropical moist broadleaf forest biome, which accounts for less than 40% of global tropical forests. With the opening of the Landsat historical archive and new satellite missions, there is no reason that the quantitative evaluation cannot be expanded to other (tropical) forest types.

3.4. Conclusions

Accurate, detailed and timely land use land cover information at both the regional and global scale is extremely valuable for helping policy makers, natural resource managers and researchers address the issues related to global environmental changes. In this study, we provided a new strategy for characterizing land use land cover change in forested areas using time series of Landsat resolution vegetation moisture. The recognition of land cover disturbances being rare events in a large geographic region allows efficient change detection by employing well-established parametric statistics. Fitting nonlinear curves to time series, continuous estimates of vegetation moisture simultaneously characterize the timing and intensity of forest cover change. The method requires little parameter fine-tuning to derive indicators of annual forest cover change but rigorous cloud screening and texture computation. It offers multiple advantages, namely (i) reliable results; (ii) computational simplicity; (iii) global applicability; (iv) flexibility to capture abrupt as well as gradual changes; and (v) capability to apply to other satellite sensors. Because increasing the frequency of forest cover change detection to annual resolution is highly desirable for understanding the global carbon cycle, further research should be broadened to include multiple and repeated disturbance at once as well as other types of disturbances. The more reliable capturing of type, timing and intensity of disturbance will also facilitate the understanding of post disturbance forest conditions, which is the topic of the next chapter. The results here will allow for segmenting forest structures at LiDAR

scales by Landsat derived time of disturbance and constructing a chronosequence to analyze how forest recovers as a function of type, time and intensity of disturbance.

CHAPTER 4 – RECOVERY DYNAMICS OF DISTURBED PEATLANDS IN NORTHWESTERN BORNEO

4.1 Introduction

4.1.1 Current knowledge on the ecology of tropical peatlands

Tropical peatlands account for less than 1% of global forest area (Page *et al.*, 2011), but contain one third of the global soil organic carbon pool (Parish *et al.*, 2008; Draper *et al.*, 2014). Southeast Asia, with Indonesia and Malaysia, collectively called the Indo-Malayan realm, is home to 56% of the tropical peatland area. The Indo-Malayan peatlands are one of the most geologically complex and biologically endemic and diverse regions in the world (Sodhi *et al.*, 2004), providing a variety of ecological services and resources such as flood mitigation and timber. The rate of deforestation targeting the economically valuable *Dipterocarp*s that dominate Indo-Malayan peatlands was twice that for other types of evergreen forests in the region during the 2000s (Miettinen *et al.*, 2011). Starting in the 1970s and accelerating through the 1990s, 80% of the pre-industrial extent of Southeast Asian peat swamp forests (PSF) has undergone some form of extraction and development (logging, draining, burning) with no ecologically and hydrologically intact peat domes remaining in Malaysia and Indonesia (Dommain *et al.*, 2016; Gaveau *et al.*, 2014, 2016; Bryan *et al.*, 2013; Miettinen *et al.*, 2012). By the 2010s, peatland deforestation and degradation represented approximately 20% of global annual CO_2 emissions from land use land cover change (van der Werf 2009, La Quere *et*

al., 2015) and substantially contributed to CH_4 and N_2O greenhouse gas emissions (Hatano *et al.*, 2016; Muller *et al.*, 2016; Mitsch *et al.*, 2010). Further, the 1997/98 and 2015/16 El Niño episodes resulted in tropical peatland fires that contributed to anomalously large rises in atmospheric CO_2 concentrations (Langman & Heil 2004, Betts *et al.*, 2016). Transboundary haze from peatland fires during the 1997/98 El Niño event caused financial damage of up to $20 billions (Varma 2003) and during the 2015/16 El Niño event was associated with 100,000 deaths (Koplitz *et al.*, 2016). If peatland deforestation and degradation is to continue unabated, PSF will disappear in 30 years (Hoojier *et al.*, 2010) and potentially produce CO_2 emissions equivalent to 11-13% of all emissions since the start of the Industrial Revolution (Donahue 2016). Conservation and restoration of PSF concerns the reduction of CO_2 emissions, protection of the region's highly endemic fauna and flora, and also regional water regulation and public health safety (Dommain *et al.*, 2016).

Policies, initiatives and conventions have thus far been largely ineffective in halting the wave of logging and agriculture conversions in peatlands despite a large body of literature dedicated to ecosystem services and ecological uniqueness of PSF, as well as the consequences of unsustainable management in this ecosystem (Anderson 1961, 1964, 1983; Bruenig 1964, 1969; Furukawa 1988a,b; Kobayashi 2000; Page 1999, 2002, 2011; Dommain 2004, 2010, 2016; Hoojier *et al.*, 2010). Broadly, logging in peat swamp forest removes up to 80% of aboveground biomass, directly reducing input to peat accumulation while also changing the peatland microclimate and impairing its water

holding capacity (Page *et al.*, 2008). Drainage of peatland results in peat oxidation and eventually subsidence to such low levels that the water table is able to reach and rise above the new surface more quickly in periods of high rainfall and dramatically increasing runoff, leading to more flooding and salinity from increased tidal influence. In some locations the peat eventually disappears leaving behind soils that hold far less water and tend to be more nutrient deficient and/or toxic (for example, sulfates in peatland of brackish water origin), which is unsuitable for agriculture and further management (Kobayashi 2016). Logging and peat drainage also increase fire risk. Fire not only destroys the aboveground biomass but also smolders in the underlying peat, resulting in high atmospheric emissions of greenhouse gases (CO_2, CO and CH_4) and particulate matter (Page *et al.*, 2016). The aboveground and belowground destructions from fires further lead to loss of the water regulation functions of the near-surface peat layer (Turetsky *et al.*, 2015), subsidence of the peat surface (Rein *et al.*, 2008), loss of the seed bank and tree bases for future vegetation re-establishment (Page *et al.*, 2009; Rein *et al.*, 2008), and damages to human health and livelihoods through loss of natural resources and high levels of air pollution (Page *et al.*, 2016). So far literature has focused on drainage and fires (Hirano *et al.*, 2012; Schrier-Uijl *et al.*, 2013), effectively assuming damages are reduced in PSF if logging occurred without subsequent drainage and fires.

Countries like Indonesia have pledged to accelerate the recovery and restoration of hydrology in degraded peatlands by rewetting 2 million hectares between 2016 and 2020. The success of these efforts will depend on the methods that can bring about an

economical, effective and permanent rise in the depth to water level and the former vegetation cover (Jaenick *et al.*, 2011). Unfortunately, our understanding of PSF ecology and its time evolution following disturbances is still very limited (Bryan *et al.*, 2013; Posa *et al.*, 2011; Dommain *et al.*, 2004). Monitoring of PSF has been extremely difficult due to the lack of baseline information, cloudy and rainy weather conditions that limit utility of satellite-based remote sensing, remote and isolated location and the microscale and mesoscale heterogeneities of this ecosystem. Improved knowledge of PSF ecology and its responses to harvesting and management practice is necessary to improve global climate models, inform sustainable peatland management practices, biodiversity conservation, and to improve carbon accounting (Page *et al.*, 2011; Posa *et al.*, 2011; Sodhi *et al.*, 2004).

4.1.2 Research objectives

The ecology of peat swamp forests is unique in many respects, including their supra-annual masting mode of reproduction (Curran *et al.*, 1999), high interdependence between peat, water and vegetation (Page *et al.*; 1999, Dommain *et al.*, 2010), and adaptation to waterlogged, nutrient-poor environmental conditions (Anderson 1983, Furakawa 1988a). This study aims to yield new insight into how the hydrological and ecological characteristics of PSF respond to natural and anthropogenic disturbances in both the short- and long-term. Specifically, we examined (i) regrowth dynamics with respect to time since last disturbance (logging and pathogen); (ii) the mesoscale patterns of hydrology with respect to disturbance dynamics and (iii) how the co-dependence

between hydrology and forest structure determines the contrasts in structure and environmental conditions between intact and logged forests.

4.2 Methodology

4.2.1 Site Description

The Damit and Mendarem peat domes occupy an area of 7,145 ha at the Malaysian

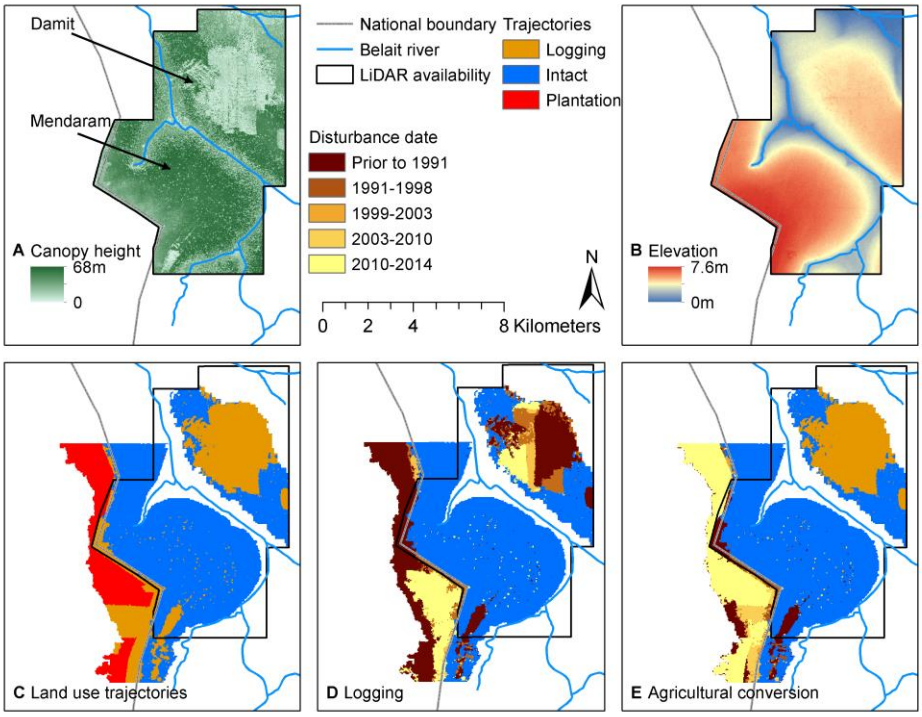

Figure 4.1: LiDAR-derived canopy height map (panel A) and dome elevation (panel B). Land use history at Sungei Damit and Ulu Mendaram (panel C: land use trajectories; panel D: years that logging was detected and panel E: years that agricultural conversion was detected) together

and Brunei border region (Figure 4.1). Figure 4.1A showed the extent of LiDAR coverage across a landscape, capturing a chronosequence of disturbance by both logging and insect infestation. In both Mendaram and Damit, the mode of logging was clear cutting with mechanical transport of logs on railroads that were laid out across the landscape (Kobayashi 2000). Both domes showed evolving disturbance dynamics associated with logging and conversion to oil palm plantations for the case of Mendaram (figure 4.1C and E). The Damit dome is in close proximity to two active river channels of the Belait system (Sungei Belait and Sungei Damit) and experienced extensive logging between the late 1980s and 2010 (Furukawa 1988b, Kobayashi 2000). In contrast, the Mendaram dome is sandwiched by the Belait system on one side (Brunei) and the Baram system on the other (Malaysia). Most of the Bruneian side of Mendaram dome is still intact with an exception of a 94-ha logged area detected on the south end of the dome that is estimated to have occurred prior to 1984 as viewed from Google Earth. The west side of the Mendaram dome is adjacent to Malaysia and was directly adjacent to logging activities from the Malaysian side of the border which also occurred prior to 1984. Although there were Landsat imagery between 1983 and 1991 for the two domes, they were not compatible in terms of atmospheric correction, coordinate system and resolution, which prevented them from being used with our land use land cover change detection algorithm. A buffer along the border was cleared between 1991 and 1994, from which logging tracks started to extend over the Malaysian side of dome to facilitate transport of logs. The heaviest period of logging occurred on the late 2010s (fig. 4.1D).

The entire Malaysian portion of Mendaram dome underwent drainage and conversion to palm oil plantation between 2010 and the present (fig. 4.1E; Dommain *et al.*, 2016).

4.2.2 Disturbance dynamics from optical imagery (Landsat)

The Baram-Belait complex, to which the peat domes at Sungei Damit and Ulu Mendaram belong, was one of the most widely documented peat complexes in northwestern Borneo (Sarawak, Malaysia and Belait, Brunei), being about 4,500 km^2 in size, about 4,500 years in age and among the few peat domes that exhibited a full catena of vegetation (Staub and Esterle 1994, Anderson 1983, 1964, 1961). By 2015, the Baram dome was completely drained and converted to oil palm plantations (Dommain *et al.*, 2016; Gaveau *et al.*, 2016). However, the rest of the Baram-Belait peatland complex, the Mendaram (MD) and Damit (DT) dome across the Malaysian border in Brunei experienced varying degrees of disturbance since the 1980s and hence could inform understanding of the differing ecology and hydrology of intact, logged, and degraded PSF. The entire Damit dome had a peat thickness of no more than 4.5m and was covered by pure stands of *Shorea albida,* an endemic species from the *Dipterocarp* family that reaches 65m in height (Furukawa 1988). On the other hand, at Mendaram, the peat depth reaches 4.5m within just 900m from the river (Dommain *et al.*, 2015), increasing toward the dome center. Mendaram contains the full catena with tree height ranging from 35 to 65m across only a 4 meter change in dome elevation (Nguyen *et al.*, 2016). Apart from anthropogenic disturbance, the forest occasionally experienced squall lines, which were

spatially localized and confined to the wet season (November-March), lightning (Bruenig 1963, 1969) and rare but extensive pathogen defoliation (Anderson 1961).

To characterize disturbance dynamics in the Damit and Mendaram peatdomes, we employed the land use/ cover change analysis approach developed in chapter 2 to analyze a time series of (208 Landsat images) that spanned 25 years (1991-2015) and detected changes using time series analysis of Landsat-pixel level reflectances and vegetation indices. In brief, a time series of the Normalized Difference Moisture Index (NDMI) was built for each pixel within the study region, screened for clouds and noise and assessed to determine whether there was a shift in its temporal trend or a change in the pixel's value with respect to the scene-wide statistical distribution during the analysis period. Quantitative metrics, such as the magnitude, rate and time of forest cover change in each pixel, were derived from the resultant logistic equations. However, if such a trend fitting procedure could not work due to data scarcity, we then assessed whether a pixel was perceived as change from the statistical distribution of its neighbors. We limited our analysis for only the extent of *Shorea albida* forests and avoid complex hydrological features such as former river channels, buried river beds and ox-bow lakes as these features can contaminate the vegetation signal and the vegetation composition is unlikely to include *Shorea albida* (Furukawa 1988). Further, noticing that when the cleared land became plantation, the presence of water in plantation canals dropped the wetness signal to below 0, we modified our algorithm to detect time of appearance of plantation canals as proxy for agricultural conversion. The algorithm achieved more than 92% user's and

producer's accuracies, making it reliable to segment higher resolution data of forest structure and radar backscatter.

4.2.3 Forest structure from Light Detection and Ranging (LiDAR) data

We characterized forest structure (individual tree canopy height, crown area, crown roughness, stem density) of the two peat domes from Light Detection and Ranging (LiDAR) observations acquired in 2010 and covering approximately 7,145 hectares of peatlands. From the raw point clouds, Canopy Height Model (CHM) for Damit at 0.5m resolution was produced following the procedure described in Nguyen *et al.* (2016). A 0.5m resolution was deemed adequate for both computational power and detailed enough for subsequent exaction of forest structure. Due to challenges associated with the signal of vegetation moisture from open mixed swamp forests, we again limited our analysis to forests dominated by *Shorea albida*, which were most affected by human activities. As there was no clear boundary to mark the transition from riverine, open mixed swamp forest to other phasic forest communities (Anderson 1983, Bruenig and Huang 1989), we delineated the analysis area using information of peat depth and drainage. The analysis area was produced in ArcGIS using a minimum elevation of 3m above mean sea level and a maximum slope of 0.10 units as proxy for poor drainage. Three meters was the reported peat depth that was beyond tidal influence and that was most like subjected to human disturbances (Esterle and Ferm 1994; Hoojer 2004; Wosten *et al.*, 2008), we therefore assumed that a minimum elevation of 3m corresponded to a minimum of 3m in

peat depth. The final analysis area for Damit and Mendaram were 1,980.5 and 5,164.6 hectares, respectively.

We extracted statistics on forest structure (gap fraction, canopy stem density, canopy stem position and height) following the methodology used in Nguyen *et al.* (2016), with improvements to account for the heterogeneity of the near-edge and logged forest areas. We first separated logged and intact forest areas by using the Landsat map of disturbance dynamics to segment the CHM by disturbance type. The intact portion of the CHM was further separated into gap and non-gap areas while the logged portion was separated into four layers: emergent/ tall canopy, mid height canopy, low stature canopy and forest floor vegetation (mainly the fern species *Pandanus andersonii* and the herb *Lephrolepis biserrata*). Assuming that the maximum height for Pandanus is 6.5m (Kobayashi 2000) and modifying Duncanson *et al.* (2014)'s approach, we inverted the logged portion of the CHM and ran ArcGIS's (Version 10.4) Basin tool to produce neighboring *watersheds* along lines of local minima. Within this section, a *watershed* represented a potential tree crown or a cluster of crowns. For each *watershed* we examined its pseudo-waveform shape of the distribution of pixels' height. We relied on Jenks' natural breaks to inform the number of layers and the thresholds at which layers within a *watershed* can be separated. After all *watersheds* were individually split into *sub-watersheds* representing separate forest layers, we merged all *sub-watersheds* that belonged to the same layer into one complete raster.

To separate the intact portion of the CHM into gaps and non-gapped areas, we relied on the knowledge that for tall, rough forests (phasic communities I, II and III), canopy height within the gaps should reach between ¼ and ¾ the surrounding canopy height (Bruenig 1964, 1973, Anderson 1963). For short, smooth forests (phasic community IV), lightning gaps are very fewer. Thus, we carried out a moving window analysis of 150m by 150m over the intact forest and calculated the ratio between mean height of a given LiDAR pixel and the maximum canopy height within the search window. On the resultant canopy fraction raster, which ran continuously between 0 and 1, we conditioned that if the maximum canopy height in the search window is more than 35m, then a canopy fraction of at most ¾ corresponded to a gap. If the maximum canopy height in the search window is less than 35m, all canopy fraction of less than 1 corresponded to a gap. On the resultant gap and non-gapped areas of the intact forest CHM, we again inverted the CHM and ran ArcGIS's Basin tool to produce neighboring *watersheds* along lines of local minima. No layering analysis was done since very little signal from LiDAR can penetrate a forest of 55-60m height.

Finally, we extracted individual stem height, crown roughness and crown areas by running a local maxima filtering algorithm on the *watersheds*. The algorithm relied on *a priori* knowledge of the relationship between stem height and crown diameter in *Dipterocarp* forest to dynamically adjust the size for the local maxima search window (Nguyen *et al.* 2016). Neighboring crowns of within 1.25 times their hypothetical crown diameter and within a 6m difference in vertical height (Osunkoya *et al.* 2007) were

merged to be one tree. The algorithm generated the location, height, crown area, crown roughness and crown depth for each tree within each layer. Crown area was calculated as the number of pixels in the crown multiplied by the area per pixel ($0.25m^2$). Crown roughness was calculated as the standard deviation of height of all pixels belonging to the same trees.

4.2.4 Hydrology and canopy-ground interactions from L-band HH backscatter (PALSAR and JERS-1)

We characterized the canopy-ground interactions (and hydrology) by analyzing multi-temporal active radar images of the peatlands between 1993 and 1998 and between 2007 and 2009. Optical satellite observations for Southeast Asian coastal peatlands are limited due to near ubiquitous cloud cover (70-80% of the year), haze from smoldering fires during the dry season (April – October), and precipitation during the wet season (November – March). Unlike optical sensors, which look at vegetation reflectance in the visible spectrum, microwave sensors measure the emissivity of surface objects (e.g. land, soil, water), given that water has a very high dielectric constant compared to other solid objects. The wavelengths of microwave are much less influenced by clouds and smoke and can better penetrate vegetation at some wavelengths, making many studies using microwave data successful for mapping wetlands and inundation (e.g. Hess *et al.*, 2003; Siqueira *et al.*, 2003). In particular, the longer wavelength of L-HH sensors such as the Japanese Earth Resource Satellite-1 (JERS-1) and the Phased Array type L-band Synthetic Aperture Radar (PALSAR) onboard the Japanese ALOS satellite have been

found to maximize canopy penetration, interaction with vegetation components (leaves, branches, trunks) and the forest floor, and discrimination between flooded and non-flooded forest (e.g. Hess *et al.*, 2003; Siqueira *et al.*, 2003; Salas *et al.*, 2002; and Lucas *et al.*, 2007).

JERS-1 was launched and operated by the National Space Development Agency of Japan (NASDA) from February 1992 until October 1998. The JERS-1 Synthetic Aperture Radar imaged the Earth on descending node with a 35-39° westward look and a ground resolution of 18m in both range and azimuth with a 44 day revisit cycle. In comparison, the ALOS PALSAR imaged on ascending node at an incidence angle of 38.8° between 2007 and 2011. The polarization mode was switched periodically between single mode (HH) during the wet season and dual mode (HH, HV) during the dry season, with a temporal resolution of 46 days. The absolute calibration accuracy of PALSAR data is 0.219 dB, using the Amazon rainforest as calibration target (Shimada *et al.*, 2009), while that for JERS-1 data was approximately 1dB (Salas *et al.*, 2002).

The Japanese Space Agency (JAXA) provided us free of charge eleven (11) radiometrically and terrain corrected, horizontally co-polarized (L-HH) JERS-1 imagery between 1993 and 1998 at 12.5m resolution. In addition, we obtained from the Alaska Space Facility eight (8) radiometrically and terrain corrected, calibrated ALOS PALSAR imagery between 2007 and 2009 with horizontal co-polarization (4 of which were also available in dual polarization) and 12.5m resolution. While ALOS PALSAR backscatter intensity was only available in the format of gamma nought (γ°) (normalized to the slant

range, which is the plane perpendicular to the ground), JERS-1 backscatter was manually normalized to the ground range and converted to intensity as sigma nought (δ°) (Shimada & Isoguchi 2002). Hence, although the images were of the same wavelength and resolution, they cannot be used together in simple one multi-temporal analysis. Nevertheless, we took advantage of the flat terrain in PSF, the zonation of vegetation structure, the availability of multiple dry-season observation dates, and similar SAR configurations between JERS-1 and ALOS (wavelength, resolution, incident angle) to deduce valuable information about the short and long-term dynamics of hydrology and forest structure in PSF.

Additional pre-processing had to be done for both JERS-1 and ALOS PALSAR to limit co-registration error and speckle noise, which contributed the most to the signal variation in L-band backscatter (Lucas *et al.*, 2007; Siqueira *et al.*, 2003; Hess *et al.*, 2003). Due to very low geometric accuracy inherent in JERS-1 imagery (406m, Shimada and Isoguchi 2002), co-registration was carried out first between Landsat and the JERS-1 imagery and then among the JERS-1 imagery. The final co-registration error between JERS-1 imagery and Landsat was reduced to 8m, or 0.7 of the horizontal resolution (12.5m). This was deemed adequate for further analysis by previous studies using JERS-1 data (Jaenick *et al.*, 2011; Almeida-Filho *et al.*, 2000, 2005, 2009). After co-registration, the images were despeckled using the enhanced Lee filter over a moving 5 by 5 window. We then segmented the L-band backscatter by disturbance epoch (section 4.2.1), then within each land use/ type (intact forest or logged forests of different epochs), sampled

and calculated the mean, standard deviation and 95% confidence interval (CI) for its backscatter.

We segmented selected JERS-1 and ALOS imagery using the Landsat-based land use/cover types (Figure 4.1), then assessed backscattering coefficients γ° for ALOS and δ° for JERS-1 across the chronosequence spatially and seasonally given three known scattering mechanisms. Despite efforts to despeckle, the images were found to be noisy and showed substantial spatial variation between forest types as expected from radar imagery (Salas *et al*, 2002). A sharp edge was consistently observed at the boundary of forests logged between 1991 and 1994 and the intact forest and was an artifact of SAR with the boundary between intact and logged forest (Salas *et al.*, 2002). By looking at statistics of L-HH backscatter between intact and logged forests at different ages and between seasons, we asked the following questions: (i) were intact and logged peatlands statistically different in terms of L-HH backscatter?; (ii) if existent, was this statistical difference changed between seasons and with logging ages?

4.2.5 Edge analysis

We characterized how the spatial and temporal extents over which disturbance influenced adjacent intact peatland forests by analyzing forest structure and surface properties (backscatter for soil moisture and EVI for greenness) in four forest edges in Damit and Medaram that were created at similar times (1991-1994), but are situated on different dome elevations (<4.5m vs. > 6m above sea level) with varying aspect with

respect to the dominant wind direction and subjected to different logging ages and modes (10 years vs 15 years, clear-cut vs selective logging). For each forest edge, we extracted forest structure (section 4.2.2), microwave data (section 4.2.3) and EVI from an area that ran from the edge and to1km away from both sides of the edge. If the intact side of the edge was less than 1km in width, we limited the area of analysis to 500m into the intact forest. The choice of 1km was the minimum predicted depth of edge effect for Borneo (Chaplin-Kramer *et al.*, 2015). Over the edge buffer areas, we laid a 100m by 100m grid and calculated the pixel-wise statistics for each variable (stem density, mean canopy height, gap fraction, dome elevation, JERS and ALOS backscatter, mean EVI for 1991, 1997, 2007 and 2008). Edge pixels were selected as those that interfaced the logged and intact forests (Fig 4.1). We then calculated the shortest Euclidean distance from a pixel to its closest edge pixel and fitted a locally weighted scatterplot smoothing (LOESS) function for each variable as a function of pixel-wise distance to the edge.

4.2.5 Statistical analysis

All statistical analysis was carried out in the R statistical software version 3.3.0 (The R Development Team 2016). Unless otherwise noted, all variables were reported as mean ± 95% confidence intervals (CI). Given the very large datasets and non-Gaussian data distributions, bootstrapping approaches were used to estimate statistics. We determined the required sample size for a variable (forest structure of land surface property) by sampling with replacement for a sample size n such that we are 95% confident that the sample percentage as a fraction of total population size N (n/N) would be within 5% error

from the true population percentage. We first calculated a preliminary sample size *m* using a Z-score of 1.96 (for 95% confidence), 5% error and a default proportion of 0.5 (Berenson *et al.*, 2013):

$$m = 1.96^2 * 0.5^2/(0.05)^2$$

We then corrected *m* for the small, finite population and output the actual sample size *n* (Berenson *et al.*, 2013):

$$n = \frac{m}{1 + \frac{(m-1)}{N}}$$

Once we determined the sample size, we sampled with replacement from the population 1000 times and calculated the means and quantiles.

For comparison of data distributions relating to forest structure (mean canopy height, stem density) and surface properties we used the two-tailed F-test against the null hypothesis that across seasons, or decades, or land use type, the two populations of the same variables assumed the same variance with 95% confidence level. We also tested the statistical relationships between EVI and backscatter, and between forest structure variables and surface properties with distance from forest edge by fitting least squares linear regression to the scatterplots. In the event that a least squares linear regression could not be fitted, we tested the lack of a relationship using the Pearson Product Moment Correlation test.

4.3 Results and Discussion

4.3.1 Vegetation structure chronosequence analysis

Much of our current knowledge of the processes of natural regeneration on degraded peatlands in the tropics comes from studies of small areas, typically tens of hectares of degraded land embedded in a forested matrix (Uhl *et al.*, 1988; Aide *et al.*, 2000; Galindo-Gonzalez *et al.*, 2000, Zimmerman *et al.*, 2000, Cubina and Aide, 2001, Ingle, 2003; Guevara *et al.*, 2004; de Melo *et al.*, 2006 and Dosch *et al.*, 2007). Logging in PSF can vary in intensity with some forests being mechanically logged, drained with canals, and/or burned. Natural regeneration of woody species in peat swamp forests has been shown to be so highly sensitive to moisture, wherein if the germinated seedlings become either submerged or desiccated they are not likely to survive (Kobayashi 2016, Blackham *et al.*, 2013, 2014). Results and synthesis from these field surveys undertaken by Bruenig and Huang (1989), Kobayashi (1998, 1999) and Anderson (1961) on the coastal peatlands in Northwestern Borneo all pointed to little natural regeneration of the canopy species, but vigorous regeneration of ferns and herbs. Logged peat domes have been observed to shift from pure stands of highly valuable and

high biomass *Shorea albida* to a new domination of wind dispersed, medium stature woody species that either dominated later vegetation communities (e.g. *Cambretocarpus rotundatus*) or did not normally grow in peatlands (e.g. *Macaranga* spp.; Blackham *et al.*, 2013, 2014); and ferns (especially *Pandanus andersonii* and *Nephrolesis biserrata*, Kobayashi 2000, Cheng 2016 - unpublished).

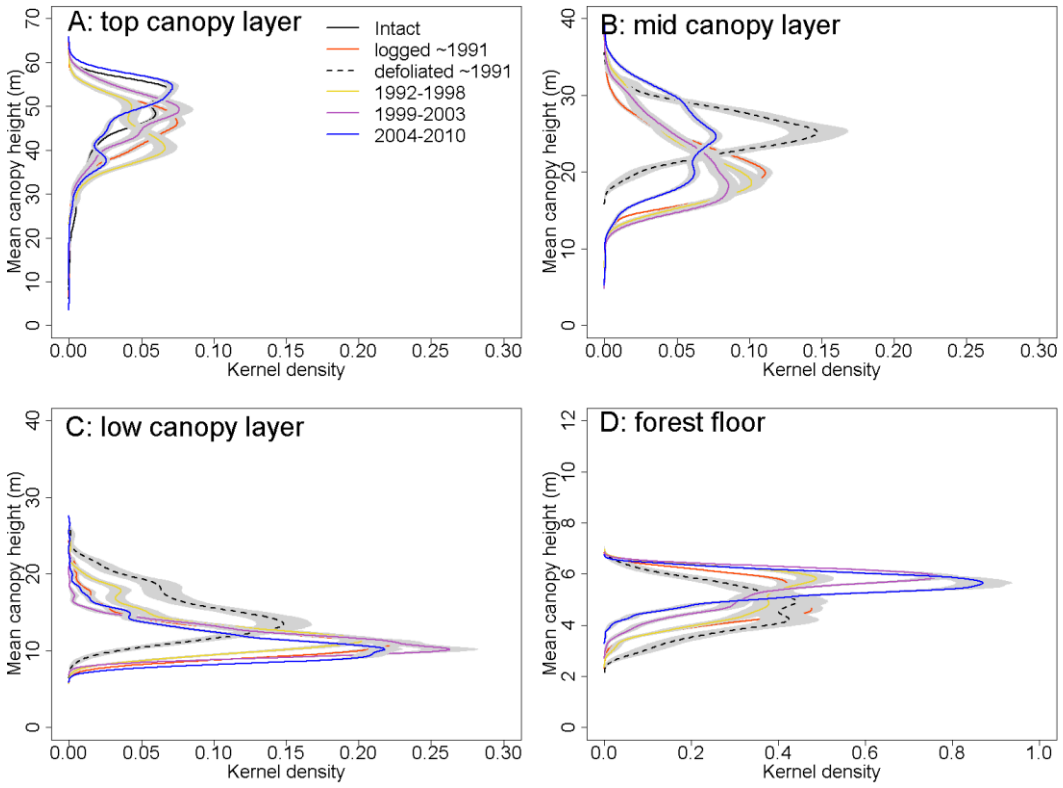

Figure 4.2: Mean canopy height observations in the top layer (>= 45m, panel A), in the mid-layer (15-45m, panel B), in the low layer (6.5-15m, panel C) and on the forest floor (<= 6.5m, panel D).

To assess recovery dynamics for different vertical strata as a function of time since disturbance, we stratified the vegetation canopy into four layers (>= 45m – top canopy layer; 25-45m – mid-canopy layer; 6.5-25m – low-canopy layer; and <= 6.5m – forest floor; figure 4.2) and partitioned the logged area by epoch of deforestation (before 1991, 1992-1998, 1999-2003 and 2004-2010) (Figure 4.2). We found that all epochs of logging retained tall stems with heights greater than 45m. The insect defoliated area did not have any trees taller than 45m, but had a substantially higher stem density for mid-canopy height trees (25-45m) than the logged areas (Table 4.1). The defoliated area was present at the start of our time series in 1991. The precise date of defoliation is unknown, but previous accounts in the area suggest it could have occurred as early as the 1960s (Anderson 1964). The observed lack of a top canopy layer (trees taller than 45m) in the defoliated area is likely due to the defoliated

Epoch	**Density of >= 45m trees (± 95 C.I)**		**Density of 25- 45m trees (± 95 C.I)**	
	Mendaram	**Damit**	**Mendaram**	**Damit**
Intact	72 ± 12	56 ± 2	238 ± 31	NA
Pest defoliation (prior to 1991)		NA		31 ± 5
Logged 1988-1991		2 ± 1		6 ± 1
Logged 1991-1994		2 ± 1		5 ± 1
Logged 1999-2003		4 ± 1		6 ± 1
Logged 2004-2010		5 ± 1		8 ± 1

Table 4.1: Stem density of trees (25-45m and >= 45m) in intact and disturbed forests

trees becoming vulnerable to mortality from lighting and further susceptible to wind throw and branch breakage. Only the defoliated area has higher mean canopy height from the other epochs of disturbance (Figure 4.2). The only epoch with vegetation present in all layers was for 2004-2010, suggesting that logging in this area was selective and did not completely clear all vegetation.

Our results temporally and spatially extend previous plot-based, episodic observations of regeneration dynamics in logged *Shorea albida* forests (Bruenig and Huang 1989, Kobayashi 1998, 1999 and Anderson 1961) to a 25-year chronosequence across more than 5,000 hectares of peatlands at various stages of degradation. The mean vegetation heights for intact forest, defoliated forest and different epochs of deforestation (before 1991, 1992-1998, 1999-2003 and 2004-2010) in Damit were 46.7 ± 0.86m, 21.0 ± 0.67m, 14.6 ± 0.90m, 14.9 ± 0.80m, 15.6 ± 0.80m, 16.1 ± 1.0m, and 20.9 ± 0.70m, respectively. For intact forest, and different epochs of deforestation (before 1991 and 1992-1998) in Mendaram, the canopy heights were 44.9 ± 1.0m, 23.3 ± 1.2m and

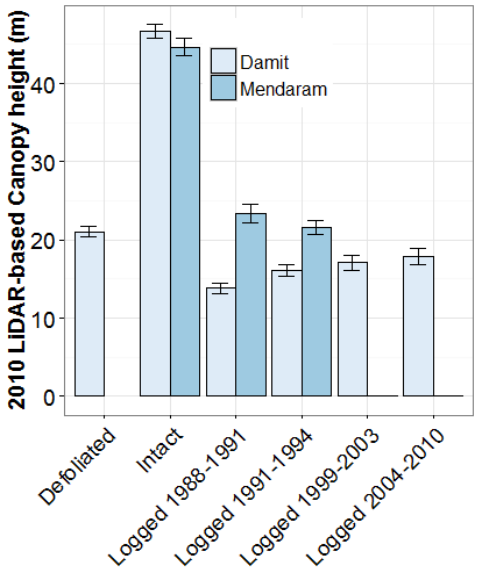

Figure 4.3: Mean canopy height by land use (Intact, logged by 1991, logged between 1991 and 1994, logged between 1999 and 2003; and logged between 2004 and 2010). Note that there was no height for Mendaram in the most recent two epochs due to LiDAR availability. Pest defoliation was only observed in Damit.

21.2 ± 0.90m (figure 4.3), suggesting little change in aggregate forest structure with time since disturbance. Canopy trees had a mean density of 2-4 trees ha^{-1} (>= 45m) and 5-8 trees ha^{-1} for mid-canopy trees (25-45m) (table 4.1). Many of the stand-alone canopy trees were left behind as seed trees or due to unsuitable timber quality. Visual inspection showed that they remarkably survived in a drastically changed post-logging environment (e.g. stronger wind disturbances, higher lightning susceptibility, higher pH and flood risk), with densities largely unchanged through time (table 4.1). Possible reasons for their survival included the lack of lianas in Bornean forests and the root mat *Shorea albida* forms with the forest floor (Furukawa 1998a; Anderson 1983).

Using the same stem recognition method (section 4.2.2), we found canopy stem densities in nearby intact forest in Damit (5-5.5m in dome elevation) and in the intact forest transect in Mendaram (~6m in dome elevation) to be 56 ± 2 trees ha^{-1} and 56 ± 8 trees ha^{-1}, respectively. The latter was within the same CI with the stem density for trees >= 45m found via ground survey in Mendaram (Nguyen *et al.*, 2016) at 72 ± 12 trees ha^{-1}, which gave us confidence to proceed and compare canopy stem densities before and after logging. At Damit, comparing the canopy stem densities before and after logging, assuming a space-for-time substitution with the chronosequence, suggested that logging removed at least 90% of the original stem density, which implied further destruction on the understory due to the felling and uprooting of these tall individuals.

The similarity of low mean canopy heights (about ¼ to 1/3 of the canopy height of the intact forest) in all layers and deforestation epoch across a 25-year chronosequence

suggested a state of arrested succession. To explore for signs of regeneration we analyzed the distributional difference in LiDAR height above 6.5m in order to avoid confusion with non-woody plants, particularly the *Pandanus andersonii*. *Pandanus* is a palm-like, dioecious early colonizer genus that typically does not grow taller than 6.5m (Kobayashi 2000). The layer between 6.5 and 25m is the area where we would expect to see a temporal evolution in stand structure associated with tree growth and woody regeneration, but there were no significant differences in the height structure as a function of time since disturbance (fig.4.2). Examining the height structure closer to the edge of the intact forest boundary (within 800m) indicated a similar lack of temporal evolution in stand structure, suggesting that both remaining forests and residual, isolated canopy trees (seed trees) did not yield a sufficient number of new viable seedlings. Alternatively, it was also possible that saplings died shortly after establishment as previously noted by Kobayashi (1998). Given that *Shorea albida* masts approximate every 3-7 years (Curran *et al.*, 1999) with an approximate dispersal distance of up to 800m from the seed tree (Blackham *et al.*, 2014), this 25-year chronosequence suggested that the business-as-usual logging operation in Brunei failed to leave the forest in a condition in which natural regeneration can proceed.

Natural regeneration of *Shorea albida* in logged peatlands is typically limited by the periodicity of masting, distance to seed source, quality of seed rain and the absence of a seed bank as well as few dispersal agents, while artificial regeneration is both costly and has not been clearly proven to be effective (Blackham *et al.*, 2013, 2014; Curran *et al.*,

1999). The challenges to seedling establishment and sapling survival in logged-over and degraded PSF could be linked back to the high interdependence between peat, vegetation and water (Page *et al.*, 1999), which would be altered by canopy removal and subsequent hydrological changes (Page *et al.*, 2008). The high water holding capacity and low bulk density in intact peatlands made it very easy to desiccate during periods of no rain but also easy to be flooded after heavy rainfall (Kobayashi 1998). Measurements in the area have found that with the removal of the vegetation cover, the peat surface oxidizes and decomposes in the presence of dissolved oxygen in pore water, has higher surface temperature and radiation inputs (Kobayashi 2016), enhanced enzyme activities (Gandois *et al.*, 2013), up to a doubling in pH level (Kobayashi 2016), and/or have the peat compact under the weight of the machinery used for extraction and transport of logs (Page *et al.*, 2008). Compaction, compression and decomposition can all lower the peat surface. At the same time, with the absence of trees and lower transpiration, more surface water may be present. As a result, there may be an increase in flood risk either from heavy precipitation or tidal influence, the latter of which can result in salt intrusion and substrate acidification from the humic acids and the underlying mangrove mud. Flood tolerant ferns, often already in the forest floor community beneath the *Shorea albida* canopies, have been previously observed to grow vigorously within 10 months of clear cut (Kobayashi 2000). The increased wetness, increased substrate acidity and salinity, competition for light on the forest floor and high sensitivity to hydrological changes all

likely contribute to low *Shorea albida* seedlings survival at Damit (Page *et al.*, 2008; Kobayashi 1998).

The changes in vegetation composition and woodiness at the Damit peat dome implied dramatic losses in aboveground biomass, which in turn may alter the amount and quality of litter inputs and affect production and biogeochemistry of the new peat. From among the few studies that attempted to estimates biomass in logged *Dipterocarp* forests, the percentage of biomass loss immediately after logging was at least 50% that of the intact forest (Berry *et al*., 2010; Saner *et al.*, 2012). After 22-40 years, recruitment of pioneer species increased biomass to about 15-28% lower than that of the intact forest (Saner *et al.*, 2012; Okuda *et al.*, 2003). For the Damit peat dome, the reduction in aboveground biomass is primarily due to the removal of woody biomass and the resultant dominance of non-woody plants in the regrowing vegetation. Laboratory experiments have demonstrated that leaves from secondary forest trees (e.g. *Macaranga* spp.) decompose faster than *Pandanus* spp., altering nutrient availability but also changing the quality of newly formed peat (Yule and Gomez 2009; Lim *et al.*, 2014).

4.3.2 Ground-hydrology-vegetation interactions

To explore short-term (0-6 years post-disturbance) and long-term (14-20 years post-disturbance) disturbance dynamics in terms of surface hydrology we characterized the active radar backscatter variations associated with forest clearing and regrowing stages across both peat domes. In forests, including forested wetlands, active radar is thought to

interact with the canopy, the forest floor and soil (moisture) via three main scattering mechanisms, which, in incremental backscatter strength, are surface, volume and double bounce scattering (fig.4.6) (e.g. Hess *et al.*, 2003; Siqueira *et al.*, 2003; Salas *et al.*, 2002; Lucas *et al.*, 2007). Surface (or specular) scattering is when only one reflection occurs (i.e. mirror-like). Volume (diffuse) scattering is where multiple reflections at differing angles occur. Double bounce scattering referred to the coherent reflection of a radar signal as it scattered from a branch or a trunk component to the ground, and back to the instrument. Double bounce is believed to be enhanced in inundated forests because the ground water surface is very reflective in the specular direction (i.e. forward scattering).

The observed backscatter for both the Damit and Mendaram domes spanned the range of all three dominant scattering mechanisms including double bounce returns from flooded forests (highest), volume scattering within dense canopy (medium) and those resulting from specular (surface) scattering over open water (lowest) or over smooth forest floor (Hess *et al.*, 2003; Siqueira *et al.*, 2003; Salas *et al.*, 2002; and Lucas *et al.*, 2007). The pre-1991 logging area in Sarawak, across the border from the Mendaram dome (area 2, figure 4.4), was dominated by surface scattering. Volume scattering was present through the interior intact forests in both Mendaram and Damit. Double bounce scattering was observed in both the open mixed swamp riverine forests and along log landings and light railways in Damit (area 3, figure 4.4). These areas had woody debris from logging and isolated standing trees that were clearly visible from Google Earth images for 2001 and high resolution aerial photos for 2010. The increase in scattering

was only temporary, as the abundance of double bounce scattering in the 1991-1994 logging area appeared in August 1993 (area 1, fig. 4.4A), but not in June 1995 (area 1, fig. 4.4C). Similarly, double bounce scattering was present in the southern portion of the pre-1991 logging area in Sarawak in January 1996 (area 4, fig. 4.4B), but not in February

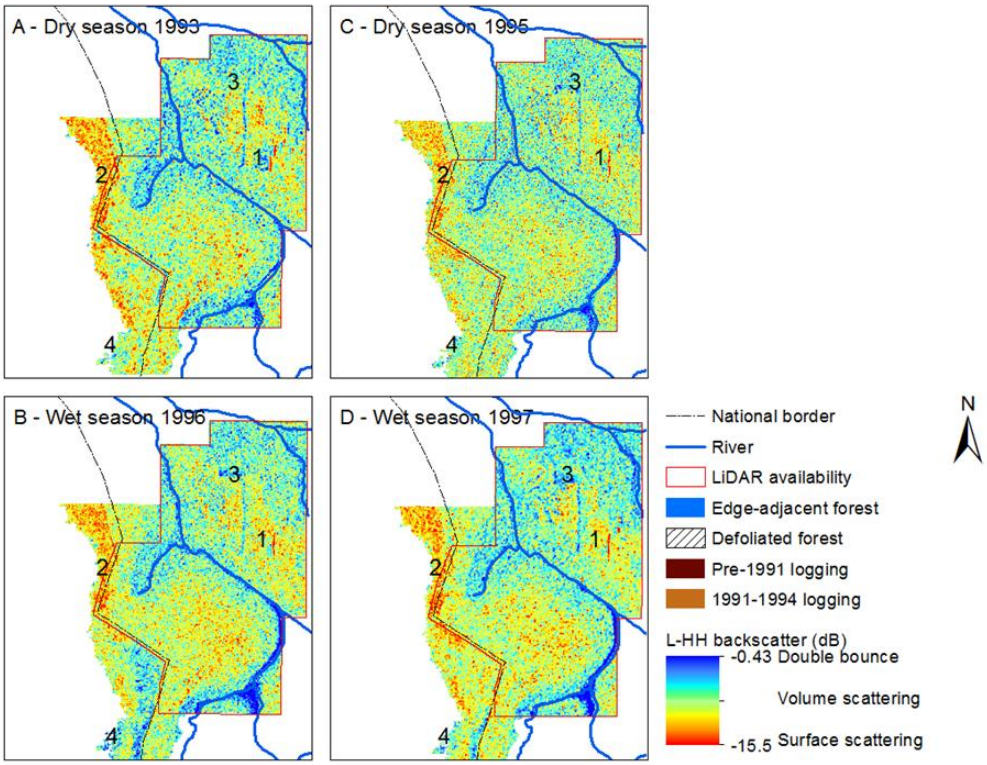

Figure 4.4: Spatial variability of JERS-1 data in August 1993 (dry season, panel A), June 1995 (dry season, panel C), January 1996 (wet season, panel B) and February 1997 (wet season, panel D).

1997 data (area 4, fig. 4.4D). This ephemeral signal was likely due to (i) vegetation regrowth attenuating or masking the ground-trunk backscatter and (ii) woody debris drying under enhanced surface temperature and radiation, lowering the dielectric constant

and the scattering ability. Signals from intact forests were stable between seasons, across the years and between two peat domes. Overall, intact PSF at -8.59 ± 0.10 had a lower

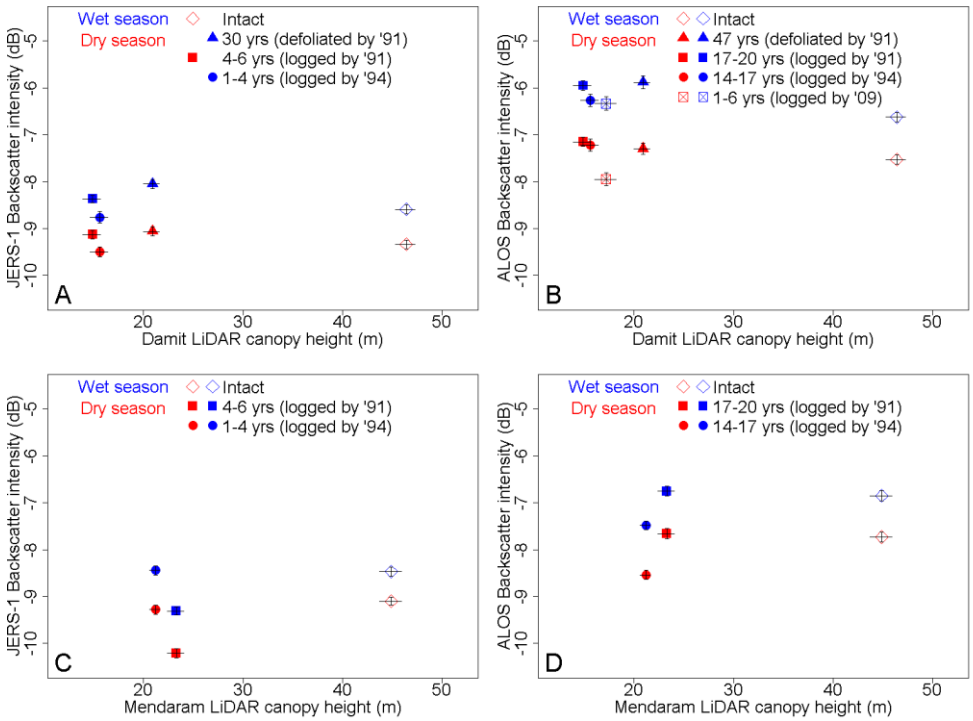

Figure 4.5: A: Means (± 95 CI) of JERS-1 L-HH backscatter for intact forest and logged forests of different ages (1-4 years, 4-6 years, 30 years) at Damit. B: Means (± 95 confidence interval) of ALOS L-HH backscatter for intact forest and logged forests of different ages (1-6 years, 14-17 years, 17-20 years and 47 years) at Damit. C: Means (± 95 CI) of JERS-1 L-HH backscatter for intact forest and logged forests of different ages (1-4 years, 4-6 years) at Mendaram. D: Means (± 95 confidence interval) of ALOS L-HH backscatter for intact forest and logged forests of different ages (1-6 years, 14-17 years, 17-20 years and 47 years) at Mendaram.

backscatter than what was reported from the Amazonia (-7.89 dB) (Siqueira *et al.*, 2003), perhaps due to its taller canopy heights (> 47m vs 35m), higher aboveground biomass (222 ± 24.4 Mg C ha^{-1} vs 150 Mg C ha^{-1} and higher percentage of biomass from the top

canopy layer (81% vs 33%) (Nguyen *et al.*, 2016 and Malhi *et al.*, 2006, respectively), which could increase signal attenuation and reduce backscatter.

We found no statistically significant differences in the backscatter between intact forest and logged forests, nor across different logging age classes in the same season in the same peat dome by land cover type nor as a function of mean canopy height (figure 4.5).

The differences in mean backscatter across land use types in the same season were within one standard deviation for backscatter of each land use type (see discussion of two exceptions below). Intact forests likely had similar backscatter with old clearings due to similar surface scattering from an even canopy in intact *Shorea albida* forest (Anderson 1964) and that from a thick herbaceous cover post-logging (Kobayashi 2000). In newly logged forest areas (1-6 years old clearing),

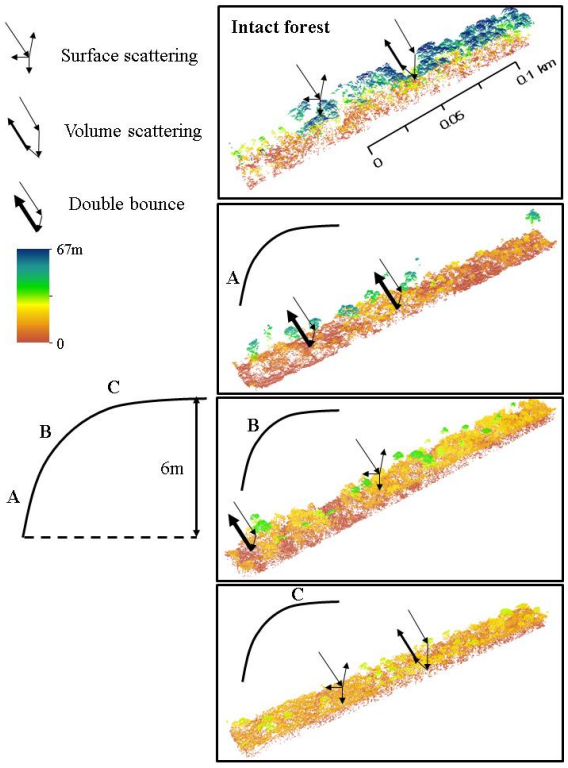

Figure 4.6: Conceptual diagram of the behavior of L-HH backscatter from an intact, forested landscape to that from a logged forest at various dome elevations in a peat dome (panels A-C). All panels displayed a 50m by 500m transect from raw LiDAR data at selected dome elevation.

all three kinds of scattering contributed to the overall backscatter (Rignot *et al.*, 1997): double bounce from either a wetter surface or felled trunks and standing trees; volume scattering from isolated stands and the thick herbaceous cover; and single scattering from lying debris and hence were not distinct from intact forests. We then compared the empirical results in table 4.2 with the theoretically expected values and trends of L-HH backscatter at 40 degrees incidence angles as a function of structural density for forest of similar biomass density with peatlands (Imhoff 1995, figure 9). Our L-HH backscatter statistics suggested four times higher vegetation density, expressed in terms of vegetation cover/ volume, from intact forest to newly cleared forest and a two times higher vegetation density from intact forest to regrowing forest. This confirmed the presence and near-term dominance of herbs and ferns and the compounding effect that forest structures had on interpreting L-HH backscatter (Imhoff 1995).

Differences between the L-HH backscatter from intact and logged forests were very small, differing by less than 1.0 dB between dry and wet seasons and between two domes for the same logging age and season (Table 4.2 and Figure 4.5). It was impossible to separately quantify the effect of dense regrowth and that of changing hydrology from these L-HH data since the height of regrowing vegetation and intact forests at 6m and more than 47m, respectively, could attenuate any signal from changing soil moisture. Moreover, due to the waterlogging nature of the soil and near-surface water table, relatively small shifts in hydrology could result in changes in L-HH backscatter. The defoliated forest (>5.5m above sea level) and recently logged forests (between 2003 and

2009) in low dome elevation (3-4m above sea level) showed significant differences in seasonal means (figure 4.5 panel B). Between a dry season mean of -7.95 ± 0.14 and a wet season mean of -6.33 ± 0.14, the seasonal difference for the recently logged forest. Between a dry season mean of -7.30 ± 0.12 and a wet season mean of -6.81 ± 0.10, the seasonal difference for the recently logged forest was 1.42dB. These seasonal differences were 1.5 and 1.25 times the seasonal difference in intact forests, implying a higher likelihood of changing soil moisture and soil-vegetation interactions. In the case of the 2003-2009 logged forests at low dome elevation, we hypothesized that the difference was due to low vegetation cover in the dry season and interactions between enhanced flooding in the wet season and woody debris from recent logging activities. Log transport railways were visible between 2004 and 2010 in the imagery, making the peat particularly vulnerable to compaction and compression. In addition, at low elevation, the surface peat tends to be more decomposed (sapric), with a higher bulk density (Esterle and Ferm 1994). Others have observed very large increases in peat pH in newly logged area and elevated surface temperature, potentially accelerating surface peat decomposition (Kobayashi 2016). The combination of compaction, compression and decomposition would increase flood risk in the wet season but also drainage in the dry season, which could widen the seasonal difference in L-HH backscatter (Dommain *et al.*, 2010). In the case of the defoliated forests, we hypothesized that a fibrous peat surface (Esterle and Ferm 1994) coupled with more isolated, defoliated trunks (Anderson 1961) were responsible for enhanced backscatter in the wet season.

Given two multi-temporal chronosequences of L-HH backscatter (1993-1998, and 2007-2009) that were 10 years apart, we proposed a conceptual model to contrast the behavior of L-HH backscatter from an intact forested peatland (top panel) to that from a logged peatland at various dome elevations (figure 4.6). Intact PSFs with a pure stand of *Shorea albida* are dominated by surface scattering and volume scattering, with the latter likely in the cases where the signal penetrated the thin, broccoli-like canopies. When logging occurs near the edge of the dome, where access was the easiest and river flooding most likely, double bounce scattering can dominate due to the interactions between flooding episodes and woody debris and standing isolated stems (fig. 4.6A). As logging proceeded upslope of the peat dome, where regrowth can be vigorous (section 4.3.1) or where a thick understory was present (fig. 4.6B), surface scattering can also occur. At the top of the peat dome (fig. 4.6C), where soil moisture is lowest and stem density is highest (Anderson 1983), surface and volume scattering occurs, producing similar overall backscatter to that of an intact forest (table 4.2 and figure 4.4).

As the temporal differences between forest conditions (intact, logging, and different domes) were within the calibration accuracy of the sensor (1.0 dB), the separability of peatlands at different clearing and regrowing stages in terms of L-HH backscatter was low. We find that the use of multi-temporal radar remote sensing for the purpose of hydrological monitoring in deforested, but undrained and unburnt peatlands for restoration and conservation purpose would be challenging given the complexity and heterogeneity of peatlands (*c.f.* Jaenicke *et al.*, 2011). As we demonstrated in section

4.3.1, even in the absence of drainage and fire, logged peatlands are likely subject to enhanced decomposition and increased flood risks, often requiring intensive restoration efforts. Further, monitoring using interferometry SAR and coupling with ground measurements of forest structure and water table could allow for the differentiation of signals from each scattering mechanism and that of changing hydrology and ground-vegetation interactions.

4.3.3 Edge dynamics

We investigated forest structure variations and canopy-soil interactions along two edge areas between logging and intact forests in Damit and Mendaram. By studying forest structure and microwave data near the edge and in the transition from the logged forest into the intact forest, we asked the following questions: (i) Do forest structures (stem density, canopy height, gap fraction) and canopy-soil interactions (indicated by microwave data) vary as a function of distance from the edge? (ii) Did the patterns of variation with distance from the forest edge change with time since edge creation (0-4 years vs 20-24 years)? and (iii) Were these patterns the same across two domes (Damit and Mendaram)? Why (not)?

When a patch of forest becomes isolated or interfaces with converted lands they can become very different environments from continuous intact forest or the central areas of large patches (Kapos 1989). Laurance *et al.* (2002) identified three phases of edge evolution: initial isolation, edge-closure, and post-closure. In the initial isolation phase

(<1 year after edge formation), the gradient between the forest interior and edge is steepest, with hot, dry conditions and increased light and wind penetrating into the fragment. There is often a dramatic pulse in tree mortality with many trees dying standing (Kapos 1989, Kapos *et al.*, 1997; Laurance *et al.*, 1998), of which large trees are particularly vulnerable (Laurance *et al.*, 2000). During the edge-closure phase (1–5 years after edge formation), secondary vegetation and lateral branching by edge trees progressively seals the edge, making it less permeable to microclimatic changes (Carmago and Kapos 1995). Edge gradients in microclimate become more complex, but do not disappear entirely (Kapos *et al.*, 1997). Broadly, plants near the edge die or become physiologically acclimated to edge conditions. Laurance *et al.* (2002) found that treefall gaps proliferate within the first 100–300 m of edges, partly as a result of increased wind throw. In the post-closure phase, wind throw remains elevated near edges, despite the fact that the edge is partially sealed by secondary growth. Turnover rates of trees increase near edges because of elevated tree mortality and recruitment of short-lived pioneer species. Pioneer plants replace leaves rapidly, contributing to the accumulation of leaf litter near edges. Although edge closure occurs quickly in tropics because of rapid plant growth, edges are still more dynamic and vulnerable to climatic vicissitudes than are forest interiors (Laurance *et al.*, 2002). Beyond changes in the energy and water budgets, edge influence can lower the biomass in the edge forests by as much as 25% compared to the forest interiors (Chaplin-Kramer *et al.*, 2015). In addition, edge-effect intensity varies markedly in space and time, and is influenced by factors such as edge

age, the number of nearby edges, and the adjoining matrix of modified vegetation surrounding fragments (Laurance *et al.*, 2011).

LiDAR data acquired in 2010 and ALOS L-HH backscatter in 2008-2009 allowed the comparison of several edges at MD and DT in their post-closure phase (figure 4.7, b and c). Data in figure 4.7 represented 100m x 100m pixels. We relied on our land use land cover change map (fig.4.1) to determine the edge zone. Distance to edge was calculated as the Euclidean distance between the center of a non-edge 1-hectare pixel and that of its closest edge pixel. Mendaram has two edges (MD1 – fig. 4.7 and MD2 – fig. 4.8) that were created in as early as 1984 and 1994, respectively, while the Damit study edge (DT1 – fig. 4.9) opened in 1994. In addition, MD1 was susceptible to several drainage canals as of 20087, while MD2 was selectively logged between 2004 and 2008, leaving DT1 the only edge that was subjected to only clear-cut and no additional disturbance. Finally, both MD1 and MD2 are down sloped from where logging occurred, whereas DT1 upslope from logging. We selected several Landsat images during the dry season (May 1994, March 1997, July 2007 and May 2008) and reported the progression of EVI and backscatter as a function of distance to edge and with time.

At MD1, 10-13 years after logging occurred, dry season EVI in 1994 were higher in the formerly logged area (0.21 ± 0.013) than that in the intact forest (0.18 ± 0.015), indicating that some regrowth occurred but the edge between intact and logged forests remained clearly delineated in the Landsat imagery (figure 4.7 panel A top plot). Dry season JERS-1 backscatter for 1994 and 1997 in logged forest was lower (-10.51 ± 0.64

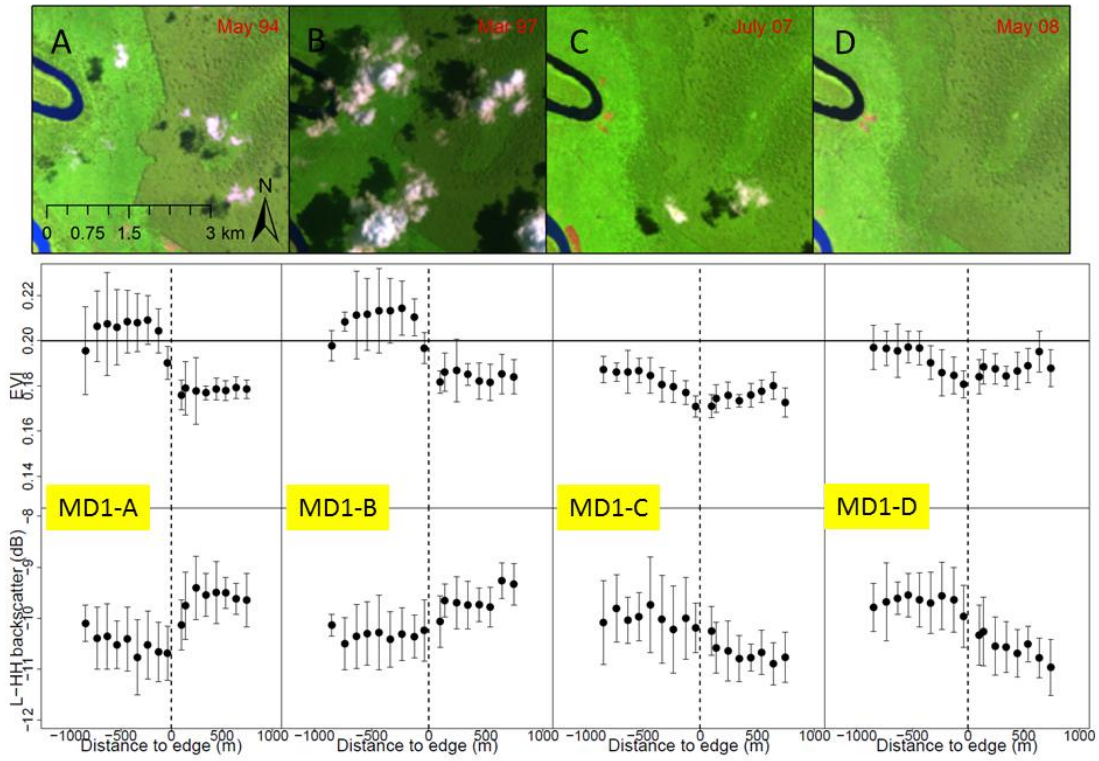

Figure 4.7: MD1 was clear-cut in as early as 1984, and then drained as of 2007, as shown in false color Landsat composite in 1994, 1997, 2007 and 2008. Edge dynamic at MD1 demonstrate a decline in 1994 EVI and an increase in backscatter (panel A top and bottom) moving from the logged to the intact forest. The 1997 EVI and backscatter (panel B top and bottom), 2007 EVI and backscatter (panel C top and bottom) and 2008 EVI and backscatter (panel D top and bottom) were plotted against distance to edge illustrating the time evolution of the signal. The edge was indicated with a dash (--) line.

dB and -10.31 ± 0.55dB, respectively) compared to intact forests (-9.77 ± 0.74 dB and -9.87 ± 0.61 dB, respectively) (figure 4.7 panels A and B bottom plot), suggesting lower surface moisture, consistent with previous observations of to reduced evapotranspiration in high EVI grasses/shrubs (citation). By 2007, 23-26 years after logging (figure 4.7

panel C top plot), the edge between intact and logged forests became blurred, indicating additional regrowth, with the mean dry season EVI in 2007 showing no significant difference between intact (0.175 ± 0.01) and logged forest (0.18 ± 0.008). However, a two-tailed F-test rejected the null hypothesis that the variance of EVI in logged and intact forests do not differ (p-value = 0.00036). In fact, ratio of variance between intact and logged forest was 0.2, suggesting that this regrowth in the logged forests may have comparable EVI, but was a different vegetation community with more woody stems compared to that in the 1990s (figure 4.7). Our stem detection algorithm (section 4.2.3) estimated stem density for trees >= 25m in 2010 in the logged and intact areas on either side of MD1 at 150 ± 10 trees ha^{-1} and 100 ± 12 trees ha^{-1} respectively. The increased abundance of woody stems might have enhanced interactions between water and vegetation, resulting in more backscatter on the logged side of the edge (fig. 4.7 panels C and D).

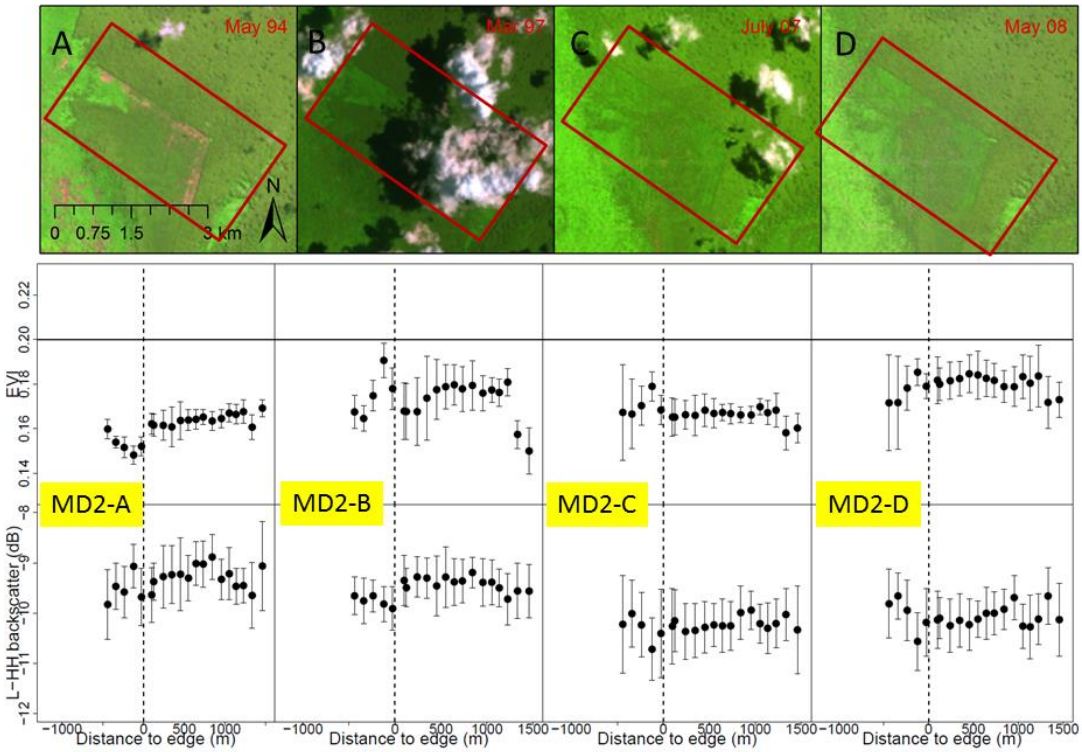

Figure 4.8: MD2 was fragmented in 1994, but selectively logged during the late 2000s, as shown in false color Landsat composite in 1994, 1997, 2007 and 2008. Edge dynamic at MD2 where 1994 EVI and backscatter (panel A top and bottom), 1997 EVI and backscatter (panel B top and bottom), 2007 EVI and backscatter (panel C top and bottom) and 2008 EVI and backscatter (panel D top and bottom) were plotted against distance to edge. The edge was indicated with a dash (--) line.

At MD2, an area fragmented in 1994 and selectively logged in the mid-2000s, dry season EVI and JERS during 1994-1997 (figure 4.8 panels A and B) were within one standard deviation between logged (0.149 ± 0.01 for EVI 1994 and -9.51 ± 0.72dB for JERS 1994) and intact forests (0.163 ± 0.109 for EVI 1994 and -9.25 ± 0.55dB for JERS 1994), with clear declines in both EVI at the Malaysia-Brunei border associated with

cutting (delineation) at the national boundary (figure 4.8). The backscatter signal at the border was less pronounced than the EVI shifts. Selective logging in the mid-2000s appeared to maintain similar EVI on both the logged and intact sides (0.169 ± 0.01 and 0.166 ± 0.005, respectively – figure 4.8 panel C and D top plots), hence the similar ALOS backscatter (-8.49 ± 0.49 and -8.23 ± 0.49, respectively – figure 4.8 panel C and D bottom plots). However, again a two-tailed F-test rejected the null hypothesis that variances of EVI in logged and intact forests are the same with p-value < 1e-9. This either indicated patchy, non-uniform ongoing regrowth in logged forests to approach that of intact forest or a level of selective logging that EVI cannot distinguish between logged and intact forests (figure 4.8). Alternatively, the presence of an edge signal persisted through time and regeneration along the edge might have contributed to the higher variance in EVI.

Finally, at DT1, within 5 years since logging, dry season EVI observations showed signs of regrowth (logged EVI = 0.19 ± 0.02, intact EVI = 0.17 ± 0.01), but the edge between intact and logged forests was still well-delineated (figure 4.9 panels A and B).

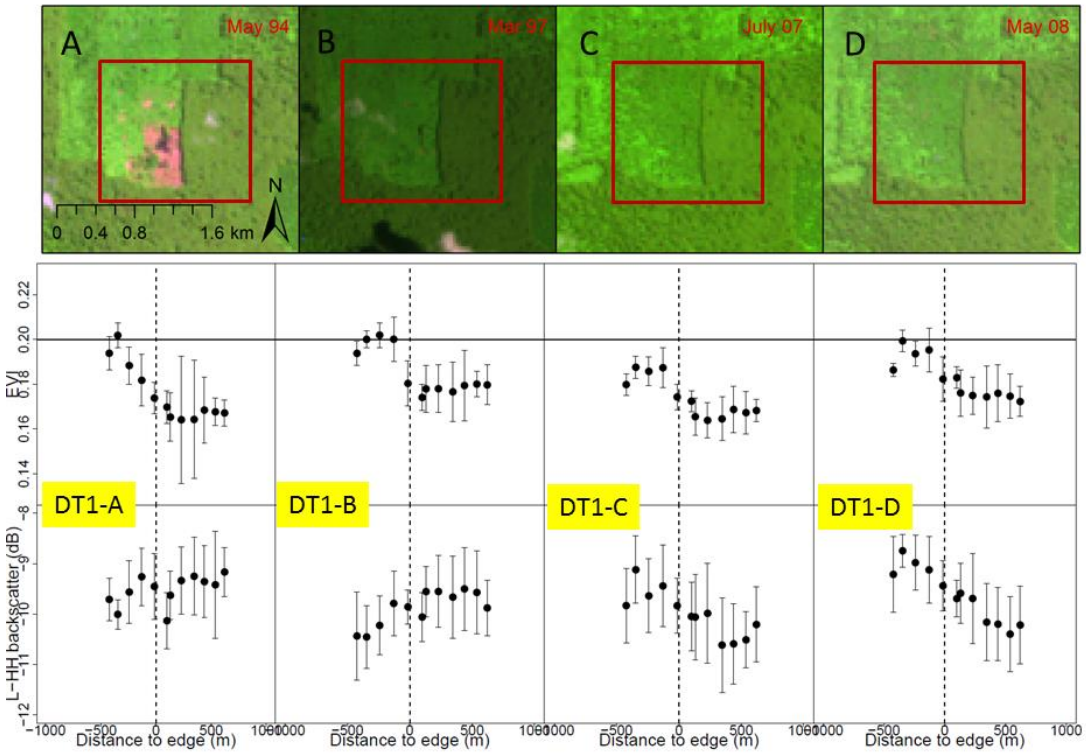

Figure 4.9: DT1 was clear-cut in 1994, as shown in false color Landsat composite in 1994, 1997, 2007 and 2008. Edge dynamic at DT1 where 1994 EVI and backscatter (panel A top and bottom), 1997 EVI and backscatter (panel B top and bottom), 2007 EVI and backscatter (panel C top and bottom) and 2008 EVI and backscatter (panel D top and bottom) were plotted against distance to edge. The edge was indicated with a dash (--) line.

However, in 2007, 13 years since logging, dry season logged EVI decreased to 0.18 ± 0.01, approaching intact forest's EVI at 0.17 ± 0.01 (figure 4.9 panel C top plot). In addition, a two-tailed F-test comparing intact and logged EVI in 1994 and then those in

2007 showed that the ratio of variance between intact and logged EVI increased from 0.2 in 1994 to 0.6 in 2007, indicating structural heterogeneity within the regrowth communities. With the increasing EVI with time since logging, the logged area also became wetter in the area downslope of intact forest (-6.80 ± 0.77 and -7.77 ± 0.79 respectively – fig.4.9 D), likely reflecting reduced evapotranspiration and drainage downslope from the remaining intact forest. The combination of patchy regeneration and increased presence of water might explain the markedly enhanced ALOS backscatter on the logged side of this edge in the late 2000s (Figure 4.9 panel C and D bottom plots).

We investigated whether we could distinguish different modes of regeneration from EVI and backscatter at each of the edges. Using the Pearson Product-Moment Correlation test, no relationship existed between backscatter and EVI within each epoch of logging or with the mode of regeneration (clearing in 1984 vs clearing all in 1994 vs selectively logged during the mid-2000s) (p-values were 0.02 for logged forest at MD1, 0.00014 for logged forest at MD2, and 0.00039 for logged forest at DT1). Moreover, despite similar technical specifications, JERS and ALOS data were not on the same numerical scales and did not seem to show consistent results across the two sensors (Figure 4.7, 4.8 and 4.9), preventing us from further exploring the backscatter time series. Wind direction, which was northeasterly and the strongest during the rainy season (November – March), did not have any detectable effect on the above trends or lack thereof.

We next looked for a relationship between mean EVI at 1 hectare grids over forests logged in 1994 and intact areas at Damit and mean canopy height as a potential indicator of different modes of regeneration. In contrast to the CHM results which indicated little changes in vegetation structure with time since disturbance (see section 4.3.1), the edge

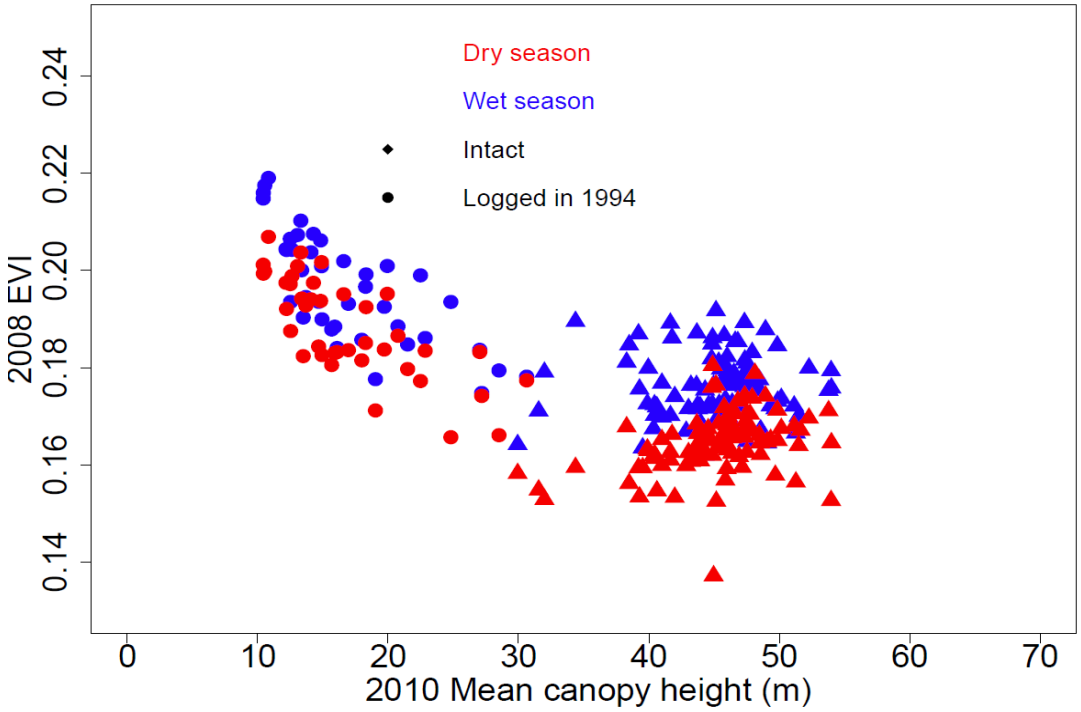

Figure 4.10: The relationships between dry season and wet season EVI and mean canopy height for logged (filled circles) and intact forests (filled triangles). Each data point represented 1 hectare. The adjusted R^2 for dry and wet season relationships were 0.47 and 0.43 respectively.

dynamics demonstrated a clear regeneration signal shortly after logging. An assessment of the EVI and CHM as a function of season and disturbance status indicated clear piecewise linear relationships. The slope of the relationship between the 2008 EVI and 2010 mean LiDAR canopy height for the logged and intact areas shifting from -0.0015 ±

0.0001 to 0 ± 0.0001, respectively (fig. 4.10). The intercept values in the logged area differed by season, but the slopes between EVI and height were indistinguishable at -0.0015 and -0.0014 for dry and wet seasons, respectively. This suggested that as more regeneration of woody biomass overtopped the colonizing *Pandanus* understory, standard deviation in EVI would keep increasing due to more vertical difference in canopy height, while mean EVI would keep decreasing due to less density in vegetation growth form. The EVI and height relationship breaks down when the top canopy layer is becomes fully established.

The three different edges in the Damit and Mendaram peat domes we just examined revealed the heterogeneous edge dynamics in peatlands through time and space, driven by harvesting history and regrowth dynamics. Edge dynamics as functions of up to 1km distance to edge in two edges on two different domes and of different edge ages (MD1 – fig.4.7 and DT1 – fig.4.9) were more similar with each other than two edges on the same dome (MD1 – fig.4.7 and MD2 – fig.4.8). At MD1 and DT1, in the edge closure phase (0-5 years after edge creation), there were clear differences in EVI (greenness), where logged forest had higher EVI than did intact forest, suggesting regrowth in the former. At the same time, logged forest had lower backscatter than intact forests, indicating more surface scattering from the regenerating non-woody vegetation, which has smoother surface. As time progressed, 13 years after edge opening at DT1 and 23 years after edge opening at MD1, continued regrowth development resulted in similar EVI in logged and intact forests, while the spatial trends in backscatter reversed with logged areas having

higher backscatter, suggesting enhanced double bounce backscatter from higher density of woody stems. MD2 differed from both MD1 and DT1 in terms of harvesting history with MD2 being only fragmented in 1994 and then selectively logged in the late 2000s while MD2 was already clear-cut as early as 1984. And despite both being opened in 1994, the DT was clear-cut in 1994 with no subsequent major disturbances. The relationship between EVI and mean canopy height above might offer some utility in seeing how harvesting history led to different EVI trajectories, and hence regrowth dynamics in the logged areas compared to the intact forests.

4.4. Summary & Conclusions

In this study, we examined the regrowth dynamics of two peat domes in Brunei, Damit and Mendaram. After more than 25 years of harvesting, management and disturbances, the remaining intact area for the two peatlands combined was approximately 40% of the original area that we investigated. Our results temporally and spatially extended previous plot-based, episodic observations of regeneration dynamics in disturbed peat swamp forests (Bruenig and Huang 1989, Kobayashi 1998, 1999 and Anderson 1961) to a 25-years chrono-sequence across more than 7,000 hectares of peatlands at various stages of degradation (intact, logged, degraded). We observed a state of widespread arrested succession in previously logged peatlands in terms of both mean canopy height and density of canopy trees. The height structure of the logged forests showed little change with time since disturbance and a dominance of low stature non-woody species. At the same time, mean canopy height in the logged area was linearly

correlated to mean EVI while standard deviation of EVI within logged forests increased with time, suggesting the potential to use EVI statistics to study the evolving structure of regrowing vegetation through time. It has been observed that deforestation can increase flood risk, substrate acidity and salinity, competition for light on the forest floor and hence reduce the ability for trees and seedlings to survive. Given the known hydrological sensitivity of peatland tree seedlings, our results are consistent with these logging practices contributing to the low woody seedlings survival at Damit and the abundance of non-woody biomass. The early colonizing species are very flood tolerant and can outcompete seedlings of the canopy species, hence preventing its returns. These non-woody species are also lower in terms of biomass and can change both new peat quality and the nutrient characteristics of the soil. For areas naturally disturbed by insect defoliation rather than logging, taller mean canopy heights were observed, which suggested more vigorous regeneration. The variable response of defoliation versus logging disturbance, coupled with the high gap fraction in an unlogged forested peatland (chapter two), indicated an important role of gaps in natural regeneration of PSF

Harvesting strategies influenced regrowth dynamics, which in turns influenced edge dynamics in peatlands. Clear-cut areas were observed to produce similar edge dynamics within 1km inside and outside the edge despite differences in elevational gradient and edge ages (13 years vs 23 years). For intact forests fragmented by clear-cutting, the edge closure phase (0-5 years after edge creation) showed clear differences in EVI (greenness), where post-logging forest had higher EVI than did intact forest, suggesting regrowth in

the former. At the same time, logged forest had lower backscatter than intact forests, indicating more surface scattering from the regenerating non-woody vegetation, which has smoother surface. Towards the post closure phase (5-10 years after edge creation), the EVI converged between the logged and intact forests. Further, the spatial trends in backscatter reversed with logged areas having higher backscatter, suggesting enhanced double bounce backscatter from higher density of woody stems. We did not observe these trends in a 13-years old edge adjacent to a selectively logged forest, suggesting varying intensity harvesting strategy can alter the regrowth dynamics.

Just as the Biological Dynamics of Forest Fragments Project (BDFFP) in the Amazon yielded new and evolving insights after 5, 20 and 32 years (Kapos *et al.*, 1997; Laurance *et al.*, 2002, 2011), only time will prove or disprove Anderson's prediction in 1961 that the once uniform and extensive peat swamp forests in Borneo will completely give way to a new ecological equilibrium of much lower ecological value. Until now, reports on vigorous regeneration in logged PSF such as in the Maludam peat dome, Sarawak, Malaysia (Mellings *et al.*, 2007) often overlooked the biomass and ecological losses associated with the failed reproduction of the original canopy species and hence may be misleading to conservation efforts. Indonesia's ambitious 2 million hectares restoration plan primarily focuses on rewetting logged, drained and burned peatlands and assumes that once hydrology is restored vegetation will return (Indonesia's Peatland Restoration Agency 2016). The results of our studies indicated that even if a peat dome is logged and degraded, but *not drained*, natural regeneration does not seem to be sufficient for forest

canopy regeneration, even on the time scale of decades. Further, in its new ecological state, the increased flood risk, acidic substrate, herbaceous competition and severe hydrological fluctuations also affects the economics and management strategies for agricultural development on post-logged peatlands (Gaveau *et al.* 2016). Future research activities are still needed for the restoration of peatlands via rewetting and assisted regeneration (Page *et al.*, 2009), the facilitation of nutrient acquisition from ectomycorrhizal fungal communities (Jones *et al.*, 2003) and protection of degraded peatlands to allow continued regeneration and carbon accumulation (Berry *et al.*, 2010). Long term monitoring of peatlands is required (Laurance *et al.*, 2011) and should include hydrology and topology in addition to ecology.

CHAPTER 5 – CONCLUSIONS

Tropical peatlands have some of the highest carbon densities of any ecosystem and are under enormous development pressure. In Southeast Asia these ecosystems are undergoing unprecedented destruction in terms of the extent of change, rate of land cover change, and impacts on the global carbon cycle. Conservation and restoration of tropical peatlands attempts to reduce the CO_2 emissions, protect the region's highly endemic fauna and flora, and also regulate regional water supplies, climate and public health safety. This dissertation aimed to provide better estimates of the scales and trends of the ecological impacts of tropical peatland deforestation and degradation through a combination of ground measurements and optical and microwave remote sensing imagery. The findings temporally and spatially extended previous plot-based, episodic observations of regeneration dynamics in logged peat swamp forests to a 25-years chronosequence across more than 7,000 hectares of peatlands at various stages of degradation (intact, logged, degraded).

Chapter two highlighted the unique ecology of an intact forested peat dome, most notably the spatial patterns of its forest structures, gap dynamics and high carbon density. Moving up a 4 m elevational gradient, stem density increased but canopy height, crown area, and crown roughness decreased. These findings were consistent with hypotheses that nutrient and hydrological dynamics co-influence forest structure and stature of the canopy individuals, leading to reduced productivity towards the dome interior. Gap

frequency as a function of gap size followed a power law distribution with a shape factor (λ) of 1.76 ± 0.06, while total gap area accounted for 10% of dome area. Ground-based and dome-wide estimates of AGB were 217.7 ± 28.3 Mg C ha^{-1} and 222.4 ± 24.4 Mg C ha^{-1}, respectively, which were higher than previously reported AGB for PSF and tropical forests in general. However, dome-wide AGB estimates were based on height statistics, and the coefficient of variation on canopy height was only 0.08, three times less than stem diameter measurements, suggesting LiDAR height metrics may not be a robust predictor of AGB in tall tropical forests with dense canopies. This structural characterization of this ecosystem advances the understanding of the ecology of intact tropical peat domes and factors that influence biomass density and landscape-scale spatial variation. Improved ecological understanding is essential accurate estimation of forest carbon density and to effectively model the effects of disturbance and deforestation in these carbon dense ecosystems.

In chapter three I developed and implemented an approach to quantifying disturbance in aseasonal peatlands using time series of Landsat resolution vegetation moisture. For each pixel, a time series of vegetation index values was compiled, screened for clouds and noise, and then analyzed to determine whether there was a shift in its temporal trend or a change in the pixel's value with respect to the scene-wide statistical distribution during the analysis period. The algorithm explicitly tracked changes in vegetation moisture over time assuming that (i) land cover disturbances were rare phenomena for a relatively large area within a short time period; and (ii) a change must warrant a

substantial and detectable drop in vegetation moisture. The final land use land cover change map achieved more than 92% user's and producer's accuracy and revealed that after more than 25 years of harvesting, management and disturbances, the remaining intact peatland area was approximately 40% of the original area that we investigated. The harvesting practices for this area involved laying railway track on the ground, clear-cutting the forest as the tracks extend and, in the case of Mendaram, drainage and eventually plantation development.

Building from the disturbance time series in chapter three, in my final data chapter, I employed a space for time substitution to examine the temporal dynamics of this ecosystem and its recovery from disturbance. Where there was no post-logging management (drainage), there was widespread and rapid regrowth, but not the structure in the short to medium terms was dominaned by low stature plants with low tree density. The height structure of the logged forests showed little change with time since disturbance and a dominance of low stature non-woody species. For an areas impacted by insect defoliation rather than logging, taller mean canopy heights were observed suggested more vigorous regeneration. The variable response of defoliated versus logging disturbance, coupled with the high gap fraction in an unlogged forested peatland (chapter two), indicated an important role of gaps in natural regeneration of PSF.

Mean canopy height in the logged area was observed to be linearly correlated with mean Enhanced Vegetation Index (EVI), while standard deviation of EVI changed with time, suggesting EVI statistics offer potential to study the evolving structure of

vegetation through time and inferring harvesting characteristics. It has been observed that clear cutting could increase flood risk, substrate acidity and salinity, competition for light on the forest floor and hence reduce the ability for trees and seedlings to survive (Kobayashi 1998, 2012). Given the known hydrological sensitivity of peatland tree seedlings, the logging practices, irrespective of drainage, seem to limit woody seedlings survival (Page *et al.*, 2008; Kobayashi 1998) and the abundance of non-woody biomass. The early colonizers species are very flood tolerant and can outcompete seedlings of the canopy species, hence preventing its returns. These non-woody species are also lower in terms of biomass and can change both new peat quality and biogeochemical properties of the soil.

Clear-cutting was observed to produce similar edge dynamics within 1km inside and outside the edge despite differences in elevational gradient and edge ages (13 years vs 23 years). In the early years following clear cut, logged forests had higher EVI than did intact forest, suggesting structural differences in vegetation between the regrowing vegetation and the undisturbed vegetation. At the same time, logged forest had lower backscatter than intact forests, indicating more surface scattering from the regenerating non-woody vegetation, which has smoother surface. Five to ten years after edge creation, the EVI converged between the logged and intact forests, suggesting more structural similarity in logged forests to intact forests. We did not observe these trends in a 13-years old edge adjacent to a selectively logged forest, suggesting a harvesting strategy with different intensity and impact, which in turns resulted in a different form of regrowth.

This dissertation advanced approaches for remote sensing analysis in aseasonal tropical peatlands, where only limited optical remote sensing imagery is often available and where the prevalence of cloud, haze and moisture can contaminate data or confound interpretations. In the case of microwave data, we caution against fusing data from different sensors and from different periods, regardless of their similar technical specifications. In the case of optical data, a proof-of-concept for a land use land cover change detection algorithm required particularly careful cloud and haze screening schemes. However, there is an opportunity cost between screening too much data, missing out on the exact timing of the event of interest and not having enough data for trend fitting. In peatlands, exposed soil after clear cut appears to have the same spectral signature with cloud, hence additional input such as image texture and spatial statistics could increase the accuracy of detection. Finally, as the same peatland often undergoes several disturbances by different agents and at different times e.g. clear cut, then left for regrowth, then drained, then developed as plantation, algorithms need to go beyond just detecting time of change and assuming only one disturbance type, but also type and rate of disturbance. These data analysis strategies presented throughout this dissertation will allow researchers to (i) spatially explicitly distinguish on the ground intact, logged and otherwise disturbed peatlands; (ii) construct a complete land use history for large areas of forested peatlands with respect type and intensity of harvesting and management practices through time and (iii) couple such history with contemporary observations of current ecologies of peatland.

Conversion of tropical peat forest areas has various consequences for the ecology, the carbon and greenhouse gas balance in the years following disturbance, which vary with the extent of disturbance and any associated change in hydrology, and which cannot be reliably inferred by short-term, infrequent measurements. Land use history provides a continuous framework to incorporate these previous lone-standing fiend campaigns and coordinate new efforts of field sampling using a space for time substitution. There still remains a clear need for additional field sampling and ground measurements of forest structures, hydrological changes, greenhouse gas fluxes and ground penetrating radar of peat layers. Several recent and upcoming satellite missions that observe forest structures (e.g. Global Ecosystem Dynamics Investigation Lidar), surface soil moisture (e.g. Advanced Land Observing Satellite 2), or detect fires (e.g. the Visible Infrared Imaging Radiometer Suite) and subsidence (e.g. interferometry Synthetic Aperture Radar) offer tremendous opportunities in improve understanding and monitor change, but these need to be carried out in conjunction with targeted field observations. These data will help constrain the greenhouse gas budgets in peatland and inform land use practices, which currently focus on rewetting of degraded peatlands and the implementation of crop and land use practices that do not involve drainage and heavy soil disturbance. As the restoration of peatland and peat quality depends on aboveground vegetation, future research activities should focus on improving our understanding of the regeneration dynamics in peatland (e.g. stand-alone trees vs gap-based regeneration), techniques and schemes to assist regeneration, and nutrient cycling in logged peatland e.g. the facilitation

of nutrient acquisition in saplings from ectomycorrhizal fungal communities (Jones *et al.*, 2003). Finally, any restoration and conservation scheme for peatlands should take into account future climate change, given the sensitivity of degraded peatlands to drought, fire, and its potential climate feedback. The stability of peatlands concerns the reduction of greenhouse gas emissions, protection of the region's highly endemic fauna and flora, the regulation of regional water and climate, regional economic activities and public health safety, to which long term continuous monitoring can offer tremendous help.

BIBLIOGRAPHY

Abrams, J. F., Hohn, S., Rixen, T., Baum, A., & Merico, A. (2016). The impact of Indonesian peatland degradation on downstream marine ecosystems and the global carbon cycle. *Global change biology*, *22*(1), 325-337.

Ahmed, O. S., Franklin, S. E., & Wulder, M. A. (2014). Interpretation of forest disturbance using a time series of Landsat imagery and canopy structure from airborne lidar. *Canadian Journal of Remote Sensing*, *39*(6), 521-542.

Aide, T. M., Zimmerman, J. K., Pascarella, J. B., Rivera, L., & Marcano-Vega, H. (2000). Forest regeneration in a chronosequence of tropical abandoned pastures: implications for restoration ecology. *Restoration ecology*, *8*(4), 328-338.

Almeida-Filho, R., & Shimabukuro, Y. E. (2000). Detecting areas disturbed by gold mining activities through JERS-1 SAR images, Roraima State, Brazilian Amazon. *International Journal of Remote Sensing*, *21*(17), 3357-3362.

Almeida-Filho, R., Rosenqvist, A., Shimabukuro, Y. E., & dos Santos, J. R. (2005). Evaluation and perspectives of using multitemporal L-band SAR data to monitor deforestation in the Brazilian Amazo/spl circ/nia. *IEEE Geoscience and Remote Sensing Letters*, *2*(4), 409-412.

Almeida-Filho, R., Shimabukuro, Y. E., Rosenqvist, A., & Sanchez, G. A. (2009). Using dual-polarized ALOS PALSAR data for detecting new fronts of deforestation in the Brazilian Amazônia. *International Journal of Remote Sensing*, *30*(14), 3735-3743.

Anderson, J. A. R. (1961). The destruction of Shorea albida forest by an unidentified insect. *Empire Forestry Review*, 19-29.

Anderson, J. A. R. (1964). Observations on climatic damage in peat swamp forest in Sarawak. *The Commonwealth Forestry Review*, 145-158.

Anderson, J. A. R., & Muller, J. (1975). Palynological study of a Holocene peat and a Miocene coal deposit from NW Borneo. *Review of Palaeobotany and Palynology*, *19*(4), 291-351.

Anderson, J. A. R. (1983). The tropical peat swamps of western Malesia. *Mires: swamp, bog, fen and moor: regional studies*.

Ashton P.S. (1983) Dipterocarpaceae. *Flora Malaesiana I*, *9*, 237–552.

Ashton, P. S., & Hall, P. (1992). Comparisons of structure among mixed dipterocarp forests of north-western Borneo. *Journal of Ecology*, 459-481.

Asner, G. P., & Mascaro, J. (2014). Mapping tropical forest carbon: Calibrating plot estimates to a simple LiDAR metric. *Remote Sensing of Environment*, *140*, 614-624.

Baccini, A., Goetz, S. J., Walker, W. S., Laporte, N. T., Sun, M., Sulla-Menashe, D., ... & Houghton, R. A. (2012). Estimated carbon dioxide emissions from tropical deforestation improved by carbon-density maps. *Nature Climate Change*, *2*(3), 182-185.

Banin, L., Lewis, S. L., Lopez-Gonzalez, G., Baker, T. R., Quesada, C. A., Chao, K. J., ... & Phillips, O. L. (2014). Tropical forest wood production: a cross-continental comparison. *Journal of Ecology*.

Berenson, M., Levine, D., Szabat, K. A., & Krehbiel, T. C. (2012). *Basic business statistics: Concepts and applications*. Pearson higher education AU.

Berry, N. J., Phillips, O. L., Lewis, S. L., Hill, J. K., Edwards, D. P., Tawatao, N. B., ... & Ong, R. C. (2010). The high value of logged tropical forests: lessons from northern Borneo. *Biodiversity and Conservation*, *19*(4), 985-997.

Betts, R. A., Jones, C. D., Knight, J. R., Keeling, R. F., & Kennedy, J. J. (2016). El Nino and a record CO2 rise. *Nature Climate Change*.

Blackham, G. V., Thomas, A., Webb, E. L., & Corlett, R. T. (2013). Seed rain into a degraded tropical peatland in Central Kalimantan, Indonesia. *Biological conservation*, *167*, 215-223.

Blackham, G. V., Webb, E. L., & Corlett, R. T. (2014). Natural regeneration in a degraded tropical peatland, Central Kalimantan, Indonesia: Implications for forest restoration. *Forest Ecology and Management*, *324*, 8-15.

Bontemps, S., Langner, A., & Defourny, P. (2012). Monitoring forest changes in Borneo on a yearly basis by an object-based change detection algorithm using SPOT-VEGETATION time series. *International journal of remote sensing*, *33*(15), 4673-4699.

Broich, M., Hansen, M., Stolle, F., Potapov, P., Margono, B. A., & Adusei, B. (2011). Remotely sensed forest cover loss shows high spatial and temporal variation across Sumatera and Kalimantan, Indonesia 2000–2008. *Environmental Research Letters*, *6*(1), 014010.

Brüenig, E. F., & Brüenig, F. E. (1964). A study of damage attributed to lightning in two areas of Shorea albida forest in Sarawak. *The Commonwealth Forestry Review*, 134-144.

Bruenig, E. F. (1969). On the seasonality of droughts in the lowlands of Sarawak (Borneo)(Über das jahreszeitliche Auftreten von Dürren im Tiefland von Sarawak (Borneo)). *Erdkunde*, 127-133.

Bruenig, E. F. (1973). Some further evidence on the amount of damage attributed to lightning and wind-throw in *Shorea Albida* forest in Sarawak. *The Commonwealth Forestry Review*, 260-265.

Brüenig, E. F. (1977). The tropical rain forest: a wasted asset or an essential biospheric resource?. *Ambio*, 187-191.

Bruenig, E. F., & Huang, Y. W. (1989). Patterns of tree species diversity and canopy structure and dynamics in humid tropical evergreen forests on Borneo and in China. *Tropical forests: botanical dynamics, speciation and diversity*, 75-88.

Bryan, J. E., Shearman, P. L., Asner, G. P., Knapp, D. E., Aoro, G., & Lokes, B. (2013). Extreme differences in forest degradation in Borneo: comparing practices in Sarawak, Sabah, and Brunei. *PloS one*, *8*(7), e69679.

Caline, B., & Huong, J. (1992). New insight into the recent evolution of the Baram Delta from satellite imagery. *Geological Society of Malaysia Bulletin*, *32*, 1-13.

Cardille, J. A., & Foley, J. A. (2003). Agricultural land-use change in Brazilian Amazonia between 1980 and 1995: Evidence from integrated satellite and census data. *Remote Sensing of Environment*, *87*(4), 551-562.

Carlson, K. M., Goodman, L. K., & May-Tobin, C. C. (2015). Modeling relationships between water table depth and peat soil carbon loss in Southeast Asian plantations. *Environmental Research Letters*, *10*(7), 074006.

Camargo, J. L. C., & Kapos, V. (1995). Complex edge effects on soil moisture and microclimate in central Amazonian forest. *Journal of Tropical Ecology*, *11*(02), 205-221.

Chambers, J. Q., Higuchi, N., Schimel, J. P., Ferreira, L. V., & Melack, J. M. (2000). Decomposition and carbon cycling of dead trees in tropical forests of the central Amazon. *Oecologia*, *122*(3), 380-388.

Chambers, J. Q., Negron-Juarez, R. I., Marra, D. M., Di Vittorio, A., Tews, J., Roberts, D., ... & Higuchi, N. (2013). The steady-state mosaic of disturbance and succession across an old-growth Central Amazon forest landscape. *Proceedings of the National Academy of Sciences, 110*(10), 3949-3954.

Chaplin-Kramer, R., Ramler, I., Sharp, R., Haddad, N. M., Gerber, J. S., West, P. C., ... & Mueller, C. (2015). Degradation in carbon stocks near tropical forest edges. *Nature communications, 6*.

Clark, D. B., & Clark, D. A. (2000). Landscape-scale variation in forest structure and biomass in a tropical rain forest. *Forest ecology and management, 137*(1), 185-198.

Chave, J., Andalo, C., Brown, S., Cairns, M. A., Chambers, J. Q., Eamus, D., ... & Yamakura, T. (2005). Tree allometry and improved estimation of carbon stocks and balance in tropical forests. *Oecologia*, *145*(1), 87-99.

Chave, J., Réjou-Méchain, M., Búrquez, A., Chidumayo, E., Colgan, M. S., Delitti, W. B., ... & Vieilledent, G. (2014). Improved allometric models to estimate the aboveground biomass of tropical trees. *Global change biology*, *20*(10), 3177-3190.

Clark, D. A. (2004). Sources or sinks? The responses of tropical forests to current and future climate and atmospheric composition. *Philosophical Transactions of the Royal Society of London. Series B: Biological Sciences*, *359*(1443), 477-491.

Couwenberg, J., Dommain, R., & Joosten, H. (2010). Greenhouse gas fluxes from tropical peatlands in south-east Asia. *Global Change Biology*, *16*(6), 1715-1732.

Cubiña, A., & Mitchell Aide, T. (2001). The effect of distance from forest edge on seed rain and soil seed bank in a tropical pasture 1. *Biotropica*, *33*(2), 260-267.

Curran, L.M. (1994). The ecology and evolution of mast-fruiting in Bornean Diptercarpaceae: a general ectomycorrhizal theory. PhD thesis, Princeton University, Princeton, NJ.

Davies, S. J., & Becker, P. (1996). Floristic composition and stand structure of mixed dipterocarp and heath forests in Brunei Darussalam. *Journal of Tropical Forest Science*, *8*(4), 542-569.

De Melo, F. P. L., Dirzo, R., & Tabarelli, M. (2006). Biased seed rain in forest edges: evidence from the Brazilian Atlantic forest. *Biological Conservation*, *132*(1), 50-60.

DeVries, B., Decuyper, M., Verbesselt, J., Zeileis, A., Herold, M., & Joseph, S. (2015). Tracking disturbance-regrowth dynamics in tropical forests using structural change detection and Landsat time series. *Remote Sensing of Environment*, *169*, 320-334.

Dixon, R. K., Solomon, A. M., Brown, S., Houghton, R. A., Trexier, M. C., & Wisniewski, J. (1994). Carbon pools and flux of global forest ecosystems. *Science*, *263*(5144), 185-190.

Dommain, R., Couwenberg, J., & Joosten, H. (2010). Hydrological self-regulation of domed peatlands in south-east Asia and consequences for conservation and restoration. *Mires and Peat*, *6*(5), 1-17.

Dommain, R., Couwenberg, J., & Joosten, H. (2011). Development and carbon sequestration of tropical peat domes in south-east Asia: links to post-glacial sea-level changes and Holocene climate variability. *Quaternary Science Reviews*, *30*(7), 999-1010.

Dommain, R., Couwenberg, J., Glaser, P. H., Joosten, H., & Suryadiputra, I. N. N. (2014). Carbon storage and release in Indonesian peatlands since the last deglaciation. *Quaternary Science Reviews*, *97*, 1-32.

Dommain, R., Cobb, A. R., Joosten, H., Glaser, P. H., Chua, A. F., Gandois, L., ... & Harvey, C. F. (2015). Forest dynamics and tip-up pools drive pulses of high carbon accumulation rates in a tropical peat dome in Borneo (Southeast Asia). *Journal of Geophysical Research: Biogeosciences*, *120*(4), 617-640.

Dommain, R. E. N. É., Dittrich, I. N. G. O., Giesen, W., Joosten, H. A. N. S., Rais, D. S., Silvius, M. A. R. C. E. L., & Wibisono, I. T. C. (2016). Ecosystem services, degradation and restoration of peat swamps in the Southeast Asian tropics. *Peatland Restoration and Ecosystem Services: Science, Policy and Practice*, 253.

Donahue, M.Z. (2016). The mad dash to figure out the fate of peatlands. [URL] http://www.smithsonianmag.com/science-nature/mad-dash-figure-out-fate-peatlands-180958841/?no-ist. Accessed October 24th, 2016.

Dosch, J. J., Peterson, C. J., & Haines, B. L. (2007). Seed rain during initial colonization of abandoned pastures in the premontane wet forest zone of southern Costa Rica. *Journal of Tropical Ecology*, 151-159.

Draper, F. C., Roucoux, K. H., Lawson, I. T., Mitchard, E. T., Coronado, E. N. H., Lähteenoja, O., ... & Baker, T. R. (2014). The distribution and amount of carbon in the largest peatland complex in Amazonia. *Environmental Research Letters*, *9*(12), 124017.

Duncanson, L. I., Cook, B. D., Hurtt, G. C., & Dubayah, R. O. (2014). An efficient, multi-layered crown delineation algorithm for mapping individual tree structure across multiple ecosystems. *Remote Sensing of Environment*, *154*, 378-386.

Dutrieux, L. P., Verbesselt, J., Kooistra, L., & Herold, M. (2015). Monitoring forest cover loss using multiple data streams, a case study of a tropical dry forest in Bolivia. *ISPRS Journal of Photogrammetry and Remote Sensing*, *107*, 112-125.

Efron, B., & Tibshirani, R. J. (1994). *An introduction to the bootstrap* (Vol. 57). CRC press.Englhart, S., Jubanski, J., & Siegert, F. (2013). Quantifying dynamics in tropical peat swamp forest biomass with multi-temporal LiDAR datasets. *Remote Sensing*, *5*(5), 2368-2388.

Espírito-Santo, F. D., Gloor, M., Keller, M., Malhi, Y., Saatchi, S., Nelson, B., ... & Phillips, O. L. (2014). Size and frequency of natural forest disturbances and the Amazon forest carbon balance. *Nature communications*, *5*.

Esterle, J. S., & Ferm, J. C. (1994). Spatial variability in modern tropical peat deposits from Sarawak, Malaysia and Sumatra, Indonesia: analogues for coal. *International Journal of Coal Geology*, *26*(1), 1-41.

FAO. 2012. FRA 2015 terms and definitions. Forest Resources Assessment Working Paper 180. Rome: Food and Agricultural Organization of the United Nations.

Falkowski, M. J., Smith, A. M., Gessler, P. E., Hudak, A. T., Vierling, L. A., & Evans, J. S. (2008). The influence of conifer forest canopy cover on the accuracy of two individual tree measurement algorithms using lidar data. *Canadian Journal of Remote Sensing*, *34*(sup2), S338-S350.

Féret, J. B., & Asner, G. P. (2012). Semi-supervised methods to identify individual crowns of lowland tropical canopy species using imaging spectroscopy and LiDAR. *Remote Sensing*, *4*(8), 2457-2476.

Fernandes, R., & Leblanc, S. G. (2005). Parametric (modified least squares) and non-parametric (Theil–Sen) linear regressions for predicting biophysical parameters in the presence of measurement errors. *Remote Sensing of Environment*, *95*(3), 303-316.

Filzmoser, P., Garrett, R. G., & Reimann, C. (2005). Multivariate outlier detection in exploration geochemistry. *Computers & geosciences*, *31*(5), 579-587.

Freitas, S. R., Mello, M. C., & Cruz, C. B. (2005). Relationships between forest structure and vegetation indices in Atlantic Rainforest. *Forest Ecology and Management*, *218*(1), 353-362.

Furukawa, H. (1988). Stratigraphic and geomorphic studies of peat and giant podzols in Brunei, 1: Peat. *Pedologist (Japan)*.

Furukawa, H. (1988). Stratigraphic and geomorphic studies of peat and giant podzols in Brunei: II. Giant Podzols. *ペドロジスト*, *32*(2), 114-126.

Galindo-González, J., Guevara, S., & Sosa, V. J. (2000). Bat-and bird-generated seed rains at isolated trees in pastures in a tropical rainforest. *Conservation biology*, *14*(6), 1693-1703.

Gamon, J. A., Field, C. B., Goulden, M. L., Griffin, K. L., Hartley, A. E., Joel, G., ... & Valentini, R. (1995). Relationships between NDVI, canopy structure, and photosynthesis in three Californian vegetation types. *Ecological Applications*, 28-41.

Gandois, L., Cobb, A. R., Hei, I. C., Lim, L. B. L., Salim, K. A., & Harvey, C. F. (2013). Impact of deforestation on solid and dissolved organic matter characteristics of tropical peat forests: implications for carbon release. *Biogeochemistry*, *114*(1-3), 183-199.

Garzon-Lopez, C. X., Jansen, P. A., Bohlman, S. A., Ordonez, A., & Olff, H. (2014). Effects of sampling scale on patterns of habitat association in tropical trees. *Journal of Vegetation Science*, *25*(2), 349-362.

Gaveau, D. L.A., Sloan, S., Molidena, E., Yaen, H., Sheil, D., Abram, N. K., ... & Meijaard, E. (2014). Four decades of forest persistence, clearance and logging on Borneo. *PloS one*, *9*(7), e101654.

Gaveau, D.L.A.; Sheil, D.; Husnayaen; Salim, M.A.; Arjasakusuma, S.; Ancrenaz, M.; Pacheco, P.; Meijaard, E. Rapid conversions and avoided deforestation: Examining four decades of industrial plantation expansion in Borneo. Scientif. Rep. **2016**, 6, 32017.

Glenn, E. P., Huete, A. R., Nagler, P. L., & Nelson, S. G. (2008). Relationship between remotely-sensed vegetation indices, canopy attributes and plant physiological processes:

What vegetation indices can and cannot tell us about the landscape. *Sensors*, *8*(4), 2136-2160.

Goodwin, N. R., Collett, L. J., Denham, R. J., Flood, N., & Tindall, D. (2013). Cloud and cloud shadow screening across Queensland, Australia: An automated method for Landsat TM/ETM+ time series. *Remote Sensing of Environment*, *134*, 50-65.

Government of Brunei Darussalam. 2009. Project Implementation Framework Negara Brunei Darussalam. URL: http://www.hobgreeneconomy.org/en/publications/ [Accessed May 11, 2016].

Guevara, S., Laborde, J., & Sanchez-Rios, G. (2004). Rain Forest Regeneration beneath the Canopy of Fig Trees Isolated in Pastures of Los Tuxtlas, Mexico 1. *Biotropica*, *36*(1), 99-108.

Hansen, M. C., Potapov, P. V., Moore, R., Hancher, M., Turubanova, S. A., Tyukavina, A., ... & Kommareddy, A. (2013). High-resolution global maps of 21st-century forest cover change. *science*, *342*(6160), 850-853.

Hatano, R., Toma, Y., Hamada, Y., Arai, H., Susilawati, H. L., & Inubushi, K. (2016). Methane and Nitrous Oxide Emissions from Tropical Peat Soil. In *Tropical Peatland Ecosystems* (pp. 339-351). Springer Japan.

Harmon, M. E., & Sexton, J. (1996). *Guidelines for measurements of woody detritus in forest ecosystems* (Vol. 20). Seattle (WA): US LTER Network Office.

Hart, T.B., Hart, J.A., Murphy, P.G. (1989) Mono-dominant and speciesrich forests of the humid tropics: causes for their occurrence. *Am Nat*, *133*, 613–633.

Hess, L. L., Melack, J. M., Novo, E. M., Barbosa, C. C., & Gastil, M. (2003). Dual-season mapping of wetland inundation and vegetation for the central Amazon basin. *Remote sensing of environment*, *87*(4), 404-428.

Hirano, T., Segah, H., Kusin, K., Limin, S., Takahashi, H., & Osaki, M. (2012). Effects of disturbances on the carbon balance of tropical peat swamp forests. *Global Change Biology*, *18*(11), 3410-3422.

Hirano, T., Kusin, K., Limin, S., & Osaki, M. (2014). Carbon dioxide emissions through oxidative peat decomposition on a burnt tropical peatland. *Global change biology*, *20*(2), 555-565.

Holden, C.E. (2015). Yet Another Time Series Model (YATSM). Zenodo. 10.5281/zenodo.17129

Hooijer, A. (2004). 17 Hydrology of tropical wetland forests: recent research results from Sarawak peat swamps. *Forests, Water and People in the Humid Tropics: Past, Present and Future Hydrological Research for Integrated Land and Water Management*, 447.

Hooijer, A., Silvius, M., Wösten, H. and Page, S. 2006. PEAT-CO2, Assessment of CO2 emissions from drained peatlands in SE Asia. Delft Hydraulics report Q3943 (2006)

Hooijer, A., Page, S., Canadell, J. G., Silvius, M., Kwadijk, J., Wösten, H., & Jauhiainen, J. (2010). Current and future CO_2 emissions from drained peatlands in Southeast Asia.

Hooijer, A., Page, S., Jauhiainen, J., Lee, W. A., Lu, X. X., Idris, A., & Anshari, G. (2012). Subsidence and carbon loss in drained tropical peatlands. *Biogeosciences*, *9*(3), 1053.

Houghton, R. A., Werf, G. V. D., DeFries, R. S., Hansen, M. C., House, J. I., Quéré, C. L., ... & Ramankutty, N. (2012). Chapter G2 Carbon emissions from land use and land-cover change. *Biogeosciences Discussions*, *9*(1), 835.

Huang, C., Goward, S. N., Masek, J. G., Thomas, N., Zhu, Z., & Vogelmann, J. E. (2010). An automated approach for reconstructing recent forest disturbance history using dense Landsat time series stacks. *Remote Sensing of Environment*, *114*(1), 183-198.

Hubbell, S. P., Foster, R. B., O'Brien, S. T., Harms, K. E., Condit, R., Wechsler, B., ... & De Lao, S. L. (1999). Light-gap disturbances, recruitment limitation, and tree diversity in a neotropical forest. *Science*, *283*(5401), 554-557.

Huete, A. R., Hua, G., Qi, J., Chehbouni, A., & Van Leeuwen, W. J. D. (1992). Normalization of multidirectional red and NIR reflectances with the SAVI. *Remote Sensing of Environment*, *41*(2-3), 143-154.

Ichikawa, M. (2007). Degradation and loss of forest land and land-use changes in Sarawak, East Malaysia: a study of native land use by the Iban. *Ecological Research*, *22*(3), 403-413.

Iida, Y., Kohyama, T. S., Kubo, T., Kassim, A. R., Poorter, L., Sterck, F., & Potts, M. D. (2011). Tree architecture and life-history strategies across 200 co-occurring tropical tree species. *Functional Ecology*, *25*(6), 1260-1268.

Imhoff, M. L. (1995). A theoretical analysis of the effect of forest structure on synthetic aperture radar backscatter and the remote sensing of biomass. *IEEE Transactions on Geoscience and Remote Sensing*, *33*(2), 341-352.

Immirzi, C.P., Maltby, E. & Clymo, R.S. (1992) The Global Status of Peatlands and their Role in Carbon Cycling. A report for Friends of the Earth by the Wetland Ecosystems Research Group. Friends of the Earth Trust Ltd.

Ingle, N. R. (2003). Seed dispersal by wind, birds, and bats between Philippine montane rainforest and successional vegetation. *Oecologia*, *134*(2), 251-261.

IPCC. 2001 Climate Change 2001: The scientific basis. Contribution of Working Group I to the Third Assessment Report of the Intergovernmental Panel on Climate Change (eds JT Houghton, Y Ding, DJ Griggs, M Noguer, PJ van der Linden, X Dai, K Maskell, CA Johnson). Cambridge, UK: Cambridge University Press.

IPCC Guidelines for national greenhouse gas inventories, agriculture, forestry and other land use. (2006) IPCC National Greenhouse Gas Inventories Programme, Technical Support Unit vol 4 (Hayama, Japan: Institute for Global Environmental Strategies (IGES))

Jauhiainen, J., Takahashi, H., Heikkinen, J. E., Martikainen, P. J., & Vasander, H. (2005). Carbon fluxes from a tropical peat swamp forest floor. *Global Change Biology*, *11*(10), 1788-1797.

Jauhiainen, J., Limin, S., Silvennoinen, H., & Vasander, H. (2008). Carbon dioxide and methane fluxes in drained tropical peat before and after hydrological restoration. *Ecology*, *89*(12), 3503-3514.

Jaenicke, J., Englhart, S., & Siegert, F. (2011). Monitoring the effect of restoration measures in Indonesian peatlands by radar satellite imagery. *Journal of Environmental Management*, *92*(3), 630-638.

Jin, S., & Sader, S. A. (2005). Comparison of time series tasseled cap wetness and the normalized difference moisture index in detecting forest disturbances. *Remote Sensing of Environment*, *94*(3), 364-372.

Jones, M. D., Durall, D. M., & Cairney, J. W. (2003). Ectomycorrhizal fungal communities in young forest stands regenerating after clearcut logging. *New Phytologist*, *157*(3), 399-422.

Jubanski, J., Ballhorn, U., Kronseder, K., Franke, J., & Siegert, F. (2013). Detection of large above-ground biomass variability in lowland forest ecosystems by airborne LiDAR. *Biogeosciences*, *10*(6), 3917-3930.

Kapos, V. (1989). Effects of isolation on the water status of forest patches in the Brazilian Amazon. *Journal of tropical ecology*, *5*(02), 173-185.

Kapos, V., Wandelli, E., Camargo, J. L., Gislene, G.. 1997. Edge-related changes in environment and plant responses due to forest fragmentation in central Amazonia. *Pages* 33–44 *in* W. F. Laurance *and* R.O.Bierregaard *(editors).* Tropical forest remnants: ecology, management and conservation of fragmented communities. *University of Chicago Press, Chicago.*

Kaur, A. (1998). A history of forestry in Sarawak. *Modern Asian Studies*, *32*(01), 117-147.

Keller, M., Palace, M., Asner, G. P., Pereira, R., & Silva, J. N. M. (2004). Coarse woody debris in undisturbed and logged forests in the eastern Brazilian Amazon. *Global change biology*, *10*(5), 784-795.

Kellner, J. R., & Asner, G. P. (2009). Convergent structural responses of tropical forests to diverse disturbance regimes. *Ecology letters*, *12*(9), 887-897.

Kennedy, R. E., Cohen, W. B., & Schroeder, T. A. (2007). Trajectory-based change detection for automated characterization of forest disturbance dynamics. *Remote Sensing of Environment*, *110*(3), 370-386.

Kennedy, R. E., Yang, Z., & Cohen, W. B. (2010). Detecting trends in forest disturbance and recovery using yearly Landsat time series: 1. LandTrendr—Temporal segmentation algorithms. *Remote Sensing of Environment*, 114(12), 2897-2910.

Kho, L. K., Malhi, Y., & Tan, S. K. S. (2013). Annual budget and seasonal variation of aboveground and belowground net primary productivity in a lowland dipterocarp forest in Borneo. *Journal of Geophysical Research: Biogeosciences*, *118*(3), 1282-1296.

Kim, D. H., Sexton, J. O., & Townshend, J. R. (2015). Accelerated deforestation in the humid tropics from the 1990s to the 2000s. *Geophysical Research Letters*, 42(9), 3495 – 3501.

Kobayashi, S. (1998). Forest structure and regeneration process of peat swamp Alan forests (Shorea albida) in Brunei Darussalam. In *Proceedings of the Second International*

Symposium on Asian Tropical Forest Management (No. PUSREHUT Special Publication).

Kobayashi, S. (2000). Initial phase of secondary succession in the exploited peat swamp forest (Shorea albida) at Sungai Damit, Belait in Brunei Darussalam. In *Proceedings of the international symposium on tropical peatlands* (pp. 205-214).

Kobayashi, S. (2016). Tropical peat Swamp Forest ecosystems and reDD+1. *Catastrophe and Regeneration in Indonesia's Peatlands: Ecology, Economy and Society*, *15*, 211.

Koplitz, S. N., Mickley, L. J., Marlier, M. E., Buonocore, J. J., Kim, P. S., Liu, T., ... & Pongsiri, M. (2016). Public health impacts of the severe haze in Equatorial Asia in September–October 2015: demonstration of a new framework for informing fire management strategies to reduce downwind smoke exposure. *Environmental Research Letters*, *11*(9), 094023.

Kronseder, K., Ballhorn, U., Böhm, V., & Siegert, F. (2012). Above ground biomass estimation across forest types at different degradation levels in Central Kalimantan using LiDAR data. *International Journal of Applied Earth Observation and Geoinformation*, *18*, 37-48.

Kumagai, T. O., Katul, G. G., Porporato, A., Saitoh, T. M., Ohashi, M., Ichie, T., & Suzuki, M. (2004). Carbon and water cycling in a Bornean tropical rainforest under current and future climate scenarios. *Advances in Water Resources*, *27*(12), 1135-1150.

Langmann, B. and Heil, A.: Release and dispersion of vegetation and peat fire emissions in the atmosphere over Indonesia 1997/1998, Atmos. Chem. Phys., 4, 2145–2160, 2004

Langner, A., Miettinen, J., & Siegert, F. (2007). Land cover change 2002–2005 in Borneo and the role of fire derived from MODIS imagery. *Global Change Biology*, *13*(11), 2329-2340. Carbon stocks and its variations with topography in an intact lowland mixed dipterocarp forest in Brunei. *Journal of Ecology and Environment*, *38(1)*, 75-84.

Langner, A., Achard, F., & Grassi, G. (2014). Can recent pan-tropical biomass maps be used to derive alternative Tier 1 values for reporting REDD+ activities under UNFCCC? *Environmental Research Letters*, *9*(12), 124008.

Laurance, W. F., Ferreira, L. V., Rankin-de Merona, J. M., & Laurance, S. G. (1998). Rain forest fragmentation and the dynamics of Amazonian tree communities. *Ecology*, *79*(6), 2032-2040.

Laurance, W. F., Delamônica, P., Laurance, S. G., Vasconcelos, H. L., & Lovejoy, T. E. (2000). Conservation: rainforest fragmentation kills big trees. *Nature*, *404*(6780), 836-836.

Laurance, W. F., Lovejoy, T. E., Vasconcelos, H. L., Bruna, E. M., Didham, R. K., Stouffer, P. C., ... & Sampaio, E. (2002). Ecosystem decay of Amazonian forest fragments: a 22-year investigation. *Conservation Biology*, *16*(3), 605-618.

Laurance, W. F., Camargo, J. L., Luizão, R. C., Laurance, S. G., Pimm, S. L., Bruna, E. M., ... & Van Houtan, K. S. (2011). The fate of Amazonian forest fragments: a 32-year investigation. *Biological Conservation*, *144*(1), 56-67.

Lee, S., Lee, D., Yoon T.K., Salim, K.A., Han, S., Yun, H.M., Yoon, M., Kim, E., Lee, W.K., Davies, S.J. & Son, Y. (2015). Carbon stocks and its variations with topography in an intact

lowland mixed dipterocarp forest in Brunei. *Journal of Ecology and Environment*, 38(1), 75-84.

Lewis, S. L., Lloyd, J., Sitch, S., Mitchard, E. T., & Laurance, W. F. (2009). Changing ecology of tropical forests: evidence and drivers. *Annual Review of Ecology, Evolution, and Systematics*, *40*, 529-549.

Lewis, S. L., Sonké, B., Sunderland, T., Begne, S. K., Lopez-Gonzalez, G., van der Heijden, G. M., ... & Simo, M. (2013). Above-ground biomass and structure of 260 African tropical forests. *Philosophical Transactions of the Royal Society B: Biological Sciences*, *368*(1625), 20120295.

Li, W., Guo, Q., Jakubowski, M. K., & Kelly, M. (2012). A new method for segmenting individual trees from the lidar point cloud. *Photogrammetric Engineering & Remote Sensing*, *78*(1), 75-84.

Lim, T. Y., Lim, Y. Y., and Yule, C. M. (2014). Bioactivity of leaves of *Macaranga* species in tropical peat swamp and non-peat swamp environments. *J. Trop. For. Sci.* 26, 134–141. Available online at: http://www.jstor.org/stable/23617022

Limpens, J., Berendse, F., Blodau, C., Canadell, J. G., Freeman, C., Holden, J., ... & Schaepman-Strub, G. (2008). Peatlands and the carbon cycle: from local processes to global implications–a synthesis. *Biogeosciences*, *5*(5), 1475-1491.

Lobo, E., & Dalling, J. W. (2014). Spatial scale and sampling resolution affect measures of gap disturbance in a lowland tropical forest: implications for understanding forest regeneration and carbon storage. *Proceedings of the Royal Society B: Biological Sciences*, *281*(1778), 20133218.

Lucas, R. M., Mitchell, A. L., Rosenqvist, A., Proisy, C., Melius, A., & Ticehurst, C. (2007). The potential of L-band SAR for quantifying mangrove characteristics and change: case studies from the tropics. *Aquatic conservation: marine and freshwater ecosystems*, *17*(3), 245-264.

Malhi, Y., Wood, D., Baker, T. R., Wright, J., Phillips, O. L., Cochrane, T., ... & Vinceti, B. (2006). The regional variation of aboveground live biomass in old-growth Amazonian forests. *Global Change Biology*, *12*(7), 1107-1138.

Malhi, Y., Gardner, T. A., Goldsmith, G. R., Silman, M. R., & Żelazowski, P. (2014). Tropical Forests in the Anthropocene. *Annual Review of Environment and Resources*, *39*(1).

Mascaro, J., Detto, M., Asner, G. P., & Muller-Landau, H. C. (2011). Evaluating uncertainty in mapping forest carbon with airborne LiDAR. *Remote Sensing of Environment*, *115*(12), 3770-3774.

Melling L, Hatano R, Goh KJ (2005) Soil CO2 flux from three ecosystems in tropical peatland of Sarawak, Malaysia. Tellus 57(B):1–11.

Melling L, Goh KJ, Uyo LJ, Hatano R (2007) Biophysical characteristics of tropical peatland. In: Jol H et al (eds) Proceedings of soil science conference of Malaysia, April 17th–19th 2007. Malaysian Soil Science Society, Sarawak.

Miettinen, J., & Liew, S. C. (2010). Degradation and development of peatlands in Peninsular Malaysia and in the islands of Sumatra and Borneo since 1990. *Land degradation & development*, *21*(3), 285-296.

Miettinen, J., Shi, C., & Liew, S. C. (2011a). Deforestation rates in insular Southeast Asia between 2000 and 2010. *Global Change Biology*, *17*(7), 2261-2270.

Miettinen, J., Shi, C., & Liew, S. C. (2011b). Two decades of destruction in Southeast Asia's peat swamp forests. *Frontiers in Ecology and the Environment*, *10*(3), 124-128.

Miettinen, J., Shi, C., & Liew, S. C. (2012). Two decades of destruction in Southeast Asia's peat swamp forests. *Frontiers in Ecology and the Environment*, *10*(3), 124-128.

Miettinen, J., Stibig, H. J., & Achard, F. (2014). Remote sensing of forest degradation in Southeast Asia—aiming for a regional view through 5–30 m satellite data. *Global Ecology and Conservation*, *2*, 24-36.

Mirmanto, E. (2010). Vegetation analyses of Sebangau peat swamp forest, Central Kalimantan. *Biodiversitas, 11*, 82-88.

Mitsch, W. J., Nahlik, A., Wolski, P., Bernal, B., Zhang, L., & Ramberg, L. (2010). Tropical wetlands: seasonal hydrologic pulsing, carbon sequestration, and methane emissions. *Wetlands ecology and management*, *18*(5), 573-586.

Momose, K., & Shimamura, T. (2002). Environment and people of Sumatran peat swamp forest I: Distribution and typology of vegetation. *Southeast Asian Studies, 40*(1), 74-86.

Monda, Y., Kiyono, Y., Melling, L., Damian, C., & Chaddy, A. (2015). Allometric equations considering the influence of hollow trees: A case study for tropical peat swamp forest in Sarawak. *Tropics, 24(1), in press.*

Moore, S., Evans, C. D., Page, S. E., Garnett, M. H., Jones, T. G., Freeman, C., et al. (2013). Deep instability of deforested tropical peatlands revealed by fluvial organic carbon fluxes. *Nature* 493, 660–663. doi: 10.1038/nature11818

Müller, D., H.W. Bange, T. Warneke, T. Rixen, M. Müller, A. Mujahid, and J. Notholt. 2016. Nitrous oxide and methane in two tropical estuaries in a peat dominated region of North-western Borneo. *Biogeosciences* 13: 2415–2428.

Neuzil SG (1997) Onset and rate of peat and carbon accumulation in four domed ombrogenous peat deposits, Indonesia. In: Rieley JO, Page SE (eds) Biodiversity and sustainability of tropical peatlands. Samara Publishing Limited, Cardigan, pp 55–72.

Nguyen, H. T., Hutyra, L. R., Hardiman, B. S. and Raciti, S. M. (2016), Characterizing forest structure variations across an intact tropical peat dome using field samplings and airborne LiDAR. Ecol Appl. Accepted Author Manuscript. doi:10.1890/15-0017.

Okuda, T., Suzuki, M., Adachi, N., Yoshida, K., Niiyama, K., Noor, N. S. M., ... & Hashim, M. (2003). Logging history and its impact on forest structure and species composition in the Pasoh forest reserve—implications for the sustainable management of natural resources and landscapes. In *Pasoh* (pp. 15-34). Springer Japan.

Olofsson, P., Foody, G. M., Stehman, S. V., & Woodcock, C. E. (2013). Making better use of accuracy data in land change studies: Estimating accuracy and area and

quantifying uncertainty using stratified estimation. *Remote Sensing of Environment*, *129*, 122-131.

Olofsson, P., Foody, G. M., Herold, M., Stehman, S. V., Woodcock, C. E., & Wulder, M. A.

(2014). Good practices for estimating area and assessing accuracy of land change. *Remote Sensing of Environment*, *148*, 42-57.

Osunkoya, O. O., Sheng, T. K., Mahund, N. A., & Damit, N. (2007). Variation in wood density, wood water content, stem growth and mortality among twenty-seven tree species in a tropical rainforest on Borneo Island. *Austral Ecology*, *32*(2), 191-201.

Ouma, Y. O., Tateishi, R., Chen, Z., Goddard, S., Hubbard, K. G., Sorensen, W. S., ... & Li, J. (2006). Optimization of second-order grey-level texture in high-resolution imagery for statistical estimation of above-ground biomass. *J. Environ. Inform*, *8*, 70-85.

Page, S. E., Rieley, J. O., Shotyk, Ø. W., & Weiss, D. (1999). Interdependence of peat and vegetation in a tropical peat swamp forest. *Philosophical Transactions of the Royal Society of London. Series B: Biological Sciences*, *354*(1391), 1885-1897.

Page, S. E., Siegert, F., Rieley, J. O., Boehm, H. D. V., Jaya, A., & Limin, S. (2002). The amount of carbon released from peat and forest fires in Indonesia during 1997. *Nature*, *420*(6911), 61-65.

Page, S. E., Wűst, R. A. J., Weiss, D., Rieley, J. O., Shotyk, W., & Limin, S. H. (2004). A record of Late Pleistocene and Holocene carbon accumulation and climate change from an equatorial peat bog (Kalimantan, Indonesia): implications for past, present and future carbon dynamics. *Journal of Quaternary Science*, *19*(7), 625-635.

Page, S. E., J. O. Rieley, & R. Wüst. (2006). "Lowland tropical peatlands of Southeast Asia." *Developments in Earth Surface Processes.* 9, 145-172.

Page, S., Graham, L., Hoscilo, A., & Limin, S. (2008). Vegetation restoration on degraded tropical peatlands: opportunities and barriers. *RESTORATION OF TROPICAL PEATLANDS*, 64.

Page S, Hoscilo A, Wosten H, Jauhiainen J, Silvius M, Rieley J, Ritzema H, Tansey K, Graham

L, Vasander H, Limin S (2009) Restoration ecology of lowland tropical peatlands in southeast Asia: current knowledge and future research directions. Ecosystems 12:888–905.

Page, S. E., Rieley, J. O., & Banks, C. J. (2011). Global and regional importance of the tropical peatland carbon pool. *Global Change Biology*, *17*(2), 798-818.

Palace, M., Keller, M., Asner, G. P., Hagen, S., & Braswell, B. (2008). Amazon forest structure from IKONOS satellite data and the automated characterization of forest canopy properties. *Biotropica*, *40*(2), 141-150.

Parish, F., et al. (Eds.) (2008), Assessment on peatlands, biodiversity and climate change: Main report, 179 pp., Global Environ. Cent., Kuala Lumpur.

Paoli, G. D., Curran, L. M., & Slik, J. W. F. (2008). Soil nutrients affect spatial patterns of aboveground biomass and emergent tree density in southwestern Borneo. *Oecologia*, *155*(2), 287-299.

Parker, G. G., Lowman, M. D., & Nadkarni, N. M. (1995). Forest canopies. *Forest canopies*.

Popescu, S. C., Wynne, R. H., & Nelson, R. F. (2002). Estimating plot-level tree heights with lidar: local filtering with a canopy-height based variable window size. *Computers and Electronics in Agriculture*, *37*(1), 71-95.

Popescu, S. C., & Wynne, R. H. (2004). Seeing the Trees in the Forest. *Photogrammetric Engineering & Remote Sensing*, *70*(5), 589-604.

Posa, M. R. C., Wijedasa, L. S., & Corlett, R. T. (2011). Biodiversity and conservation of tropical peat swamp forests. *BioScience*, *61*(1), 49-57.

Potts, M. D., Ashton, P. S., Kaufman, L. S., & Plotkin, J. B. (2002). Habitat patterns in tropical rain forests: a comparison of 105 plots in northwest Borneo. *Ecology*, *83*(10), 2782-2797.

Poulsen, A. D., Nielsen, I. C., Tan, S., & Balslev, H. (1996). A quantitative inventory of trees in one hectare of mixed dipterocarp forest in Temburong, Brunei Darussalam. In *Tropical Rainforest Research—Current Issues* (pp. 139-150). Springer Netherlands.

Proctor, J., Anderson, J. M., Chai, P., & Vallack, H. W. (1983). Ecological studies in four contrasting lowland rain forests in Gunung Mulu National Park, Sarawak: I. Forest environment, structure and floristics. *The Journal of Ecology*, 237-260.

Quéré, C. L., Moriarty, R., Andrew, R. M., Canadell, J. G., Sitch, S., Korsbakken, J. I., ... & Houghton, R. A. (2015). Global Carbon Budget 2015. *Earth System Science Data*, *7*(2), 349-396.

R Development Core Team. 2016. R: a language and environment for statistical computing. Reference index version 3.3.0. R Foundation for Statistical Computing,Vienna, Austria.

Rein, G., Cleaver, N., Ashton, C., Pironi, P., & Torero, J. L. (2008). The severity of smouldering peat fires and damage to the forest soil. *Catena*, *74*(3), 304-309.

Richter, R. (1996). Atmospheric correction of satellite data with haze removal including a haze/clear transition region. *Computers & Geosciences*, *22*(6), 675-681.

Rieley, J. O., & Page, S. E. (2005). Wise use of tropical peatlands. *ALTERRA, Wageningen, the Netherlands*.

Rice, A. H., Pyle, E. H., Saleska, S. R., Hutyra, L., Palace, M., Keller, M., ... & Wofsy, S. C. (2004). Carbon balance and vegetation dynamics in an old-growth Amazonian forest. *Ecological Applications*, *14*(sp4), 55-71.

Rignot, E., Salas, W. A., & Skole, D. L. (1997). Mapping deforestation and secondary growth in Rondônia, Brazil, using imaging radar and Thematic Mapper data. *Remote Sensing of Environment*, *59*(2), 167-179.

Rogan, J., & Chen, D. (2004). Remote sensing technology for mapping and monitoring land-cover and land-use change. *Progress in planning*, *61*(4), 301-325.

Saatchi, S. S., Harris, N. L., Brown, S., Lefsky, M., Mitchard, E. T., Salas, W., ... & Morel, A. (2011). Benchmark map of forest carbon stocks in tropical regions across three continents. *Proceedings of the National Academy of Sciences*, *108*(24), 9899-9904.

Salas, W. A., Ducey, M. J., Rignot, E., & Skole, D. (2002). Assessment of JERS-1 SAR for monitoring secondary vegetation in Amazonia: I. Spatial and temporal variability in backscatter across a chrono-sequence of secondary vegetation stands in Rondonia. *International Journal of Remote Sensing*, *23*(7), 1357-1379.

Saner, P., Loh, Y. Y., Ong, R. C., & Hector, A. (2012). Carbon stocks and fluxes in tropical lowland dipterocarp rainforests in Sabah, Malaysian Borneo. *PloS one, 7*(1), e29642.

Schrier-Uijl, A. P., Silvius, M., Parish, F., Lim, K. H., Rosediana, S., & Anshari, G. (2013). Environmental and social impacts of oil palm cultivation on tropical peat: a scientific review. *Reports from the Science Panel of the Second RSPO GHG Working Group. Kuala Lumpur, Malaysia: Roundtable for Sustainable Palm Oil*.

Shimada, M., & Isoguchi, O. (2002). JERS-1 SAR mosaics of Southeast Asia using calibrated path images. *International Journal of Remote Sensing*, *23*(7), 1507-1526.

Shimada, S., Takahashi, H., Osaki, M, & Tsuji, N. (2016). Carbon Stock Estimate. In: Osaki, M, & Tsuji, N. (eds) Tropical Peatland Ecosystems, pp. 353-365. http://dx.doi.org/10.1007/978-4-431-55681-7_23

Shimamura, T., & Momose, K. (2005). Organic matter dynamics control plant species coexistence in a tropical peat swamp forest. *Proceedings of the Royal Society B: Biological Sciences*, *272*(1571), 1503-1510.

Sieffermann, R. G., Fournier, M., Triutomo, S., Sadelman, M. T., & Semah, A. M. (1988, August). Velocity of tropical forest peat accumulation in Central Kalimantan Province, Indonesia (Borneo). In *Proceedings of the 8th International Peat Congress, August 1988, Leningrad* (pp. 90-98).

Siddique, S. (1992). Brunei Darussalam 1991: The Non-Secular Nation. *Southeast Asian Affairs*, 91-100.

Siqueira, P., Chapman, B., & McGarragh, G. (2004). The coregistration, calibration, and interpretation of multiseason JERS-1 SAR data over South America. *Remote Sensing of Environment*, *90*(4), 536-550.

Slik, J. W. F., Poulsen, A. D., Ashton, P. S., Cannon, C. H., Eichhorn, K. A. O., Kartawinata, K., ... & Wilkie, P. (2003). A floristic analysis of the lowland dipterocarp forests of Borneo. *Journal of Biogeography*, *30*(10), 1517-1531.

Slik, J. W. F., Aiba, S. I., Brearley, F. Q., Cannon, C. H., Forshed, O., Kitayama, K., ... & van Valkenburg, J. L. (2010). Environmental correlates of tree biomass, basal area, wood specific gravity and stem density gradients in Borneo's tropical forests. *Global Ecology and Biogeography*, *19*(1), 50-60.

Small, A., Martin, T. G., Kitching, R. L., & Wong, K. M. (2004). Contribution of tree species to the biodiversity of a 1ha Old World rainforest in Brunei, Borneo. *Biodiversity & Conservation*, *13*(11), 2067-2088.

Sodhi, N. S., Koh, L. P., Brook, B. W., & Ng, P. K. (2004). Southeast Asian biodiversity: an impending disaster. *Trends in Ecology & Evolution*, *19*(12), 654-660.

Solberg, S., Naesset, E., & Bollandsas, O. M. (2006). Single tree segmentation using airborne laser scanner data in a structurally heterogeneous spruce forest. *Photogrammetric Engineering & Remote Sensing*, *72*(12), 1369-1378.

Song, X. P., Huang, C., Sexton, J. O., Channan, S., & Townshend, J. R. (2014). Annual detection of forest cover loss using time series satellite measurements of percent tree cover. *Remote Sensing*, *6*(9), 8878-8903.

Staub, J. R., & Esterle, J. S. (1994). Peat-accumulating depositional systems of Sarawak, East Malaysia. *Sedimentary Geology*, *89*(1-2), 91-106.

Stibig, H. J., Achard, F., Carboni, S., Raši, R., & Miettinen, J. (2014). Change in tropical forest cover of Southeast Asia from 1990 to 2010. *Biogeosciences*, *11*(2), 247-258.

Strack, M. (Ed.). (2008). *Peatlands and climate change*. IPS, International Peat Society.

Turetsky M, Benscoter B, Page SE, Rein G, van der Werf G, Watts A. (2015). *Global vulnerability of peatlands to fire and carbon loss. Nat. Geosci. 8, 11–14.*

Uhl, C., Clark, K., Dezzeo, N., & Maquirino, P. (1988). Vegetation dynamics in Amazonian treefall gaps. *Ecology*, *69*(3), 751-763.

van der Meer, Peter J., and Caspar C. Verwer. "Towards a reference carbon value for peat swamp forest in Southeast Asia based on historical inventory data." *Workshop on Tropical Wetland Ecosystems of Indonesia: Science Needs To Address Climate Change Adaptation And Mitigation. Watilan Convention Center, Sanur Beach Hotel, Bali*. 2011.

Van der Werf, G. R., Morton, D. C., DeFries, R. S., Olivier, J. G., Kasibhatla, P. S., Jackson, R. B., ... & Randerson, J. T. (2009). CO2 emissions from forest loss. *Nature geoscience*, *2*(11), 737-738.

van der Werf 2015. URL: http://www.globalfiredata.org/updates.html. [Accessed May 11, 2016].

Varma, A. (2003). The economics of slash and burn: a case study of the 1997–1998 Indonesian forest fires. *Ecological Economics*, *46*(1), 159-171.

Vauhkonen, J., Ene, L., Gupta, S., Heinzel, J., Holmgren, J., Pitkänen, J., ... & Maltamo, M. (2011). Comparative testing of single-tree detection algorithms under different types of forest. *Forestry*, cpr051.

Vega, C., Hamrouni, A., El Mokhtari, S., Morel, J., Bock, J., Renaud, J. P., ... & Durrieu, S. (2014). PTrees: A point-based approach to forest tree extraction from lidar data. *International Journal of Applied Earth Observation and Geoinformation*, *33*, 98-108.

Verbesselt, J., Hyndman, R., Newnham, G., & Culvenor, D. (2010). Detecting trend and seasonal changes in satellite image time series. *Remote sensing of Environment*, *114*(1), 106-115.

Viedma, O., Melia, J., Segarra, D., & Garcia-Haro, J. (1997). Modeling rates of ecosystem recovery after fires by using Landsat TM data. *Remote Sensing of Environment*, *61*(3), 383-398.

Wang, Y., Weinacker, H., & Koch, B. (2008). A lidar point cloud based procedure for vertical canopy structure analysis and 3D single tree modelling in forest. *Sensors*, *8*(6), 3938-3951.

Wetlands International. 2010. A quick scan of peatlands in Malaysia. Wetlands International-Malaysia: Petaling Jaya, Malaysia. 74 pp.

Wösten, J. H. M., Clymans, E., Page, S. E., Rieley, J. O., & Limin, S. H. (2008). Peat–water interrelationships in a tropical peatland ecosystem in Southeast Asia. *Catena*, *73*(2), 212-224.

Whigham, D. F., Dickinson, M. B., & Brokaw, N. V. (1999). Background canopy gap and catastrophic wind disturbances in tropical forests. *Ecosystems of the World*, 223-252.

Whitmore, T. C. (1984). Tropical forests of the Far East. *Tropical forests of the Far East*.

Yule, C. M., & Gomez, L. N. (2009). Leaf litter decomposition in a tropical peat swamp forest in Peninsular Malaysia. *Wetlands ecology and management*, *17*(3), 231-241.

Zhu, Z., & Woodcock, C. E. (2014). Continuous change detection and classification of land cover using all available Landsat data. *Remote sensing of Environment*, *144*, 152-171.

Zhu, Z., & Woodcock, C. E. (2012). Object-based cloud and cloud shadow detection in Landsat imagery. *Remote Sensing of Environment*, *118*, 83-94.

Zimmerman, J. K., Pascarella, J. B., & Aide, T. M. (2000). Barriers to forest regeneration in an abandoned pasture in Puerto Rico. *Restoration ecology*, *8*(4), 350-360.